NASA CONTRACTOR REPORT

NASA CR-1560

INVESTIGATION OF THE VIBRATION ISOLATION OF COMMERCIAL JET TRANSPORT PILOTS DURING TURBULENT AIR PENETRATION

by Dale W. Schubert, Jerome S. Pepi, and Frank E. Roman

Prepared by
BARRY WRIGHT CORPORATION
Watertown, Mass.
for Langley Research Center

NATIONAL AERONAUTICS AND SPACE ADMINISTRATION • WASHINGTON, D. C. • JULY 1970

NASA CR-1560

INVESTIGATION OF THE VIBRATION ISOLATION OF COMMERCIAL JET TRANSPORT PILOTS DURING TURBULENT AIR PENETRATION

By Dale W. Schubert, Jerome S. Pepi, and Frank E. Roman

Prepared under Contract No. NAS 1-8060 by
BARRY WRIGHT CORPORATION
Watertown, Mass.

for Langley Research Center

NATIONAL AERONAUTICS AND SPACE ADMINISTRATION

For sale by the Clearinghouse for Federal Scientific and Technical Information
Springfield, Virginia 22151 – CFSTI price $3.00

INVESTIGATION OF THE VIBRATION ISOLATION OF COMMERCIAL JET TRANSPORT PILOTS DURING TURBULENT AIR PENETRATION

by Dale W. Schubert, Jerome S. Pepi, and Frank E. Roman

ABSTRACT

This report presents the results of an analytical and experimental investigation of the configuration of an electrohydraulic pilot seat isolation system which would provide commercial jet transport pilots with maximum protection from the dynamic response of the aircraft during turbulent air penetration. A literature survey was conducted into the effects of vibration on the visual and motor performance of seated human subjects (based on equal excitation of the subject and his controls) and the vibration levels encountered at the cockpit of present and future commercial jet transport aircraft during the penetration of turbulence. It was determined that active vibration isolation of the pilot was required in the vertical direction with a resonant frequency of nominally 2 Hz, a resonant transmissibility of less than 2, and better than 70 percent isolation at 4.5 Hz. In addition, it was necessary that the performance of the active isolation system be essentially independent of pilot reactions and variations in weight. The survey also indicated that conventional passive isolation of the pilot in the horizontal directions was sufficient. The active isolator selected for analysis and experimental evaluation was of the electrohydraulic feedback control type. Test data indicates that the laboratory model of the electrohydraulic pilot seat isolation system developed under this contract met all design goals. It was also determined in preliminary subjective evaluation tests (based on the simultaneous excitation of the pilot seat and cockpit simulator) that, although the vibrations transmitted to the pilot's legs via the rudder pedals was somewhat disconcerting (vibration of the arms via the control column was of less importance), the electrohydraulic pilot seat isolation system had the potential for providing a significant improvement in pilot performance capability during turbulent air penetration.

CONTENTS

INVESTIGATION OF THE VIBRATION ISOLATION OF COMMERCIAL JET TRANSPORT PILOTS DURING TURBULENT AIR PENETRATION

by Dale W. Schubert, Jerome S. Pepi, and Frank E. Roman

Barry Controls, Division of Barry Wright Corporation
Watertown, Massachusetts

SUMMARY

In order to select parameters for the design of the pilot seat isolation system, a literature survey was made of the vibration levels present in the cockpit of commercial jet transport aircraft during turbulent flight. It was determined that the primary excitation frequency of concern occurred between 4 and 5 Hz and was due to the first fuselage flexible bending mode of the aircraft. This excitation frequency coincides with the primary whole body resonant frequency of seated human subjects. Based on a comparison of the input with criteria for the maximum vibration levels which should be transmitted to the pilot in order to minimize the reduction in performance, it was concluded that active vibration isolation was required in the vertical direction with a high-isolation notch centered about the first fuselage flexible bending mode frequency (nominally 4.5 Hz), a resonant frequency of nominally 2 Hz and a resonant transmissibility less than 2. In this investigation, an active electrohydraulic isolation system was selected for evaluation. Conventional passive isolation was sufficient in the horizontal direction.

A theoretical investigation was conducted into the type of motion sensors and feedback compensation which should be employed with the electrohydraulic vibration isolation system. A digital computer analysis was made of the control system taking into account the dynamic characteristics of all components which could influence its performance. Isolation performance tests were performed on a laboratory model of the electrohydraulic pilot seat isolation system, the results of which indicated that the model met all design goals.

Subjective tests were also performed to determine the potential effectiveness of the laboratory model of the electrohydraulic pilot seat isolation system in improving the performance of commercial jet transport pilots. The subjects were required to perform a combination visual/motor (hand) task with their feet on a simulated cockpit floor and their hands grasping a simulated control column. It was demonstrated that the active electrohydraulic isolation system provided substantially less vibration interference and annoyance than a conventional commercial jet transport pilot seat.

SECTION 1: INTRODUCTION

Preliminary studies of the flight recorders from commercial jet transport aircraft during "jet upset" conditions as well as the results of flight simulator tests, indicated that the vibration levels imposed on the cockpit due to turbulent air penetration placed severe limitations on the ability of the pilot to take appropriate corrective action. Consequently, an analytical and experimental investigation was conducted into the configuration of a pilot seat isolation system which would provide commercial jet transport pilots with maximum protection from the dynamic response of the aircraft during turbulent air penetration. This report presents the results of this investigation. Goals for the maximum vibration levels which should be transmitted to the pilot, based on the same vibration input to the subject's buttocks and instrument panel, are established in Section 2. These vibration levels have been defined considering the ability of the pilot to perform. Available data on the dynamic environment existing in the cockpit of present and future generation commercial jet transport aircraft during turbulent air penetration are presented in Section 3. In Section 4, the excitation and desired response spectra are compared and a determination is made of the necessary performance characteristics of the pilot seat isolation system. It is concluded that active vibration isolation is required in the vertical direction, while conventional passive isolation is sufficient in the horizontal directions.

In this study, an active electrohydraulic vibration isolation system was selected for evaluation. The general principles of electrohydraulic vibration isolation are presented in Section 5. Consideration is given to the application of broad-band and broad-band plus high-isolation notch electrohydraulic vibration isolation to the pilot seat problem. It is concluded that the latter approach is required. A detailed theoretical analysis of

the laboratory model of the electrohydraulic pilot seat isolation system developed under this contract is presented in Section 6. The electrical and mechanical design of the unit is also discussed in this section.

Both objective and subjective tests were performed on the electrohydraulic pilot seat isolation system. The results of the tests are presented in Section 7. The objective tests were performed with the subject's legs hanging free and his arms on the arm rests. Transmissibility functions between the input and various points on the isolation system and the subjects were determined. During the subjective tests, the subject's feet were positioned on the floor of a cockpit simulator and their hands grasped a simulated control column. Qualitative reactions as to the potential effectiveness of the electrohydraulic vibration isolation system developed during this program in improving the performance of commercial jet transport pilots were recorded. The detailed conclusions from this investigation are presented in Section 8 and recommendations for further work are discussed in Section 9.

SECTION 2: HUMAN REACTION TO WHOLE BODY VIBRATIONS AND SUSTAINED ACCELERATIONS

Introduction

The ability of a pilot to maintain control of his aircraft following the penetration of atmospheric turbulence is predicated on his being able to perform the necessary flight control tasks, while being subjected to the dynamic environment imposed by the turbulence. The pilot must, of course, be able to survive the dynamic environment without physical injury. Studies have shown, however, that the excitation levels which would cause a degradation in the visual and motor performance of the pilot are substantially below those which would cause physical injury. The purpose of this section is to present the results of a literature survey on this subject; to establish goals for the maximum vibration levels which should be transmitted to the pilot, based on in-phase and equal vibration amplitudes of the subject's buttocks and his instrument panel; and to discuss the effects of sustained accelerations on the performance characteristics of seated human subjects.

Whole Body Vibration

Literature Survey: The majority of early research on human performance under whole body vibration was oriented towards determining subjective response characteristics. The test subject was normally instructed to describe the excitation as being perceptible, strongly noticeable, unpleasant, and so forth. Not until the past ten years have closely controlled visual and motor performance studies been conducted on seated subjects, while they were being subjected to various excitation amplitudes and frequencies of whole body vibration. The available data summarized herein, includes information on the tolerance and performance characteristics of seated human subjects exposed to vertical and transverse (left to right) vibration. Similar data is not presented for the longi-

tudinal (fore/aft) direction since pilots who have flown through turbulence have not indicated that fore/aft vibrations were a problem.

The Human Factors Unit of the Boeing Company has performed an extensive series of studies on both human tolerance to and performance under vertical sinusoidal vibration. The first of the series, as reported in Reference 1, investigated the tolerance levels of seated human subjects exposed to vertical sinusoidal vibration. The seat employed during the tests consisted of a standard aircraft pilot's seat with harness but reinforced with plywood inserts and covered with 3/4 inch of hard felt in place of the normal seat cushion, to insure the full transmission of the vibration to the subject. A heavy aircraft control wheel and column was installed in the normal operating position with respect to the seated test subject. The test subjects were required to hold down a fail-safe switch on the wheel, which was located under the fingers of the left hand. In addition to the wheel and column, the test structure was equipped with an instrument panel containing various switches, gauges, and lights typical of those employed in a cockpit. The entire structure was subjected to the vibration and the test room was finished in a light green to minimize visual clues as to the level of vibration. Figure 1 illustrates the average test results for nine subjects. The subjects were instructed to describe the vibration level as definitely perceptible, mildly annoying, extremely annoying, or alarming. The duration of the exposure to each of the vibration levels was relatively short, since the excitation level was increased until the subject indicated that the predescribed level had been reached, at which time the test was terminated. Also illustrated in Figure 1, for the purpose of comparison, is the one-minute tolerance level as reported in Reference 2.

Many other investigations have been conducted on the tolerance of seated human subjects to vertical vibration [Refs. 3

through 10], the results of which are in minor disagreement with References 1 and 2. The differences, which occur primarily in the frequency region from 1 to 5 Hz, appear to be due to variations in seat design, restraint conditions, experience and physique of the test subjects, and definitions of the various tolerance levels. Only the data reported on in References 1 and 2 have been selected for presentation in this report since, in the opinion of Barry Controls, it was obtained in an environment most closely simulating actual cockpit conditions.

Reference 11 discusses the results of a series of two-dimensional tracking performance tests conducted on a total of seven seated subjects by the Boeing Company. The excitation was vertical sinusoidal vibration and the test equipment and seat design were identical to that employed during the Reference 1 tolerance tests. Average error scores for wheel tracking and column tracking tests were obtained with and without vibration over a constant time interval. The error scores obtained without vibration served as the standard of reference. The subjects were also required to perform various tasks in addition to the primary tracking assignment; including the reading of four counters, manipulation of three toggle switches, the adjustment of four throttles, and the adjustment of four knobs, levers, and thumbwheels. These additional tasks in combination with the primary tracking assignment provided a realistic simulation of actual flight control problems. The amplitudes and frequency range of excitation corresponded to the definitely perceptible, mildly annoying, extremely annoying, and alarming levels reported in Reference 1, except that the annoying and alarming levels were omitted throughout the frequency range from 1.5 to 6 Hz, to avoid possible injury to the test subjects.

Figure 2 represents the results of these tests in terms of relative wheel tracking error as a function of the amplitude and frequency of vertical sinusoidal vibration. The relative tracking

error is defined as the ratio of the number of tracking errors with vibration, to that without. Figure 2 shows that there is a rapid increase in relative tracking error for combinations of excitation amplitude and frequency sufficient to cause a relative tracking error greater than 1.1. Since it is desirable to minimize the probability of pilot error due to vibration to less than 10 percent, the vertical vibration levels associated with a relative tracking error of 1.1 will be employed along with other performance criteria presented herein, when establishing the maximum sinusoidal accelerations which should be transmitted to commercial jet transport pilots during turbulence encounters.

The purpose of a series of tests conducted by C. S. Harris, et al., [Ref. 12] was to evaluate the relationship between two dimensional tracking error and excitation amplitude, for an excitation frequency of 5 Hz. The subject, while being exposed to various amplitudes of vertical sinusoidal vibration at 5 Hz, was required to perform both vertical and horizontal (left to right) tracking tasks with a stick type control. It was determined that increasing the peak sinusoidal acceleration levels above 0.2 g resulted in a significant increase in the errors associated with the vertical component of the tracking tasks. This finding agrees with the results of the Reference 11 tests illustrated in Figure 2. Contrary to the results of the Reference 11 tests, however, C. S. Harris, et al., did not observe a significant degredation in the horizontal component of the tracking tasks. This suggests that pilot tracking by wheel and column movements is more difficult than tracking by the horizontal (left to right) movement of a control stick, when he is subjected to vertical vibrations alone.

Another in the series of tests conducted by the Boeing Company [Ref. 13] evaluated the response time and ability of several subjects exposed to vertical sinusoidal vibration, to adjust various size control knobs to a predetermined setting. Some of the controls

required vertical adjustments while others required horizontal adjustment. Although this task differs from normal tracking tests, since locating the required setting is not a continuous operation, the results of these tests indicated that considerably more time was required to adjust the vertical moving controls than the horizontal moving controls, which confirms the finds of Reference 12. The study also found, as expected, that the time required to achieve the required setting and the offset error increased with the amplitude of vibration; however, the work load imposed upon the subject (number of settings required per unit time) was a more dominating factor. In addition, the final accuracy of adjustment was not a function of the direction of control motion.

R. Buckhout reported in Reference 14 on tracking tests performed during vertical vibration at excitation frequencies of 5, 7, and 11 Hz and peak acceleration values of 25, 30, and 35 percent of the one-minute tolerance criteria established by Magid, Coermann, and Ziegenruecker in Reference 2 (see Figure 1). The resulting data, which indicated tracking errors between 34 and 74 percent, corroborates the data presented in Figure 2. This report also discusses the fact that some individuals show a marked susceptibility to vertical vibration, while the others are not affected significantly; this phenomenon being observed even for experienced pilots.

Harris and Shoenberger reiterate in Reference 15 that the primary loss in tracking performance is due to excitation frequencies between 1 and 20 Hz, with the dominant effect occurring at the shoulder resonance between 4 and 6 Hz. Employing a collection of data from several investigators, a one-hour endurance curve was formulated for seated subjects exposed to vertical sinusoidal vibration. They employed an allowable percentage tracking error of 15 percent or an acceleration level at which significant increases in error resulted from slight increases in the amplitude of excitation, whichever was less, as criteria in obtaining the

endurance threshold. Figure 3 illustrates the results of their study. There is an adequate correlation between the data presented in Figures 2 and 3; and, as would be expected, the endurance curve is slightly less than that shown in Figure 2 for a relative tracking error of 1.15 which was obtained on a short term basis.

The evaluation of the effects of horizontal vibration on the performance of seated human subjects has not received the attention afforded to the vertical direction, since most aircraft and land vehicles do not generate significant amplitudes of vibration in these directions. Although some information does exist, the relative unimportance of horizontal vibration in the past has led to a general lack of performance data which can be compared and applied to commercial jet transports flying under turbulent conditions.

Bostrum Research Laboratories has conducted an evaluation of the effects of transverse (left to right) vibrations on both visual acuity and tracking tasks [Ref. 16]. Two series of tests, which employed a rigid seat, were performed. In the first series, the subjects were required to track a point on an oscilloscope screen by the turning of a wheel similar to the steering wheel of an automobile. In the second series, the subjects were required to track a meter representing a speedometer, by variations of foot pressure upon a floor pedal. Three levels of vibrations were tested: 0.15 g, 0.25 g, and 0.35 g. The vibration response curves illustrated in Figures 4 and 5 were generated from this report.

The Boeing Company has also performed tests on the effects of vertical sinusoidal vibration on the visual performance of seated subjects [Ref. 17]. The subjects were seated in the simulated cockpit described previously and subjected to vertical sinusoidal vibrations corresponding to the definitely perceptible, mildly annoying, extremely annoying, and alarming levels illustrated in

Figure 1. The subjects were commanded by means of amber colored signal lights to read one of five, five-digit counters. The five counters had different numeral heights ranging from 0.05 inches to 0.2 inches and visual angles ranging from 6 to 24 arc minutes. The light level of the counters in the plane of the panel was about 32 foot-candles and the average viewing distance was 28 inches. Figure 6, which illustrates average constant percentage (average of visual angles tested) visual tracking error as a function of the amplitude and frequency of vibration, was computed from the test data provided in Reference 17. Harris and Shoenberger also employed in Reference 15, which was discussed earlier, a collection of data from several sources to relate the effects of vertical sinusoidal vibration on the visual acuity of seated human subjects. The results of the study, which established maximum and minimum thresholds of vibration that will cause a significant reduction in visual acuity, are in general agreement with the data illustrated in Figure 6.

Summary: Many analytical and experimental studies have been conducted on the dynamic analog of the human body, with varying degrees of complexity. Some of these studies are described in References 2, and 18 through 22. Although these data do not provide quantitative information on the tracking and visual acuity thresholds, they do indicate the excitation frequencies for which the human body is particularly sensitive to vibration. Consequently, a certain confidence level can be derived by comparing this information to that previously presented.

A vertical dynamic model of the human body developed by Coermann [Ref. 22] consisted of seven masses representing the lower leg, upper leg, hips, right and left thorax-abdomen, upper torso, and head. These various masses were interconnected by linear springs and viscous dampers. It was determined that the principal vertical resonant frequencies are: the resonance of the entire torso upon the lower spine and pelvis, in the frequency

range from 4 to 6 Hz; the resonance of the upper torso which involves the movements of the upper vertebral column, in the frequency range from 10 to 15 Hz; and the head/shoulder resonance which normally occurs in the frequency range from 20 to 30 Hz.

Figure 7 illustrates average test data on the vertical transmissibilities of various parts of the human body relative to the seat, and between parts of the body, as a function of frequency [Refs. 23 and 24]. Resonances are again indicated in the frequency regions from 4 to 6 Hz, 10 to 15 Hz, and 20 to 30 Hz. However, it appears that the head/shoulder resonance in the region from 10 to 15 Hz would have a small effect on the performance of seated subjects in relation to the effects the shoulder/seat and head/shoulder resonances. The head/shoulder resonance between 20 and 30 Hz is of importance in connection with the deterioration of visual acuity under vibration. Examination of the tolerance and performance threshold levels illustrated in Figures 1 through 6 indicates that seated subjects are indeed primarily affected by excitation in the frequency region from 4 to 6 Hz and 20 to 30 Hz and that the head/seat resonance in the frequency region from 10 to 15 Hz is a less significant factor.

Based upon this verification and the others previously presented, it is concluded that there is sufficient justification to employ a composite of Figures 2 and 6 as guides in establishing a design goal for the maximum vertical vibration levels, and a composite of Figures 4 and 5 as guides in establishing a design goal for the maximum transverse vibration levels, which should be transmitted to the pilots of commercial jet transports.

The vertical vibration threshold for 10 percent wheel tracking error illustrated in Figure 2 and the vertical threshold for 10 percent visual tracking error illustrated in Figure 6 have been superimposed in Figure 8. Also included is: discrete frequency data given in References 25 and 26 on the effects of vertical vibration on the error thresholds of visual, tracking, and foot

pressure tasks; the 10-minute fatigue-decreased proficiency level recommended in Reference 27; the 20-minute motion sickness threshold from Reference 28; and the mildly annoying level shown in Figure 1. The 10-minute fatigue-decreased proficiency level recommended in Reference 27 was included to provide a guide as to the maximum vertical vibration levels which should be transmitted to the pilots of commercial jet transports, for excitation frequencies greater than 30 Hz. The author of Reference 27 states that when this criteria (which was derived from studies on aircraft pilots and vehicle operators) is exceeded, noticeable fatigue and decreased job proficiency will result in most tasks. Motion sickness is the most critical factor effecting pilot performance under very low-frequency vertical oscillations [Refs. 28 and 29]. Data point (6) indicated in Figure 8 represents the peak acceleration level which produced motion sickness in 53 percent of a group of naval officers in 20 minutes.

The design goal for the maximum vertical sinusoidal vibration levels which should be transmitted to commercial jet transport pilots, illustrated in Figure 8, has been selected using a composite of the previously discussed data as a guide. The mildly annoying tolerance level [Ref. 1] has also been illustrated in Figure 8 to indicate that the design goal is in fact determined by pilot performance criteria (visual, tracking, etc.) and not tolerance criteria, as stated in the introduction to this section.

The transverse vibration threshold for 10 percent wheel tracking error illustrated in Figure 4, and the transverse vibration threshold for 10 percent foot tracking error illustrated in Figure 5, have been superimposed in Figure 9. Also included in the 10-minute fatigue-decreased proficiency level recommended in Reference 27. Obviously, the indicated data is insufficient in the frequency ranges from 0.2 to 1 Hz and 6 to 30 Hz, to make a firm selection of a design goal. Consequently, as a first approximation only, the design goal for the vertical direction has also been applied to the transverse direction.

Figures 8 and 9 illustrate the design goals for the maximum vertical and transverse sinusoidal acceleration levels which should be transmitted to a commercial pilot. The actual dynamic environment encountered during turbulence is a combination of broad and narrow-band random excitation in which the narrow-band excitations are dominant. It has been necessary to present data on the effects of sinusoidal rather than random vibration on pilot performance since there have been no extensive investigations into the latter. The authors of References 21, 30, and 31 have, however, performed sufficient investigations to conclude that sinusoidal and narrow-band random vibration equated on the basis of rms levels result in similar degradations in the performance of seated human subjects. This criteria, which has been verified over the frequency range from 0.75 to 30 Hz, applies to vibration excitations beneath the high stress level (beneath the Extremely Annoying Level defined in Figure 1), as in this case. Consequently, the design goals for the maximum rms vertical and transverse narrow-band random accelerations which should be transmitted to commercial jet transport pilots will be taken as 0.707 times the design goals illustrated in Figures 8 and 9.

Sustained Accelerations

Research [Refs. 32 through 37] on the effects of rapidly applied and sustained accelerations has been primarily oriented toward three fields of study: (1) impact accelerations caused by crash landings, falls, etc; (2) extremely short rise time accelerations with high peak magnitudes of the type encountered during ejection from a jet aircraft; and (3) long duration sustained accelerations with relatively low onset rates of the type encountered during rocket launch and reentry into the atmosphere. The evaluation criteria in the first two cases are concerned only with the ability of the subject to survive, since performance tasks are not generally required under these conditions; while performance criteria are a consideration in the third case. The jet upset

problem is concerned, however, with the necessity for pilot performance under the conditions of multiple acceleration pulses of short rise times and relatively low magnitudes, which places the required data somewhat between the extremes of the three previously mentioned fields of study. Based on actual jet upset conditions, of greatest interest is the effect upon pilot performance of short rise time (0.2 to 2 sec) accelerations in the vertical direction (i.e., perpendicular to the plane of the aircraft) having peak magnitudes ranging from -2.5 g to + 2.5 g.

The major effects of both the level of sustained acceleration and the rate of onset of the acceleration are lowering of the blood pressure at head level, reduction of vision, and increase in the muscular exertion required to perform a required task. The effect of decreasing the onset time is to shorten the conscious period of the pilot. Based upon an investigation of available literature, however, there is no known basis for establishing the allowable onset rate of repeated acceleration pulses which should be transmitted to the pilots of commercial jet transports. Consequently, it can only be said that as a design goal the pilot seat isolation system should decrease the onset rate of the sustained acceleration such that the conscious period of the pilot is maximized (consideration of allowable sway space must also be included). The isolation system cannot, of course, lower the magnitude of the sustained acceleration. Thus, it is of paramount importance for the pilot to exercise muscular actions during sustained accelerations which will help maintain the blood pressure at head level and prevent or at least prolong the time to blackout.

SECTION 3: DYNAMIC ENVIRONMENT EXISTING ON COMMERCIAL JET TRANSPORTS DURING TURBULENT AIR PENETRATION

The purpose of this section is to present available data on the dynamic environment existing at the pilot station on present and future generation jet transport aircraft during turbulent flight. A comparison can then be made between the desired input to the pilot established in Section 2 with the amplitude of aircraft excitation, in order to determine the desired transmissibility of the pilot seat isolation system as a function of frequency. The overall spectrum of motion transmitted to the pilot is a function of the dynamic response of the aircraft to: (1) atmospheric turbulence; (2) buffeting resulting from unsteady aerodynamic flow conditions; and (3) its internal mechanical components (i.e., engines, compressors, etc.).

Figure 10 illustrates the envelope of the maximum equivalent sinusoidal vibrations measured in the transverse (i.e., left to right) and normal (i.e., perpendicular to the plane of the aircraft) directions on a KC-135 [Ref. 37] which is the military version of Boeing 707 and on a turboprop aircraft [Ref. 38] during all normal flight conditions such as cruise and maneuvers (i.e., except for "rough air"). Since both of these curves represent envelopes of dominant vibrations, they are probably more severe than actual at many excitation frequencies. Nevertheless, they can be applied as the worst case environment imposed on commercial jet transport pilots during normal flight conditions, at excitation frequencies greater than 5 Hz.

Aircraft buffet loads depend on many factors such as the aircraft configuration, Mach number, gross weight, altitude, and normal acceleration. Buffeting of an aircraft in a deep stall can result in peak accelerations approaching 1 g at excitation frequencies of approximately 1 Hz. Buffeting also excites the fundamental fuselage bending mode of the aircraft which is

normally close to the fundamental resonance of the human body at 4 Hz [Refs. 40-42]. The peak accelerations which occur in the cockpit during a heavy buffet condition, are well in excess of the levels under which the pilot can maintain control over the aircraft and clearly see the critical flight control instruments. Figure 11 illustrates a typical time history of the normal CG acceleration of a jet transport aircraft undergoing heavy buffet conditions during uncontrolled flight resulting from an upset in severe turbulence. The data was obtained from the crash flight recorders of the aircraft as reported in Reference 43. The flight recorder data does not show the high frequency accelerations which result from the fuselage bending modes and high frequency gust excitations.

The composite spectrum of aircraft excitations during turbulent air penetration is primarily a function of the response of its rigid body and flexible bending modes. The rigid body pitch and roll rotational resonant frequencies of commercial jet transports normally occur in the frequency range from 0.15 to 0.4 Hz. The excitation of the fuselage bending modes of the aircraft can result in large amplitude normal and transverse accelerations in the frequency range from 2 to 6 Hz, depending upon the type of aircraft and the flight conditions. This frequency range of excitations is of particular importance since it is in this range that the human body is most sensitive to mechanical vibration.

Figures 12 and 13 illustrate the power spectral densities of the normal (i.e., vertical) and transverse vibrations which would be experienced at the pilot's cabin of a representative present-day (subsonic) commercial jet transport, during turbulent flight. Figures 12 and 13 were obtained by multiplying the power spectral density data given in Reference 44 by a factor of 2.5 to take into account the ratio of the maximum rms gust velocity known to exist in thunderstorms (i.e., 20 ft/sec), to that present during the Reference 44 tests. Figures 14 and 15 illustrate the power

spectral densities of the normal and transverse vibrations measured in the pilot's cabin of a large supersonic aircraft during a penetration of clear air turbulence at 55,000 feet [Ref. 45]. The speed of the aircraft was mach 2.4. Unfortunately, the data provided by Reference 45 is not low enough in frequency for determination of the response of the longitudinal stability modes of the supersonic aircraft. However, it can be readily seen from a comparison of Figure 12 with Figure 14 and Figure 13 with Figure 15, that the spectral density of the vibrations expected at the pilot's cabin in present day subsonic jet transports is the determining factor in establishing the degree of isolation required by the pilot seat isolation system.

Table I summarizes the dominant response characteristics predicted at the pilot station for the representative subsonic commercial jet transport during turbulent flight. The average frequencies of the normal vibrations due to the rigid body aircraft resonance at 0.35 Hz and the fuselage bending mode resonance at 4.7 Hz, as well as the transverse vibrations due to the rigid body resonance, are well defined. There are several aircraft resonances which occur in the transverse direction over the frequency range from 3.7 to 7.2 Hz. However, they tend to form a single or composite narrow-band resonance with an average frequency of 5.5 Hz. The rms value of the excitation in this composite band has been taken equal to the square root of the sum of the mean square values of the excitation in each of the individual bands.

SECTION 4: DESIGN GOALS FOR PERFORMANCE OF PILOT SEAT ISOLATION SYSTEM

Introduction

Design goals for the maximum sinusoidal and random vibration levels that should be allowed to be transmitted to the pilot of commercial jet transports in the normal and transverse directions were established in Section 2. In Section 3, the available data on the equivalent sinusoidal and random vibration levels which can be expected at the base of the pilot's seat during various flight conditions were presented. The purpose of this section is to compare the excitation and desired response spectrums, and to determine the necessary performance characteristics of the pilot seat vibration isolation system.

Isolation System Performance

Consider first the aircraft response to turbulence in the lateral and longitudinal rigid body stability modes. As summarized in Table I, the worst-case rigid body response occurs in the normal direction with an rms acceleration of 0.28 g at a statistical average frequency of 0.35 Hz. This is less than the design goal of a maximum acceleration of 0.4 g which should be transmitted to the pilot at this frequency (see Figure 8). Thus, vibration isolation of the rigid body modes of the aircraft is not required. It should be noted, however, that the rms displacement associated with the rms acceleration of 0.28 g at 0.35 Hz is nominally 23 inches or a 3 sigma value of 69 inches. Since the input at 0.35 Hz is continuous with time, the isolation system must be designed such that it does not bottom due to the relative deflections caused by this input. Bottoming would result in a degradation of the high frequency isolation and undesirable shock inputs.

Consider secondly the degree of vibration isolation required in the normal and transverse directions above 3 Hz. The dashed curve illustrated in Figure 16 indicates the degree of isolation required in the normal direction necessary to reduce the rms acceleration transmitted to the pilot to 0.07 g in the frequency band from 3.5 to 5.5 Hz. This performance requirement is in general agreement with the conceptual recommendations made in References 46 and 47. Vibration isolation is not required in the transverse direction over the frequency range from 3.7 to 7.2 Hz since the rms acceleration input due to the flexible bending modes of the aircraft is less than the maximum allowable input to the pilot of 0.07 g rms. The degree of isolation required in the normal and transverse directions above 6 Hz, as illustrated in Figure 16, was obtained by computing the ratio (as a function of frequency) of the maximum sinusoidal vibration levels which should be transmitted to the pilot to the vibration levels experienced in turboprop aircraft during cruise conditions (Figure 10).

Consider next the peak aircraft response due to buffeting which is 0.9 g at nominally 1.3 Hz, as estimated from Figure 11. Buffeting, which primarily results in increased vibrations of the aircraft in the vertical direction, is an abnormal condition. Also, since buffeting provides the pilot with a "seat-of-the-pants" aircraft stall alarm, it is probably undesirable to provide vibration isolation at the buffeting frequency. However, in an attempt to provide the pilot with every possible advantage during buffeting, it is concluded that as a design goal, isolation at the fundamental fuselage bending mode of the aircraft (nominally 4.5 Hz) should not be appreciably degraded due to the high input displacement levels encountered under severe buffeting conditions. In any event, the absolute displacement transmissibility of the isolation system at 4.5 Hz should not exceed unity in the vertical direction during buffet conditions.

Based on discussions with jet transport pilots, it was concluded that the steady-state relative deflections between the pilot and the aircraft structure, due to the resilience of the isolation system, should not exceed ± 1 inch and the relative deflections due to any abnormal or transient conditions should be maintained less than ± 2 inches. The isolation system cannot lower the magnitude of the sustained accelerations which are transmitted to the pilot during jet upset. It must, however, be able to generate sufficient reaction forces to return and maintain the pilot seat at its mean position as soon as possible after the onset of the acceleration and thus provide its full linear range for vibration isolation. Based on Reference 43 (worst case of available data), the pilot seat must be designed to provide steady-state vibration isolation while support its payload under vertical sustained acceleration conditions of ± 3 g. In addition, the vertical performance of the isolation system must be essentially independent of variations in pilot weight as well as reactions induced by the pilot.

Consequently, it is concluded that in the vertical direction, active (electrohydraulic) vibration isolation is required at the fundamental flexural bending mode of the aircraft at nominally 4.5 Hz and above 8 Hz, as specified in Figure 16. Active isolation is not required in the horizontal direction since the passive isolation provided by conventional aircraft pilot seats in the horizontal plane is sufficient to meet the requirements of Figure 16 above 8 Hz.

Finally, it was concluded from discussions with NASA, that it would be desirable for the active portion of the pilot seat isolation system to have two modes of operation. In one mode, the pilot seat would provide the required isolation at the fundamental fuselage frequency of the aircraft as well as at the high frequencies. In the second mode, the system would only provide high frequency

vibration isolation. With this capability, the effects of the added isolation at nominally 4.5 Hz on pilot performance could be determined during landing and takeoff conditions as well as other maneuvers.

SECTION 5: THEORETICAL ANALYSIS OF ELECTROHYDRAULIC VIBRATION ISOLATION

General Principles

The prime objectives of an active electrohydraulic vibration isolation system are to exhibit the characteristics of a very stiff system for DC excitations (static conditions and sustained acceleration), the isolation characteristics associated with a low resonant frequency vibration isolation system, as well as to return the isolated mass to its neutral position following the onset of sustained accelerations and to eliminate the large static deflections associated with low resonant frequency isolation systems. The operation of such a system is based on sensing the dynamic response of the isolated body and/or the source of excitation, and employing automatic feedback control techniques to control an actuator which produces relative motions to oppose and cancel the accelerations of the source of excitation.

Figure 17 illustrates schematically an electrohydraulic vibration isolation system with acceleration feedback and a flexible coupling located outside the loop. The associated signal flow diagram is illustrated in Figure 18. In the case of a pilot seat isolation system, the intermediate mass would be representative of the seat structure, the secondary passive isolator of the seat cushion, and the payload mass would represent the subject. The basic components of the active isolation system are the feedback transducers, a servoamplifier and servovalve, and the hydraulic actuator. Signals from the acceleration and relative position transducers are modified, summed, and compensated in the servoamplifier which delivers an error signal to the servovalve. Flow from a fluid power source is supplied to the actuator according to the signal delivered to the servovalve. Forces are thus generated by the actuator proportional to the differential

pressure across the piston, to limit the vibrations experienced by the mass and null the relative displacement between the mass and the source of excitation.

The dynamic range of a closed loop electrohydraulic vibration isolation system is nominally less than 40 Hz. Therefore, the purpose of the secondary passive isolator (i.e., seat cushion in the case of the pilot seat) is to provide the desired high frequency isolation. The purpose of the flexible coupling is to decouple the intermediate mass from the hydraulic actuator above nominally 100 Hz, therefore, maximizing the actuator resonant frequency and the stability of the servo system. If it was necessary for the active isolation system which is inserted between the support structure and payload to provide high frequency broad-band isolation (i.e., there was no secondary passive isolator), then the accelerometer would have to be located on the payload. This latter technique is described more fully in References 48 through 50.

The following simplified example will serve to demonstrate the theory and advantages of electrohydraulic vibration isolation. Consider the case of an infinitely stiff secondary passive isolator. The equations of motion of the resulting single-degree-of-freedom system can be derived by equating the flow into the actuator chamber to the flow delivered by the servovalve. Assuming zero leakage across the actuator piston, the flow from the servovalve Q can be expressed in Laplace notation by [Refs. 51 and 52]

$$Q(s) = -As\,[r(s) - w(s)] - \frac{V}{2\beta_f}\,s\,[\Delta P(s)] \qquad (1)$$

where A is the average actuator cross-sectional area, r is the displacement of the actuator rod, w is the displacement of the support structure, V is the mean volume of the upper and lower actuator chambers, β_f is the bulk modulus of the hydraulic fluid, and ΔP is the differential pressure across the actuator. Assuming that the mass of the piston is negligible with respect to that

of the isolated body, the equation of motion of the isolated mass is given by

$$ms^2z(s) = - csz(s) - k[z(s)-r(s)] = A[\Delta P(s)] \tag{2}$$

where c is the absolute velocity damping constant of the isolator and k is the stiffness of the coupling. The coupling will normally be fabricated from an elastomeric material and it has been found from experience that the relation expressed by Equation (2) models its absolute isolation characteristics more closely than the assumption of relative velocity damping.

Combining Equations (1) and (2) yields

$$\left[1 + \frac{kV}{2A^2\beta_f}\right] ms^2z(s) + csz(s) + k\delta(s) + \frac{k}{As} Q(s) = 0 \tag{3}$$

where

$$\delta(s) = z(s)-w(s) \tag{4}$$

Since the hydraulic fluid is virtually imcompressible (i.e., $\beta_f >> kV/2A^2$) it follows that

$$ms^2z(s) + csz(s) + k\delta(s) + \frac{k}{As} Q(s) = 0 \tag{5}$$

Assume that the resonant frequency of the servovalve is well above the frequency range of interest and let the net flow from the cylinder be given by

$$Q = C_1\ddot{r} + C_2[\dot{r}-\dot{w}] + C_3[r-w] \tag{6}$$

In Laplace notation

$$Q(s) = C_1 s^2 r(s) + C_2 s[r(s)-w(s)] + C_3[r(s)-w(s)] \qquad (7)$$

where C_1, C_2, and C_3 are constants representing acceleration, relative velocity (obtained by differentiating signal from relative displacement transducer), and relative displacement gains respectively. The relative magnitude of each of these feedback signals can be manipulated to minimize the response of the isolated body due to the excitation imposed by the support structure.

Combining Equations (2), (3), and (7) and solving for the absolute displacement transfer function

$$\frac{z(s)}{w(s)} = \frac{\left[\frac{C_2+A}{C_1}\right]s + \frac{C_3}{C_1}}{s^2 + \left[\frac{C_2+A}{C_1}\right]s + \frac{C_3}{C_1} + \left\{\frac{s(ms+c)}{k}\left[s^2 + \frac{(C_2+A)s}{C_1} + \frac{C_3}{C_1}\right]\right\}} \qquad (8)$$

Due to the high values of the acceleration feedback C_1 and the coupling stiffness k (the coupling-isolated mass resonance is normally greater than 20 Hz), for excitation frequencies less than 10 Hz the fourth term in the denominator of Equation (8) can be considered small relative to the remainder of the terms in the denominator. Consequently, for frequencies less than 10 Hz

$$\frac{z(s)}{w(s)} = \frac{s\left[\frac{C_2+A}{C_1}\right] + \frac{C_3}{C_1}}{s^2 + s\left[\frac{C_2+A}{C_1}\right] + \frac{C_3}{C_1}} \qquad (9)$$

Notice that Equation (9) is identical in form to the expression for the absolute displacement transmissibility (in Laplace Transform notation) of a conventional passive isolation

system defined by resonant frequency ω_n and damping ratio ζ where

$$\omega_n = \sqrt{\frac{C_3}{C_1}} \tag{10}$$

$$\zeta = \frac{1}{2} \frac{C_2+A}{\sqrt{C_1 C_3}} \tag{11}$$

Thus, it is possible to establish the resonant frequency and transmissibility characteristics of the isolation system in the low frequency region simply by electronically adjusting the relation between the feedback parameter gains C_1, C_2, and C_3. The relative displacement feedback gain C_3 can also be made a nonlinear function of relative deflection to provide a near linear stiffness about the null position for vibration isolation and a rapidly increasing but continuous hardening stiffness for limiting relative deflections due to shock excitations without bottoming. The isolation system will act as a stiffer system, however, only for a very short period of time due to the displacement feedback restoring forces which will rapidly return the isolated body to its initial position following transient excitations. In addition, the relative displacement feedback allows the static position of the isolated body to be nulled at a preselected equilibrium position [Refs. 50 and 53].

However, since $z(s)/w(s)$ has the same form as that for a passive isolation system, the relative displacement between the initial and final position of the mass will be g/ω_n^2 for each g of sustained acceleration input, which is contrary to the goals established for an active isolation system in the beginning of this section. The explanation for this is based on the assumption up to this point that C_1, C_2, and C_3 are independent of the

excitation frequency. Therefore, under static or sustained acceleration conditions with no oscillatory motion, in order to maintain zero relative velocity between the isolated mass and the actuator, the relative displacement feedback signal must cancel the acceleration feedback signal of the isolated mass so that there will be no net feedback. To counter this effect and null the relative deflection during sustained acceleration conditions, it is necessary to add a network to the acceleration feedback signal so that it will decrease to zero when the frequency of oscillation is zero.

Also, it should be noted that Equation (9) is unconditionally stable. That is, the active control system is stable for any attainable combination of positive values for parameters C_1, C_2, and C_3 when they are independent of the frequency of excitation. Introducing networks similar to that described above will introduce the possibility of instability and the variation in the feedback gains will become limited.

Notice also that at low frequencies, Equation (9) is independent of the weight of the isolated body and any forces F imposed on it (Figure 17). Consequently, due to the feedback characteristics of the motion sensors, the maximum force sensitivity of the system is governed by the stiffness of the flexible coupling, which is normally many times stiffer than the effective stiffness associated with the electronically created resonant frequency. This approaches the ideal situation for the case in which an electrohydraulic isolation system is employed in the isolation of a payload which generates reaction forces, such as in the case of a pilot operating the aircraft controls.

An electrohydraulic isolation system which functions according to a relation similar to Equation (9) is termed a broad-band isolation system. It is also possible to provide a very high degree of vibration isolation in a narrow-band centered about a

discrete frequency (termed a notch type isolation system) by incorporating a frequency response shaping network having an undamped resonance in the acceleration feedforward loop. One such network is a second order resonance defined by the transfer function [Ref. 54]

$$\frac{\omega_1^2}{s^2 + \omega_1^2} \tag{12}$$

This network provides an infinite dynamic feedforward gain in the acceleration loop at the frequency $\omega = \omega_1$, thereby resulting in an absolute transmissibility of zero, as will be demonstrated by the following equations. Modifying Equation (7) to include the second order notch network

$$Q(s) = C_1 s^2 \left[\frac{\omega_1^2}{s^2+\omega_1^2}\right] r(s) + C_2 s[r(s)-w(s)] + C_3[r(s)-w(s)] \tag{13}$$

Combining Equations (2), (3), and (13), solving for the absolute displacement transmissibility, and then simplifying the expression for excitation frequencies less than 10 Hz

$$\frac{z(s)}{w(s)} = \frac{s[C_2+A] + C_3}{\frac{C_1\omega_1^2}{s^2+\omega_1^2} + s[C_2+A] + C_3} \tag{14}$$

Substitution of $s = j\omega_1$ into Equation (14) indicates that the absolute displacement transmissibility equals zero at the notch resonant frequency. The absolute displacement transmissibility associated with a typical notch type electrohydraulic vibration isolation system is illustrated in Figure 19. Examination of Equation (14) also shows (as illustrated in Figure 19) that this idealized notch isolation system does not provide vibration

isolation for frequencies greater than twice the notch frequency. It is necessary, therefore, to combine the functions of Equations (9) and (14) if a combination of broad-band plus notch type isolation is required.

Application of Broad-Band Electrohydraulic Isolation to the Pilot Seat Problem

Consider an electrohydraulic vibration isolation system with the net flow from the cylinder defined by the relation (Figure 17)

$$Q(s) = C_1 G_1(s) s^2 r(s) + [C_2 G_2(s) s + C_3]\, G_3(s)[r(s)-w(s)] \qquad (15)$$

where

$$G_1(s) = \frac{\tau_1 s}{1 + \tau_1 s} \qquad (16)$$

$G_2(s)$ and $G_3(s)$ are the relative velocity and relative deflection feedback networks, respectively. The acceleration feedback networks $G_1(s)$ reduces the acceleration feedback signal to zero, at zero excitation frequency, thus allowing the displacement feedback control system to null the static deflection (as discussed in the previous sub-section). Decreasing the time constant τ_1 has three effects. First, it tightens the relative displacement feedback loop by lowering the acceleration gain with decreasing frequency. Second, it increases the resonant frequency of the isolation system and third, it decreases the system stability margin which results in a higher resonant transmissibility.

For a coupling-mass resonant frequency greater than 20 Hz, a rigid payload, and for excitation frequencies less than 10 Hz, then

$$\frac{z(s)}{w(s)} = \frac{s + \left[\frac{C_2}{A} G_2(s) s + \frac{C_3}{A}\right] G_3(s)}{\frac{C_1}{A}\,\frac{\tau_1 s^3}{(1+\tau_1 s)} + s + \left[\frac{C_2}{A} s G_2(s) + \frac{C_3}{A}\right] G_3(s)} \qquad (17)$$

and

$$\frac{\delta(s)}{w(s)} = - \frac{\frac{C_1}{A} \frac{\tau_1 s^3}{(1+\tau_1 s)}}{\frac{C_1}{A} \frac{\tau_1 s^3}{(1+\tau_1 s)} + s + \left[\frac{C_2}{A} sG_2(s) + \frac{C_3}{A}\right] G_3(s)} \tag{18}$$

The absolute displacement transmissibility of the isolation system is given by

$$T_A = \left| \mathcal{L}^{-1} \left\{ \frac{z(s)}{w(s)} \right\} \right| = \left| \frac{z_o}{w_o} \right| \tag{19}$$

where w_o represents the amplitude of the sinusoidal base excitation and z_o is the amplitude of the response of the isolated mass. The relative displacement transmissibility of the isolation system is given by

$$T_R = \left| \mathcal{L}^{-1} \left\{ \frac{\delta(s)}{w(s)} \right\} \right| = \left| \frac{\delta_o}{w_o} \right| = \left| \frac{z_o - w_o}{w_o} \right| \tag{20}$$

Figure 20 illustrates the absolute displacement and relative displacement transmissibilities for a 2.5 Hz resonant frequency electrohydraulic broad-band vibration isolation system. The open loop transfer function of the isolation system has been checked to insure that the values of the selected parameters result in a stable control system. The relative displacement transmissibility peaks at a slightly higher frequency than the absolute displacement transmissibility, which is characteristic of this type of control system. Substantially lower resonant frequencies (i.e., 0.1 Hz) are achievable with electrohydraulic vibration isolation systems. As will be demonstrated, however, the displacement inputs

associated with the aircraft rigid body pitch resonant frequency and buffeting negates their application in this instance.

If the resonant frequency of the isolation system was located below 1 Hz, say 0.5 Hz, then the relative displacement transmissibility would be essentially 1 at 0.35 Hz. Referring to Table I, the rms vertical acceleration of the typical jet transport aircraft is 0.28 g at this frequency. Since the rms aircraft displacement associated with the rms acceleration of 0.28 g is 23 inches (3 sigma level of 69 inches), this means that the isolation system would be in its nonlinear control region the majority of the time and very little high frequency isolation would be provided.

A 0.5 Hz resonant frequency isolation system could provide isolation at 1.3 Hz (which is not stipulated by the isolation system performance requirements derived in Section 4) if there was a negligible input at 0.35 Hz. However, an increasing input at the buffeting frequency would force the isolation system into its nonlinear range, thus raising the resonant frequency and further amplifying the excitation and associated relative deflections.

A 2.5 Hz resonant frequency isolation system was selected for evaluation since it falls in the frequency region of minimum effect on the performance capabilities of a human subject, as can be seen from Figure 8, and since it also falls in the region of minimum excitation for typical subsonic aircraft (refer to Figure 12). The peak expected relative deflection of an active system with isolation characteristics as illustrated in Figure 20 is obtained by multiplying the rms relative displacement of 0.38 inches computed for the frequency range of 0.2 to 7 Hz by a factor of 3 to arrive at the 3 sigma level, and then adding 0.04 inches which is an estimate of the relative deflection due to the aircraft excitations above 7 Hz (Figure 10), for a total of ± 1.18 inches. The rms relative deflection for excitation frequencies between

0.2 and 7 Hz was computed from the expression

$$\delta_{rms} = \sqrt{\int_{0.2(2\pi)}^{7(2\pi)} S_{\ddot{w}}(\omega) \left[\omega^2 T_R\right]^2 \, d\omega} \qquad (21)$$

where $S_{\ddot{w}}(\omega)$ is the power spectral density of the vertical vibrations given by Figure 12.

In addition to the fact that the steady-state relative deflection is greater than the design goal of ± 1 inch established in Section 4, only 30 percent isolation is provided at 4.5 Hz rather than the minimum required value of 70 percent isolation (see Figure 16). Also, the acceleration input to the pilot at 2.5 Hz due to the resonance of the isolation system is 0.15 g rms. Although the pilot could probably tolerate greater excitations at 2.5 Hz than the 0.07 g rms design goal, it is felt that the 0.15 g rms level is excessively greater than the design goal.

During the analytical phase of the program, various types of feedback functions were investigated for $G_1(s)$, $G_2(s)$, and $G_3(s)$. However, it was not possible to optimize the isolation performance of the broad-band isolation system any further than the characteristics illustrated in Figure 20. Therefore, it was concluded that a broad-band electrohydraulic vibration isolation system is not capable of providing a complete solution to the problem of isolating commercial jet transport pilots during turbulence encounters.

Application of Broad-Band Plus Notch Electrohydraulic Isolation to the Pilot Seat Problem

Since it was concluded that broad-band isolation alone could not solve the problem of isolating commercial jet transports during severe turbulence, consideration was then given to use of circuits which detect discrete excitation frequencies and apply high isolation notches at these frequencies, in conjunction with the broad-band isolation. In this case, a single high-isolation notch would be required at the first fuselage bending-mode frequency of the aircraft (i.e., 4.5 Hz).

The most advantageous approach for providing this type of performance, for this application, is employing a notch network similar to that described in the "General Principles" sub-section in conjunction with a second accelerometer sensing the input acceleration which will provide the broad-band isolation. A schematic diagram of this sytem is illustrated in Figure 21 for the case of a rigid payload and no flexible coupling. This simplified example will serve to demonstrate the applicability of the approach.

The servovalve flow equation will be defined in this case by

$$Q(s) = C_1 G_1(s) s^2 w(s) + [C_2 s G_2(s) + C_3]\delta(s) + \frac{C_4 \omega_1^2}{s^2+\omega_1^2} s^2 G_4(s) z(s) \tag{22}$$

where

$$G_1(s) = \frac{\tau_1 s}{1+\tau_1 s} \tag{23}$$

$$G_2(s) = \frac{1}{1+\tau_2 s} \tag{24}$$

$$G_4(s) = \frac{\tau_4 s}{1+\tau_4 s} \tag{25}$$

Combining Equations (1), (2), and (22) and neglecting the compressibility term yields

$$\frac{z(s)}{w(s)} = \frac{s + \frac{C_2}{A}\, s\, G_2(s) + \frac{C_3}{A} - \left(\frac{C_1}{A}\right) G_1(s) s^2}{\left(\frac{C_4}{A}\right) G_4(s)\, \frac{^2\omega_1{}^2}{s^2+\omega_1{}^2} + \frac{C_2}{A}\, s\, G_2(s) + s + \frac{C_3}{A}} \tag{26}$$

$$\frac{\delta(s)}{w(s)} = -\frac{\left(\frac{C_1}{A}\right) G_1(s) s + \left(\frac{C_4}{A}\right) G_4(s)\, \frac{s^2\omega_1{}^2}{s^2+\omega_1{}^2}}{\left(\frac{C_4}{A}\right) G_4(s)\, \frac{s^2\omega_1{}^2}{s^2+\omega_1{}^2} + \frac{C_2}{A}\, s\, G_2(s) + s + \frac{C_3}{A}} \tag{27}$$

Figure 22 illustrates the absolute displacement and relative displacement transmissibilities for a 2.5 Hz resonant frequency broad-band plus notch system as computed from Equations (26) and (27). In addition to the fact that this scheme provides the desired isolation characteristics, the resonant transmissibilities are lower than those for the broad-band isolation system alone (Figure 20). Also, the relative displacement transmissibility is 1 at 4.5 Hz rather than 1.4 as for the broad-band system, since 100 percent isolation is provided at the notch frequency. The peak expected relative deflection of this idealized system due to the dynamic environments defined in Figure 12 is 0.91 inches which was computed in the same manner as for the broad-band system discussed in the previous sub-section. The acceleration input to the pilot at 2.5 Hz due to the resonance of the isolation system is 0.1 g rms. This is slightly greater than the design goal of 0.07 g rms. However, it is in a frequency region of minimum effect on human performance and therefore considered acceptable.

Stiffening of this type of isolation system beyond its linear range can be readily achieved by decreasing the broad-band and notch acceleration feedback gains as an inverse function of the relative displacement feedback voltage. Decreasing the broad-band and notch acceleration gains increases the phase and gain margin of the control system thus making it more stable as it goes into its nonlinear range. Figure 23 illustrates the isolation characteristics which could be expected for small relative deflections (less than ± 0.1 inch) about a mean relative deflection (for example 1.5 inches) in the nonlinear range of the broad-band plus notch isolation system. The isolation characteristics of the broad-band plus notch system, with relative deflections in the order of ± 2 inches, would be intermediate between those of Figures 22 and 23. Note from Figure 23 that the relative displacement transmissibility is 0.1 at 1.3 Hz (i.e., buffeting frequency described in Section 3). Consequently, the isolation system will not hard bottom with the 6 inch amplitude input at 1.3 Hz when combined with the other sources of excitation. Although, the amount of high frequency isolation and notch bandwidth are reduced, a significant amount of isolation is still provided at the first fuselage flexible bending mode, thus meeting the design goal for nonlinear operation set forth in Section 4.

Therefore, it is concluded that: a broad-band plus notch isolation system with linear isolation characteristics as illustrated in Figure 22 and nonlinear characteristics as illustrated in Figure 23, would be capable of providing a satisfactory solution to the problem of isolating commercial jet transport pilots during turbulence encounters, as defined in Section 4.

The isolation system transfer functions examined thus far have been for idealized system elements (actuator, servovalve, payload and foundation dynamics) having unity transfer functions. This simplification was introduced to demonstrate clearly the

basic low frequency response characteristics of the electro-hydraulic vibration isolation system. As a practical matter, however, the effect of fixed element dynamics on the isolation system performance must be considered along with the dynamics of the payload and foundation. These factors will be taken into account in the following section on the detail design of the laboratory model of the electrohydraulic isolation system developed in this program.

SECTION 6: DESIGN OF LABORATORY MODEL OF ELECTROHYDRAULIC PILOT SEAT ISOLATION SYSTEM

Analysis

Figure 24 illustrates the model of the support structure, seat, actuator, and pilot selected for evaluation of finite foundation and payload impedances on the performance of the pilot seat isolation system. The mass of the upper torso of the pilot, in addition to his arms and head, is represented by m_t; m_ℓ represents the weight of the pilot's legs and buttocks; and m_s represents the mass of the seat and seat support structure. The spring stiffness of the pilot's spine is described by k_m and c_m represents the damping in the spine. The stiffness and damping of the seat cushion are represented by k_s and c_s, respectively. The spring stiffness and damping of the coupling are represented by k_c and c_c, respectively. Damping in the flexible coupling has been modeled as inertial viscous damping for the reason discussed in Section 5. The actuator is considered to have a negligible weight in relation to the other system components. The spring stiffness of the support structure is represented by k_i and has been assumed to be undamped in order to simulate the worst case insofar as the stability of the control system is concerned.

The dynamic characteristics of a man could be simulated more closely by employing several spring-mass systems to represent the lower leg, upper leg, hips, thorax-abdomen, upper torso, and head. However, as a first order approximation, the model employed in Figure 24 will be sufficient to indicate how the impedance of the pilot effects the performance of the composite isolation system. An actual aircraft support structure will, of course, have several localized resonant frequencies (which are not simulated by the stiffness k_i) and some additional high frequency compensation in

the acceleration feedback loop may be required in actual applications in order to obtain the desired system response.

The relations governing the motion of the dynamic system illustrated in Figure 24 are defined below. Including the effects of leakage across the actuator piston, the flow from the servovalve is defined by [Ref. 48].

$$Q(s) = - As[R(s) - X(s)] - \frac{V}{2\beta_f} s\, \Delta P(s) - C_\ell \Delta P(s) \tag{28}$$

where C_ℓ is the leakage coefficient. The equation relating the motion of the seat support structure to the actuator piston is given by

$$A\Delta P(s) = - k_c[C(s) - R(s)] \tag{29}$$

and that relating the cylinder motion to the input from the support structure is given by

$$\Delta P(s) = - k_i[X(s) - Y(s)] \tag{30}$$

The equation relating the upper torso motion to the lower torso motion is

$$[m_t s^2 + c_m s + k_m]A(s) = [c_m s + k_m]B(s) \tag{31}$$

The equation relating the lower torso motion to the upper torso and seat structure motion is given by

$$[m_\ell s^2 + c_m s + k_m + c_s s + k_s]B(s) = [c_m s + k_m]A(s) + [c_s s + k_s]C(s) \tag{32}$$

The equation relating the seat structure motion to the lower torso motion and piston motion is defined by

$$[m_s s^2+c_s s+k_s+c_c s+k_c]C(s) = [c_s s+k_s]B(s) + k_c R(s) \tag{33}$$

The isolation control system is designed such that the net flow from the cylinder is given by

$$Q(s) = G_{sv}(s)\left\{\left[\frac{\tau_{1a}s}{1+\tau_{1a}s}\right]\left[\frac{\tau_{1b}s}{1+\tau_{1b}s}\right]\left[\frac{1}{1+\tau_{1c}s}\right]C_1 s^2 X(s)+\left[\frac{C_2 s}{1+\tau_2 s}+C_3\right]\left[R(s)-X(s)\right]\right.$$

$$\left. + \left[\frac{\tau_4 s}{1+\tau_4 s}\right]\left[\frac{\omega_1{}^2}{s^2+\omega_1{}^2}\right]C_4 s^2 R(s)\right\} \tag{34}$$

where G_{sv} is the transfer function of the servovalve defined by

$$G_{sv} = \frac{1}{\left(\frac{s}{\omega_{sv}}\right)^2 + 2\zeta_{sv}\left(\frac{s}{\omega_{sv}}\right) + 1} \tag{35}$$

The damping constant of the servovalve is defined by ζ_{sv} and ω_{sv} is the resonant frequency of the servovalve. The input accelerometer is located on the actuator cylinder structure and the feedback accelerometer is located on the actuator rod.

In order to provide a physical understanding of the value of k_i selected for analysis, an equivalent base resonant frequency ω_i in radians per second is defined as

$$\omega_i = \sqrt{\frac{k_i}{m_t+m_\ell+m_s}} \tag{36}$$

The sitting weight of the pilot will, of course, vary with the amount of weight supported by the rudder pedals via his legs, from a maximum value with the legs fully tucked in, to a minimum with them fully extended. According to data transmitted informally from the 6570th Aerospace Medical Research Laboratories at WPAFB, the average sitting weight of a pilot with a body weight of 175 pounds is 135 pounds. In the following analysis, the total weight of m_t plus m_ℓ has been specified at 135 pounds. Also, m_t has been assumed to be twice m_ℓ. In order to provide a physical comprehension of the spring stiffnesses and damping constants of the spine and seat, an equivalent whole body resonant frequency ω_m and whole body damping ratio ζ_m have been defined as

$$\omega_m = \sqrt{\frac{k_m}{m_t}} \tag{37}$$

$$\zeta_m = \frac{c_m}{2\sqrt{k_m m_t}} \tag{38}$$

A seat resonant frequency ω_s and seat damping ratio ζ_s have been defined as

$$\omega_s = \sqrt{\frac{k_s}{m_t+m_\ell}} \tag{39}$$

$$\zeta_s = \frac{c_s}{2\sqrt{k_s(m_t+m_\ell)}} \tag{40}$$

It should be noted that the resonant frequencies defined by Equations (36), (37), and (39) would not appear as second order resonances in any of the transmissibility functions of interest since the response of the system is governed by the interaction of all its components.

The absolute displacement transmissibility of primary interest is that of $|B_o/X_o|$ and the relative displacement transmissibility of primary interest is that of $|(B_o - X_o)/X_o|$ where X_o represents the amplitude of the actuator cylinder motion assuming sinusoidal oscillations and B_o represents the amplitude of motion of the seat cushion or the pilot's buttocks. The magnitude of $|B_o/X_o|$ must meet the isolation design goals established in Section 4. Figure 25 illustrates the theoretical vertical absolute and relative displacement transmissibilities for the pilot seat isolation system with a rigid payload (i.e., $k_s = k_m = \infty$ and $A_o = B_o = C_o$) and $\omega_i = 2\pi(20)$ radians per second. The transmissibilities were obtained from the simultaneous solution of Equations (27) through (34) by means of a digital computer program. The notch frequency was located at 4.2 Hz rather than 4.5 Hz in order to more nearly center the notch on the isolation requirements of Figure 16. The relative displacement transmissibility being less than one over the frequency range from 4.2 to 30 Hz is associated with the relative decrease in isolation over the frequency range from 6 to 10 Hz (i.e., decreasing phase difference between excitation and response over this frequency range). Although non-intentional, this feature is of particular value in the application of active isolation to commercial jet transport pilots since it minimizes the phase difference between the pilot and his controls, while providing the required degree of isolation. The relative transmissibility values of less than one above 50 Hz is also associated with the relative decrease in isolation provided by the active system.

Figure 26 illustrates the theoretical absolute and relative displacement transmissibilities for the pilot seat isolation system with the stiffness and damping models of a DC-8 seat cushion and 175 pound subject included in the analysis. The DC-8 seat cushion was incorporated in the analysis since a unit was obtained for use with the laboratory model of the electrohydraulic pilot seat isolation system. The primary effects of the seat cushion are to slightly increase the effective resonant transmissibilities of the isolation system (which is, of course, undesirable) and to provide additional high frequency broad-band isolation. Figure 27 illustrates the theoretical horizontal passive absolute and relative displacement transmissibilities for the pilot seat isolation system with a DC-8 seat cushion and a 175 pound rigid payload. The masses m_t and m_ℓ have been assumed to be rigidly connected due to the lack of any data on the horizontal resonant characteristics of the human torso. The location of the excitation source and response are defined in Figure 24. The resonance at 25 Hz is due to the flexible coupling which acts in the horizontal as well as in the vertical directions. Rotational resonances have been neglected in the horizontal analysis. Figure 28 illustrates the pertinent theoretical vertical transmissibilities for the isolation system when it is operating at the extremes of its nonlinear range. The derivation of Figure 28 was based on the same assumptions described for Figure 23 in Section 5.

A comparison of Figures 26 and 27 with Figure 16 shows that this isolation system meets the design goals for isolation established in Section 4. The vertical and horizontal relative displacement transmissibilities will result in peak steady-state relative deflections less than ± 1 inch due to the dynamic environment defined in Section 4, and the nonlinear characteristics of the isolation system meet the pertinent design goals established in Section 4. Consequently, the control system modeled by Equation (34) was employed in the design of the laboratory model of the electrohydraulic pilot seat isolation system.

Electrical and Mechanical Design

Figure 29 is a diagrammatic representation of the major functional components of the laboratory model of the pilot seat employed during the experimental phase of the program being reported on. The seat support structure was obtained from a DC-8 pilot seat. The major portion of the testing program, which will be discussed in the following section, was conducted with a DC-8 seat cushion. In addition, tests were performed with the DC-8 seat cushion replaced by a balsa wood seat in order to determine the effects of seat cushion stiffness on the overall isolation characteristics of the system.

Referring again to Figure 29, the actuator piston rod is fastened to a horizontal plate which supports four elastomeric isolators (flexible couplings). The horizontal plate is guided in the vertical direction by two guide rods mounted fore and aft of the actuator. The guide rods are accurately aligned by four linear bearings to minimize the transmission of any horizontal loads to the actuator piston rod. The principal elastic axes of the flexible couplings have been inclined with respect to the principal inertia axes of the payload to minimize the effects of the lower and upper rocking modes caused by the imbalance between the center of gravity of the isolated body and the horizontal elastic axes of the flexible couplings. When the center of gravity of the payload is offset from the elastic axis of the isolators (i.e., coupled condition) the uncoupled rotational resonant frequency about the pitch or roll axis degenerates into two frequencies defined by the horizontal as well as the vertical stiffness of the isolators. The stroke of the hydraulic actuator is ± 1.5 inches. This is less than the ± 2 inches allowed during transient conditions since a portion of the relative deflection occurs across the seat cushion. The actuator is rated for 3,000 psig normal operation although only 2,000 psig supply pressure to the servovalve was employed during the tests. The servovalve is

a two-stage, mechanical feedback, flow control valve similar to those normally employed in electrohydraulic position control servomechanisms. The relative position transducer is of the linear variable differential transformer type (LVDT). The input accelerometer which is of the strain gage type is mounted on the actuator housing at the base of the actuator and the output accelerometer which is of the servo type is located on the horizontal plate adjacent to the actuator rod.

Figure 30 is a photograph of the laboratory model of the electrohydraulic pilot seat mounted on the cockpit simulator employed during the testing program. The cockpit simulator consisted of a control column meter panel and foot rests, the locations of which are representative of the DC-8 cockpit. The active portion of the isolation system was designed to fit in the same space provided for the seat substructure in the DC-8. The size of the isolation system is also compatible with present commercial jet transports such as the DC-9 and Boeing 727 aircraft. The lap belt and shoulder straps with inertia reel were retained in the design in order to simulate an actual seating system as closely as possible. The test subject in Figure 30 is shown wearing the helmet and accelerometer employed during the testing program to monitor the accelerations of the subject's head. Figure 31 is a photograph of the active portion of the electrohydraulic pilot seat showing the details of the actuator mounting.

Figure 32 illustrates the signal flow diagram for the electrohydraulic pilot seat isolation system. The control system has two modes of operation: the "flight" mode; and the "landing/takeoff" mode. In the flight mode, the control system has been designed to provide the isolation characteristics described in the previous section. In the landing/takeoff mode, the control system is employed in a tight relative position feedback loop such that isolation is only provided by the seat cushion in combination with the flexible couplings. Figure 33 illustrates the servo control

console for the electrohydraulic pilot seat isolation system, which is of a modular board type construction. Except for the input accelerometer pre-amplifier which was mounted on the actuator housing, all other electronic components were mounted in the servo control console. In addition to the power and mode controls, all the system feedback gains and compensation network time constants were controllable by potentiometers mounted on the front panel of the console. The notch frequency was adjustable to ± 0.75 Hz about a mean frequency of 4.5 Hz. The results of the testing program on the electrohydraulic pilot seat isolation system are described in the following section.

SECTION 7: EXPERIMENTAL EVALUATION OF THE ELECTROHYDRAULIC PILOT SEAT ISOLATION SYSTEM

Introduction

A test program, primarily objective in nature, was conducted with both sinusoidal and random excitation to determine: (a) the absolute transmissibility characteristics of the active portion of the isolation system; (b) the ratio of the absolute acceleration of various parts of a human subject to that of the input; (c) the effects of seat belt restraint on the response of the test subject; (d) the effects of a finite impedance support structure on the stability and performance characteristics of the isolation system; and (e) the effects of seat cushion stiffness on the overall performance of the isolation system. The purpose of the shoulder straps is to provide restraint due to the rapid transient forward motion of the pilot and do not provide any restriction of the vertical and horizontal motion of the subject within the range of excitations defined in Section 4. Consequently, no tests were run with the shoulder straps fastened. Subjective tests with sinusoidal and random inputs were also performed with two test subjects to obtain qualitative reactions to the performance of the isolation system and the effects of the pilot's controls vibrating at the full excitation amplitude.

Figure 34 illustrates the various locations and directions which were monitored for acceleration levels during the testing program. The sensor for monitoring the acceleration of the subject's buttocks (i.e., location B) was mounted in a metal capsule nominally 1.75 inches in diameter and 1 inch high in order to minimize the effects of secondary disturbances on the accelerometer readings. The buttocks accelerometer housing was designed such that it press fit between the rectal cavity and the seat cushion. The sensor for monitoring the acceleration of the subject's head was mounted on the top of a tightly strapped

helmet. The sensor for monitoring the fore/aft acceleration of the subject's waist was press fit between his belt and the back cushion while that for monitoring the lateral acceleration of his waist was press fit between his belt and his torso.

Vertical sinusoidal testing was performed with a hydraulic shaker from 1 to 100 Hz. The input was 0.05 inch D.A. from 1 to 6 Hz, a 0.032 inch D.A. input from 6 to 50 Hz, and ± 4 g from 50 to 100 Hz. Horizontal testing (excitation at base of actuator housing) was performed with an electrodynamic shaker from 5 to 50 Hz with a 0.032 inch D.A. input and from 50 to 100 Hz with a ± 4 g input. Random vibration testing was performed in the vertical direction only. The power spectral density function (PSD) consisted of a narrow-band input centered at 4.5 Hz with an rms value of 0.1 g. The total rms acceleration over the frequency range from 2 to 15 Hz, during the random testing, was 0.27 g. This input is scaled down from that encountered during turbulent flight (Figure 12) due to the limitation in the double displacement amplitude capability of the shaker. However, this is not considered to be a serious shortcoming since the primary purpose of the random vibration testing was to verify that the isolation system provided the same transfer function whether excited by sinusoidal or random vibrations. Figure 35 illustrates the pilot seat and cockpit simulator mounted on the hydraulic shaker. The plate mounted between the shaker fixture and simulator was employed to simulate the effects of a flexible foundation.

Objective Testing

Unless otherwise stated, the experimental data on the transmissibilities presented herein were obtained with the sinusoidal excitation spectrum defined in the introduction to this section. Also, the tests are performed with the hydraulic actuator operating about its null position, unless otherwise stated. All inputs were measured from points U, X, and V.

Figure 36 illustrates test data on the absolute and relative vertical transmissibility between the input and the output of the flexible coupling with: a 160 pound subject, the DC-8 seat cushion; seat belt tight; and with the isolation system in the flight mode. These tests were also performed with a 175 pound rigid payload and there was no measurable difference in the results, within an estimated testing error of ± 10 percent, which indicates that the performance of the active portion of the isolation system is independent of payload dynamics. The performance of the isolation system agrees very well with that predicted below 20 Hz (Figure 25). The resonant frequency and resonant transmissibility of the isolation system are slightly lower than expected and the bandwidth of the notch at an absolute transmissibility of 0.3 is greater than expected. The slight degradation in performance from that computed above 20 Hz and, therefore, the variation in the relative transmissibility, is primarily due to a higher than predicted seat support structure flexible coupling resonant frequency. The performance of the isolation system was linear over the relative deflection range from -1 inch to +1 inch with essentially the same isolation characteristics as at a zero mean relative deflection. Figure 37 illustrates the absolute vertical transmissibility measured between the input and output of the flexible coupling with the isolation system in the landing/takeoff mode. The response characteristics are primarily due to those of the flexible coupling. This latter test was also performed with a 175 pound rigid payload and there was no measurable difference in the results.

Figure 38 illustrates test data on the absolute horizontal transmissibilities between the input and output of the flexible coupling. The secondary resonance at 80 Hz which occurs in the lateral direction is due to a structural resonance in the actuator housing. The tests were performed with the isolation system in the flight and landing/takeoff modes, with no differences in the

results. Figure 39 illustrates the absolute vertical transmissibility $|C_o/X_o|$ with the mean position of the hydraulic actuator 1.25 inches above its null position and excitation levels as defined in the introduction to this section. The variation in the mean position of the actuator was accomplished by inserting a DC offset voltage in the relative position feedback control loop. The resonant frequency of the active portion of the isolation system increases while the bandwidth of the notch and the amount of high frequency isolation decreases, thus verifying the design calculations presented in the previous section.

Figure 40 illustrates test data on the absolute transmissibilities measured between the input and the buttocks with a 160 pound subject on the DC-8 seat cushion. The differences between the flight and landing/takeoff modes and the effects of the seat belt are also illustrated. Measurements were only made up to 15 Hz since this was considered to be the upper limit of reliable data. Above this frequency, localized variations in the dynamics of the seat cushion and motions of the subject had a marked effect on accelerometer readings. The absolute transmissibility provided by the composite isolation system (i.e., active isolation system plus seat cushion) meets the design goals established in Section 4. However, notice that the 4 Hz subject seat cushion resonant frequency results in a degredation of the bandwidth of the notch rather than a slight improvement as predicted by a comparison of Figures 25 and 26. Since the isolation provided by the active portion of the isolation system (Figure 36) meets the design goals below 15 Hz with a substantial safety margin, it is concluded that a higher stiffness seat cushion would provide more optimum performance. This would also have the effect of decreasing the low frequency relative deflections between the pilot and his cockpit controls. Figure 41 illustrates results of tests similar to that described in Figure 40 except with a 200 pound subject. In order to verify the previously discussed effects of the seat cushion

stiffness on $|B_o/X_o|$, this function was measured in the flight mode with a balsa wood seat in place of the DC-8 seat cushion. The results were identical to those for $|C_o/X_o|$ indicated in Figure 36, below 15 Hz.

Figure 42 illustrates data on the absolute vertical transmissibility $|B_o/X_o|$ with the mean position of the hydraulic actuator 1.25 inches above its null position and sinusoidal excitation levels as defined in the introduction to this section. The performance characteristics of the isolation system in its nonlinear range closely follow the trends predicted analytically. Figure 43 indicates measured data on the absolute vertical transmissibility $|B_o/X_o|$ with a 175 pound rigid payload on the DC-8 seat cushion and the isolation system in the flight mode. The response of the isolation system with the rigid payload is representative of that with a human subject (Figures 40 and 41) and thus a rigid payload could be employed in long duration reliability testing of an electrohydraulic pilot seat isolation system.

Figure 44 illustrates the absolute vertical transmissibilities between the input and the buttocks with the random vibration input. The transmissibilities were determined by computing the square root of the ratio of the output spectral density to the input spectral density. The bandwidth of the filters employed in the analysis was 6 percent of the mean analysis frequency. A comparison between Figure 44 and the data illustrated in Figure 40 which was obtained with a sinusoidal input, demonstrates that the active electrohydraulic isolation system acts as a linear transfer function about its null position.

Figures 45 and 46 illustrate the absolute fore/aft and lateral transmissibilities measured between the input (at base of actuator housing) and the waist. The accuracy of the test data is somewhat in doubt due to the localized flexibility of the subject's torso at the location of the accelerometers. The information does

indicate, however, that the isolation provided by the seat cushion is comparable to the design goals.

Figure 47 illustrates test data on the absolute vertical transmissibility measured between the input and an accelerometer mounted on a helmet that was firmly strapped to the subject's head. Tests were performed on 160 and 200 pound subjects. As expected, the bandwidth of the notch is less than that for $|B_o/X_o|$ (Figure 40) due to the resonance of the subject's torso. Figure 48 illustrates test data on the absolute vertical transmissibility between the input and head with a 200 pound subject on a balsa wood seat. A comparison between Figures 47 and 48 shows that the dynamic characteristics of the DC-8 seat cushion, increases the response amplitude of the subject's head, over that associated with the balsa wood seat in the frequency range from 4 to 15 Hz. Figure 49 illustrates test data on the absolute transmissibilities between the input and head for the 160 and 200 pound subjects and the isolation system in the landing/takeoff mode. Figure 50 illustrates the absolute vertical transmissibilities between the buttocks and the head for the 160 and 200 pound subjects. The response curves were obtained by dividing $|A_o/X_o|$ by $|B_o/X_o|$ as determined from the landing/takeoff mode tests with the DC-8 seat cushion. The resonance at 4.5 Hz is the primary body resonance and that at 8-9 Hz is the head/shoulder resonant frequency. The fact that the head/shoulder resonant frequency is lower than the 10-12 Hz indicated in the literature is attributed to the weight of the helmet. Figure 50 further points out that a seat cushion resonant frequency between 4 and 5 Hz should be avoided. Figures 51 and 52 illustrate the absolute fore/aft transmissibilities measured between the input and head for the 160 pound subject on the DC-8 seat cushion.

Subjective Testing

The tests reported on in the previous sub-section on "Objective Testing" of the electrohydraulic pilot seat isolation system were performed with the subject's legs hanging free and his arms on the arm rests. There was no physical contact between the subjects and the simulator during the tests. The purpose of this section is to report on two days of tests which were performed with two NASA Langley representatives in order to obtain qualitative reactions as to the potential effectiveness of the laboratory model of the electrohydraulic pilot seat isolation system in improving the performance of commercial jet transport pilots during turbulence penetration. In this series of tests, the subjects were in a normal seated position with their feet positioned on the simulator cockpit floor and their hands grasping the control column. A helmet was not employed during the subjective tests since subject performance might have been effected by its jostling. The test setup is illustrated in Figure 35. The cockpit floor and control column were subjected to the same dynamic inputs as the isolation system since the structural resonances of the simulator were well above the frequency range of interest. Tests were performed with sinusoidal and random excitation.

The subjects were required to perform a task and then make a judgement as to the effect of the vibration on task performance immediately following task completion. The subjects were required to perform a Discrimination Reaction Time test with the active isolation system "off" (i.e., landing/takeoff mode) and with the active isolation system "on" (i.e., flight mode) while being subjected to various vibration levels and excitation frequencies. The test apparatus, provided by NASA Langley, was an adaption of a Discrimination Reaction Time Testing device developed at the U. S. Naval Air Development Center and employed in studies of pilot fatigue in aircraft cockpits during transoceanic flight as

well as in studies of human responses to acceleration and vibration stress in the human centrifuge at NADC. The tasks required by the Discrimination Reaction Time Testing device were not sufficiently difficult, in this case, to measure any consistent trends in the performance of the test subjects. The tasks did, however, provide a basis for the subjects to make judgements as to the degree of "Vibration Interference" which they experienced in performing the task and the degree of "Vibration Annoyance".

The term "Vibration Interference" was employed as a measure of how much extra effort the subject had to exert in order to perform the task with vibration present as compared to the zero vibration condition. The term "Vibration Annoyance", although related to comfort, was employed as a measure of long term fatigue and impairment of performance. These evaluations utilized a 10 point rating scale which was based on the Cooper Pilot Opinion Rating System for Universal Use. The scale, adopted for use in these vibration studies, was originally based on aircraft flying qualities. The vibration interference and vibration annoyance rating scale is defined in Table II. Ratings 1, 2, or 3 are considered satisfactory; ratings 4, 5, or 6 are unsatisfactory; ratings 7, 8, or 9 are unacceptable; and rating 10 is completely unacceptable (i.e., catastrophic).

Tables III and IV summarize the average Vibration Annoyance and Vibration Interference ratings by the two subjects while the isolation system and simulator were being exposed to various levels and frequencies of vertical sinusoidal excitation. Each rating represents the average rating for three tests which were performed at each excitation level and frequency. The length of each test was approximately 35 seconds. The tests were performed in a random sequence so that the subjects did not know whether the active isolation system was "off" (Landing/Takeoff Mode) or "on" (Flight Mode). Test subject A (Ref. Table III) also employed observation of the gauges mounted on the cockpit simulator (Ref.

Figure 30) as a reference in establishing the ratings. As would be expected, the ratings at 2 Hz are slightly higher with the active system "on" than with it "off". This is due to the resonance of the active portion of the isolation system in the flight mode. Considering the fact that the active isolation system has a resonant transmissibility of 2 at this frequency and the ratings only increased by 0.3 with the active system "on", does indicate that human subjects have a relatively low sensitivity to vibration inputs at this frequency as compared to other frequencies. Also, reducing the value of the resonant transmissibility of the active portion of the isolation system in the flight mode is not sufficiently profitable since this could only be accomplished by decreasing the bandwidth of the notch. The reason for the slightly higher ratings at 3 Hz with the active system "on" than with it "off", appears to be due to the fact that the relative displacement transmissibility at that frequency is less with the active system "off", although the absolute transmissibility is less with the active system "on".

The active isolation system shows a substantial improvement over the non-active condition at 4.2 Hz. At 6, 9, and 12 Hz, the active isolation system also showed a consistent improvement over the non-active case. It should be noted that the hydraulic power supply for the shaker was somewhat noisy and could have had an effect on the minimum level (i.e., threshold) of judgements since the subjects did not have helmets during the subjective tests. Tests were not performed to isolate the effects of environmental noise. The common reaction of the test subjects was that the annoyance and interference ratings for 4.2, 6, 9, and 12 Hz would be even lower in the case of the active system "on", if it were not for the vibrations induced in their legs. The vibrations induced in their arms via the control column appeared to be a secondary factor. Also, the absolute level of the leg vibrations appeared to be the problem, rather than the phase lag between

the leg vibrations and the response of the subjects. Tables V and VI summarize the average Vibration Annoyance and Vibration Interference ratings by the two subjects while the isolation system and simulator were being exposed to various random excitation levels. Each excitation level consisted of a broad-band input over the frequency range from 2-15 Hz, and a narrow-band input centered at 4.5 Hz which simulated the fuselage bending mode of the aircraft. Each judgement level represents an average of three tests and each test ran 1 minute. The active system shows a consistent improvement over the non-active case.

SECTION 8: CONCLUSIONS

Conclusions based on the results of this investigation into the vibration isolation of commercial jet transport pilots during turbulent air penetration are:

1. Based on a literature survey on the effects of vibration on the visual and motor performance of seated subjects, the maximum rms vertical and transverse narrow-band random accelerations which should be transmitted to the pilot over the frequency range from 1 to 20 Hz is 0.07 g.

2. The vertical whole body resonant frequency of a seated human subject (i.e., 4 to 5 Hz) is coincident with the primary excitation frequency of commercial jet transport aircraft (i.e., first fuselage flexible bending mode).

3. Conventional passive vibration isolation of the pilot is sufficient in the fore/aft and lateral directions. An active vibration isolation system is required in the vertical direction with a nominally 2 Hz resonant frequency, better than 70 percent isolation between 4 and 5 Hz, and greater than 85 percent isolation for excitation frequencies between 20 and 50 Hz. Also, the resonant transmissibility of the isolation system in the vertical direction must be maintained less than 2.

4. In addition to providing the required isolation, the active isolation system must be designed to limit the relative deflections between the pilot and the cockpit controls to ± 1 inch during turbulence penetration, with peak relative deflection of ± 2 inches only allowable during severe transients such as buffeting.

5. The active isolation system must automatically reposition the pilot seat to its equilibrium position and provide isolation during sustained acceleration conditions of ± 3 g.

6. The performance of the active isolation system must be independent of variations in pilot weight.

7. The laboratory model of the electrohydraulic pilot seat isolation system developed under this contract met all the design goals outlined in statements 3 through 6 above.

8. Based on preliminary subjective evaluation tests, it can be said that the electrohydraulic pilot seat isolation system offers the potential for providing a substantial improvement in pilot performance during turbulent air penetration.

9. The vibration which is transmitted directly to the pilot's legs via the rudder pedals and in the arms via the control column may be a source of degradation in pilot performance.

In summary, the preliminary subjective evaluation tests performed on the laboratory model of the electrohydraulic pilot seat isolation system have shown that it is capable of providing a substantial reduction in dynamic excitation imposed on the pilot's torso during turbulent air penetration. However, the results of the tests also indicate that the vibration which is transmitted directly to the pilot's legs via the rudder pedals and that induced in the arms through the controls may play a significant role in the overall degradation of pilot performance. It appears that, although the vibration reaching the pilot through the seat is virtually eliminated by the electrohydraulic seat isolation system developed, overall pilot disturbance can be further reduced by decreasing the level of vibrations induced in the pilot's legs and arms. The relative improvement in performance which can be obtained by reducing the level of pilot vibration should be validated by a comprehensive human factors test program.

SECTION 9: RECOMMENDATIONS

Based on the results and conclusions of the investigation, it is recommended that an evaluation be made of rudder pedal and control column designs representative of that utilized in present commercial jet transports, and that an engineering study be conducted to devise means by which vibrations induced in the pilot's legs and arms could be reduced. It is recommended that detailed subjective response tests, simulator tests and flight tests be conducted so that the performance improvement to be accrued by electrohydraulic seat isolation system configurations over that provided by existing seats can be validated.

The subjective response tests should employ a hydraulic shaker with a minimum double displacement capability of 6 inches so that the buffeting input at 1.3 Hz, the first fuselage bending mode at 4.5 Hz, and the broad-band input from 1 to 50 Hz can be more accurately simulated. Also, rudder pedal and control column designs representative of that utilized in present commercial jet transports (i.e., simulate effects of pin joints and linkages between controls and aircraft) should be employed in the subjective tests, so that the effect of vibrations induced in the pilot's legs and arms can be more accurately evaluated.

It is recommended that a program be formulated to accomplish the following:

1. Engineering study of potential ways in which the vibrations induced in the pilot's legs and arms could be reduced in order to obtain a more satisfactory solution to the problem of reducing the overall disturbances induced in commercial jet transport pilots during turbulent air penetration.
2. Accurate evaluation of the improvement in the motor and visual performance capabilities of test subjects (commercial jet transport pilots should be employed) with the

active isolation system configurations as compared to conventional commercial seats. It is proposed that the tracking tasks be of the compensatory type with a controlled element having a first-order unstable divergence such as that described in NASA CR-616 and CR-674. During these tests, the subject should employ a headset representative of that in use by commercial pilots.

3. Manual control dexterity tests as a means of further evaluating the effect of relative deflection between the pilot and the cockpit and the absolute level of cockpit vibrations on the ability of the pilot to perform required flight control tasks. A headset should also be employed in these tests.

4. Test the effects of the various isolation system configurations on ability of the subject to communicate. The subject's speech should be recorded and the headset should be representative of that in use by commercial pilots (for the purpose of evaluating the effect of microphone vibrations).

5. Motor and visual performance as well as manual control dexterity tests should be performed for long durations (such as 1 hour) to determine the effects of fatigue.

6. Tests on the selected seat isolation system configuration in the Vertical Acceleration and Roll Device designated as S.07 at Ames Research Center. The S.07 is a dynamic flight simulator capable of ± 10 feet vertical displacements and ± 5 g acceleration and is capable of generating the vibratory motion over the frequency range from 0.1 to 10 Hz.

7. Flight tests (under turbulent conditions) in a typical commercial jet transport aircraft.

APPENDIX A

LIST OF SYMBOLS

A	Average actuator cross-sectional area, $in.^2$
$A(t)$	Vertical motion time history of subject's head, in.
A_o	Vertical sinusoidal motion amplitude of subject's head, in.
$B(t)$	Vertical motion time history of subject's buttocks, in.
B_o	Vertical sinusoidal motion amplitude of subject's buttocks, in.
c	Absolute velocity damping constant of isolator lb.sec./in.
c_c	Absolute velocity damping constant of flexible coupling lb.sec./in.
c_m	Relative velocity damping constant of subject's spine, lb.sec./in.
c_s	Relative velocity damping constant of seat cushion, lb.sec./in.
$C(t)$	Vertical motion time history of seat structure, in.
C_ℓ	Leakage coefficient across actuator piston, $(in.^3/sec.)/(lb./in.^2)$
C_o	Vertical sinusoidal motion amplitude of seat structure, in.
C_1	Acceleration feedback or feed-forward gain, $(in.^3/sec.)/(in./sec.^2)$
C_2	Relative velocity feedback gain, $(in.^3/sec.)/(in./sec.)$
C_3	Relative displacement feedback gain, $(in.^3/sec.)/in.$
C_4	Acceleration feedback gain, $(in.^3/sec.)/(in./sec.^2)$
D_o	Fore/aft sinusoidal motion amplitude of seat structure, in.
E_o	Fore/aft sinusoidal motion amplitude of subject's head, in.
$F(t)$	Vertical time history of force, lb.
F_o	Fore/aft sinusoidal motion amplitude of subject's waist, in.

g	Acceleration due to gravity, 386 in./sec.^{2}
$G_{sv}(s)$	Transfer function of servovalve, dimensionless
G_o	Lateral sinusoidal motion amplitude of subject's head, in.
$G_1(s)$	Acceleration feedback or feed-forward compensation, dimensionless
$G_2(s)$	Relative velocity feedback compensation, dimensionless
$G_3(s)$	Relative displacement feedback compensation, dimensionless
$G_4(s)$	Acceleration feedback compensation dimensionless
H_o	Lateral sinusoidal motion amplitude of subject's waist, in.
J_o	Lateral sinusoidal motion amplitude of seat structure, in.
k	Stiffness of isolator, lb./in.
k_c	Stiffness of flexible coupling, lb./in.
k_i	Stiffness of foundation, lb./in.
k_m	Stiffness of subject's spine, lb./in.
k_s	Stiffness of seat cushion, lb./in.
$L( )$	Laplace transform of, dimensionless
$L^{-1}( )$	Inverse Laplace transform of, dimensionless
m	Mass of isolated body, lb.sec.^{2}/in.
m_ℓ	Mass of lower torso, lb.sec.^{2}/in.
m_s	Mass of seat structure, lb.sec.^{2}/in.
m_t	Mass of upper torso, lb.sec.^{2}/in.
Q	Flow from the servovalve, in.^{3}/sec.
$r(t)$	Vertical motion time history of actuator piston, in.
$R(t)$	Vertical motion time history of actuator piston, in.
s	Laplace transform operator, radians per sec.
$S_{\ddot{w}}(\omega)$	Power spectral density of normal vibrations, g^2/Hz

T_A Absolute displacement transmissibility, dimensionless

T_R Relative displacement transmissibility, dimensionless

U_o Lateral sinusoidal motion amplitude of actuator housing, in.

V Mean volume of upper and lower actuator chambers, $in.^3$

V_o Fore/aft sinusoidal motion amplitude of actuator housing, in.

$w(t)$ Vertical motion time history of support structure, in.

w_o Vertical sinusoidal motion amplitude of support structure,in.

$X(t)$ Vertical motion time history of actuator housing, in.

X_o Vertical sinusoidal motion amplitude of actuator housing,in.

$Y(t)$ Vertical motion time history of flexible foundation, in.

$z(t)$ Vertical motion time history of payload, in.

z_o Vertical sinusoidal motion amplitude of payload, in.

β_F Bulk modulus of hydraulic Fluid, lb./in.

δ Relative displacement, in.

ΔP Differential pressure across actuator piston, lb./in.

ζ Ratio of coefficient of viscous damping to that for a critically damped second order system, dimensionless

ζ_m Equivalent whole body damping ratio, dimensionless

ζ_s Equivalent seat damping ratio, dimensionless

ζ_{sv} Damping constant of servovalve, dimensionless

τ_1 Time constant for acceleration feedback or feed-forward shaping network, sec.

τ_2 Time constant for relative velocity shaping network, sec.

τ_3 Time constant for relative displacement feedback shaping network, sec.

τ_4 Time constant for acceleration feedback shaping network,sec.

τ_{1a} Time constant for acceleration feed-forward shaping network, sec.

τ_{1b} Time constant for acceleration feed-forward shaping network, sec.

τ_{1c} Time constant for acceleration feed-forward shaping network, sec.

ω Frequency, radians per second

ω_i Equivalent base resonant frequency, radians per second

ω_m Equivalent whole body resonant frequency, radians per second

ω_n Resonant frequency of isolation system, radians per second

ω_s Equivalent seat resonant frequency, radians per second

ω_1 Notch frequency, radians per second

ω_{sv} Resonant frequency of servovalve, radians per second

REFERENCES

1. Parks, D. L.; and Snyder, F. W.: Human Reaction to Low Frequency Vibration, AD 261330 (Boeing, Wichita D3-3512-1), July 1961.

2. Magid, E. B.; Coermann, R. R.; and Ziegenruecker, G. H.: Human Tolerance to Whole Body Sinusoidal Vibration, Aerospace Medicine, vol. 31, 1960.

3. Goldman, D. E.; and von Gierke, H. E.: Shock and Vibration Limits of Comfort and Safety, Shock and Vibration Handbook, C. M. Harris and C. E. Crede eds., McGraw-Hill Book Co., 1961.

4. Goldman, D. E.: A Review of Subjective Responses to Vibration Motion of the Human Body in the Frequency Range from 1 to 70 Cycles per Second, Report No. 1, Project NM-004-001, U. S. Naval Medical Research Institute, 1948.

5. Magid, E. B.: Human Tolerance to Whole Body Sinusoidal Vibrations Short Time, One Minute, and Three Minutes, Aerospace Medicine, vol. 31, 1960.

6. Ziegenruecker, G. H.; and Magid, E. B.: Short Time Human Tolerance to Sinusoidal Vibrations, AD 227341, July 1959.

7. Chaney, R. E.: Subjective Reaction to Whole Body Vibration, AD 607462, September 1964.

8. Goldman, D. E.: The Biological Effects of Vibration, AD 256926, April 1961.

9. Temple, W. E.; et al.: Man's Short-Time Tolerance to Sinusoidal Vibrations, Aerospace Medicine, vol. 35, 1964.

10. Guignard, J. C.: Effects of Vibration on Man, Royal Air Force Institute of Aviation Medicine, Journal of Environmental Sciences, August 1966.

11. Chaney, R. E.; and Parks, D. L.: Tracking Performance During Whole Body Vibration, AD 456277 (Boeing, Wichita D3-3512-6), November 1964.

12. Harris, C. S.; Chiles, W. D.; and Touchstone, R. M.: Human Performance as a Function of Intensity of Vibration at 5 cps, AD 607760, September 1964.

13. Chaney, R. E.; and Parks, D. L.: Visual-Motor Performance During Whole Body Vibrations, AD 456271 (Boeing, Wichita D3-3512-5), November 1964.

14. Buckhout, R.: Effect of Whole Body Sinusoidal Vibration on Human Performance, Human Factors, vol. 6, 1964.

15. Harris, C. S.; and Shoenberger, R. W.: Human Performance During Vibration, AD 624196, November 1965.

16. Hornich, R. J.; Boettcher, C. A.; and Simons, A. K.: The Effect of Low Frequency, High Amplitude, Whole Body, Longitudinal and Transverse Performance Upon Human Performance, Final Report Contract No. DA-11-022-509-ORD-3300, July 1961.

17. Teare, J. R.; and Parks, D. L.: Visual Performance During Whole Body Vibration, AD 427254 (Boeing, Wichita D3-3512-4), November 1963.

18. Goldman, D. E.; and von Gierke, H. E.: The Effect of Shock and Vibrations on Man, Lecture and Review Series No. 60-3, Naval Medical Research Institute, 1960.

19. von Gierke, H. E.: Biodynamic Response of the Human Body, Applied Mechanics Reviews, vol. 17, December 1964.

20. Edwards, R. G.; and Lange, K. O.: A Mechanical Impedance Investigation of Human Response to Vibration, AD 609006, October 1964.

21. Pradko, F.; Lee, R. A.; and Green, J. D.: Human Vibration-Response Theory, ASME Publication 65-WA/HUF-19, November 1965.

22. Coermann, R. R.; et al.: The Passive Dynamic Mechanical Properties of the Human Thorax-Abdomen System and of the Whole Body System, Aerospace Medicine, vol. 31, June 1960.

23. Coermann, R. R.: The Mechanical Impedance of the Human Body in Sitting and Standing Position at Low Frequencies, ASD Technical Report 61-492, September 1961.

24. Nadel, A. B.; Burns, N. M.; Chambers, M.; and Hendler, E.: Unusual Environments and Human Behavior, Chapter 10, Collier-Macmillan, 1963.

25. Schmitz, M. A.; Simons, A. K.; and Boettcher, C. A.: The Effect of Low Frequency, High Amplitude Whole Body Vertical Vibration on Human Performance, Final Report Contract No. DA-49-007-MD-797, January 1960.

26. Linder, G. S.: Mechanical Vibration Effects on Human Beings, Aerospace Medicine, vol. 33, 1962.

27. von Gierke, H. E.: Proposed Standard: Recommendation for Evaluating Vibration Exposure of Humans, International Organization For Standards Document 108/7 N21, February 1967.

28. Wendt, G. R.: Vestibular Functions, Handbook of Experimental Psychology, S. S. Stevens, ed., John Wiley and Sons, 1951.

29. Kerr, T. H.; Nethaway, J. E.; and Chinn, H. W.: Aircraft Tests in High-Speed Low-Level Flight, Including Impressions of a Spring-Mounted Seat, AD 431319 (NATA Report 442), April 1963.

30. Parks, D. L.: A Comparison of Sinusoidal and Random Vibration Effects on Human Performance, AD 261331 (Boeing, Wichita D3-3512-2), July 1961.

31. Weisz, A. Z.; Goddard, C.: and Allen, R. W.: Human Performance Under Random and Sinusoidal Vibration, AD 631457, December 1965.

32. Sadoff, M.; and Dolkas, C. B.: Acceleration Stress Effects on Pilot Performance and Dynamic Response, NASA SP-128, 1967.

33. Fraser, T. M.: Human Response to Sustained Acceleration, NASA SP-103, 1966.

34. Lambert, E. H.: Physiologic Studies of Man's G Tolerance in Aircraft, Federation Proceedings, vol. 5, 1946.

35. Wells, J. G.; and Morehouse, L. E.: Electromyographic Study of the Effects of Various Headward Accelerative Forces Upon Pilot's Ability to Perform Standardized Pulls on an Aircraft Control Stick, Journal of Aviation Medicine, vol. 21, 1950.

36. Stoll, A. M.: Human Tolerance to Positive G as Determined by the Physiological End Points, Journal of Aviation Medicine, vol. 27, 1956.

37. Chambers, R. M.; and Hitchcock, L.: The Effects of Acceleration on Pilot Performance, NADC-6219, 1963.

38. Casper, R.: Resolution of Vibration Isolated Cameras, Photogrammetric Engineering, July 1964.

39. Magrath, H. A.; Rogers, O. R.; and Grimes, C. K.: Shock and Vibration in Aircraft and Missiles, Shock and Vibration Handbook, C. M. Harris and C. E. Crede eds., McGraw-Hill Book Co., 1961.

40. Northwest Airlines, Inc.: Jet Turbulence Penetration, Flight Standards Bulletin No. 8-63, November 1963.

41. Northwest Airlines, Inc.: Operation in Turbulence, Flight Standards Bulletin No. 3-65, February 1965.

42. Civil Aeronautics Board: Aircraft Accident Report No. SA-366, File No. 1-0001, March 1962.

43. Civil Aeronautics Board: Aircraft Accident Report SA-372, File No. 1-0006, February 1963.

44. Sadoff, M.; Bray, R. S.; and Andrews, W. H.: Summary of NASA Research on Jet Transport Control Problems in Severe Turbulence, Journal of Aircraft, vol. 3, May 1966.

45. Kordes, E. E.; and Love, B. J.: Preliminary Evaluation of XB-70 Airplane Encounters With High Altitude Turbulence, NASA TN D-4209, October 1967.

46. Bray, R. S.; and Larsen, W. E.: Simulator Investigations of the Problems of Flying a Swept-Wing Transport in Heavy Turbulence, Conference on Aircraft Operating Problems, NASA SP-83, 1965.

47. Andrews, W. H.; Butchart, S. P.; Sisk, T. R.; and Hughes, D. L.: Flight Tests Related to Jet-Transport Upset and Turbulent-Air Penetration, Conference on Aircraft Operating Problems, NASA SP-83, 1965.

48. Ruzicka, J. E.: Active Vibration and Shock Isolation, SAE Transactions, vol. 77, 1969, pp 2872-2886.

49. Schubert, D. W.; and Ruzicka, J. E.: Theoretical and Experimental Investigation of Electrohydraulic Vibration Isolation Systems, Transactions ASME, Journal of Engineering for Industry, vol. 91, Series B, No. 4, November 1969, pp 981-990.

50. Calcaterra, P. C.; and Schubert, D. W.: Active Vibration Isolation of Human Subjects from Severe Dynamic Environments, ASME Paper No. 69-Vibr-65.

51. D'Azzo, J. J.; and Houpis, C. H.: Feedback Control System Analysis and Synthesis, 1960, McGraw-Hill Book Co., Inc.

52. Calcaterra, P. C.; and Schubert, D. W.: Research on Active Vibration Isolation Techniques for Aircraft Pilot Protection, AMRL-TR-67-138, March 1967.

53. Pepi, J. S.: Active Vibration Isolation of Aerial Cameras, 1968 Proceedings of the Institute of Environmental Sciences, page 389, April 1968.

54. Calcaterra, P. C.; and Schubert, D. W.: Isolation of Helicopter Rotor-Induced Vibrations Using Active Elements, USAAVLABS Technical Report 69-8, April 1969.

TABLE I

SUMMARY OF DOMINANT RESPONSE CHARACTERISTICS AT PILOT STATION PREDICTED FOR REPRESENTATIVE SUBSONIC COMMERCIAL JET TRANSPORT DURING TURBULENT FLIGHT

Direction of Excitation	Rigid Body Resonant Frequency, Hz	Bandwidth of Rigid Body Resonance Analysis, Hz	Acceleration at Rigid Body Resonance g_{rms}	Average Dominant Fuselage Bending Mode Frequency Hz	Bandwidth of Dominant Bending Mode Analysis, Hz	Acceleration at Dominant Bending Mode, g_{rms}
Normal	0.35	0.2-0.6	0.28	4.7	3.5-5.5	0.18
Transverse	0.45	0.2-0.7	0.05	5.5	3.7-7.2	0.05

TABLE II

VIBRATION INTERFERENCE AND ANNOYANCE RATING SCALE

Numerical Rating	Description
1	Excellent
2	Good, pleasant to fly
3	Satisfactory, but with some mildly unpleasant characteristics
4	Acceptable, but with unpleasant characteristics
5	Unacceptable for normal operation
6	Acceptable for emergency operation
7	Unacceptable even for emergency conditions
8	Unacceptable - dangerous
9	Unacceptable - uncontrollable
10	Completely unacceptable - catastrophic

TABLE III

AVERAGE SUBJECTIVE REACTIONS OF TEST SUBJECT A TO EFFECTS OF VERTICAL SINUSOIDAL EXCITATION OF ELECTROHYDRAULIC PILOT SEAT ISOLATION SYSTEM AND COCKPIT SIMULATOR

Excitation	Vibration Annoyance Rating		Vibration Interference Rating	
	Active System Off	Active System On	Active System Off	Active System On
0.04g @ 2 Hz	5.5	5	4.5	4
0.09g @ 3 Hz	6	6	5	5
0.25g @ 4.2 Hz	9	4.8	7.7	6
0.09g @ 6 Hz	5	4	4	4
0.09g @ 9 Hz	5	4	4	4
0.09g @ 12 Hz	5	3	4	4.5

TABLE IV

AVERAGE SUBJECTIVE REACTIONS OF TEST SUBJECT B TO EFFECTS OF VERTICAL SINUSOIDAL EXCITATION OF ELECTROHYDRAULIC PILOT SEAT ISOLATION SYSTEM AND COCKPIT SIMULATOR

Excitation	Vibration Annoyance Rating		Vibration Interference Rating	
	Active System Off	Active System On	Active System Off	Active System On
0.04g @ 2 Hz	4	5	4	5
0.09g @ 3 Hz	5	6	5	6
0.25g @ 4.2 Hz	8	3	8	3
0.09g @ 6 Hz	5	4	5	4
0.09g @ 9 Hz	4.7	4	5	4
0.09g @ 12 Hz	4.7	4	4.7	3

TABLE V

AVERAGE SUBJECTIVE REACTIONS OF TEST SUBJECT A TO EFFECTS OF VERTICAL RANDOM EXCITATION OF ELECTROHYDRAULIC PILOT SEAT ISOLATION SYSTEM AND COCKPIT SIMULATOR

RMS Acc. 3.9-5.1 Hz	RMS Acc. 2-15 Hz	Vibration Annoyance Rating		Vibration Interference Rating	
		Active System Off	Active System On	Active System Off	Active System On
0.05	0.13	4	4	3.2	3
0.07	0.19	5	4	4.8	4
0.1	0.27	6	3	5.2	4

TABLE VI

AVERAGE SUBJECTIVE REACTIONS OF TEST SUBJECT B TO EFFECTS OF VERTICAL RANDOM EXCITATION OF ELECTROHYDRAULIC PILOT SEAT ISOLATION SYSTEM AND COCKPIT SIMULATOR

RMS Acc. 3.9-5.1 Hz	RMS Acc. 2-15 Hz	Vibration Annoyance Rating		Vibration Interference Rating	
		Active System Off	Active System On	Active System Off	Active System On
0.05	0.13	5	3	5	3
0.07	0.19	6	3	6	3
0.1	0.27	7.3	4	7.3	4

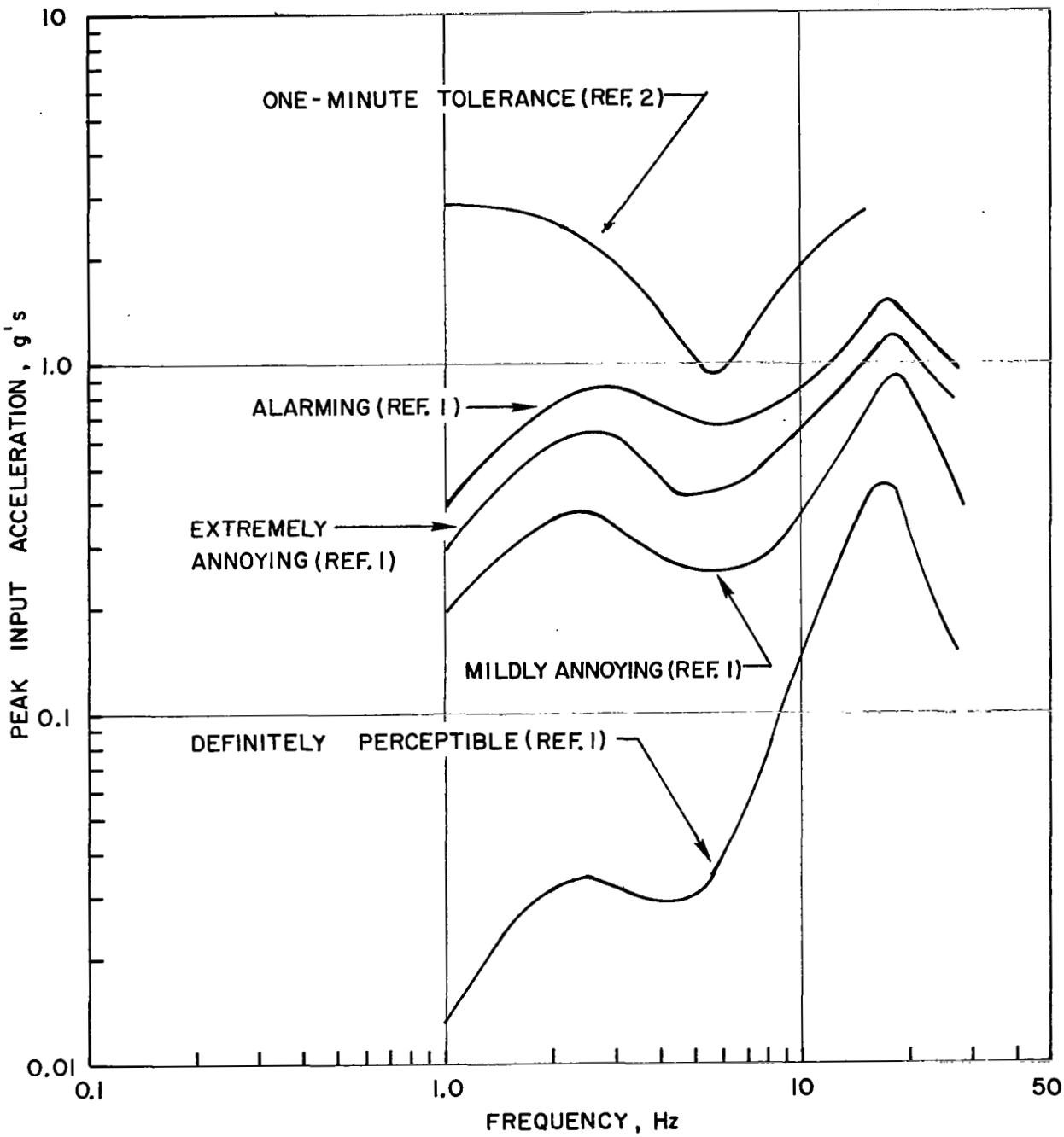

Figure 1: Vertical Sinusoidal Vibration Tolerance Levels of Seated Human Subjects

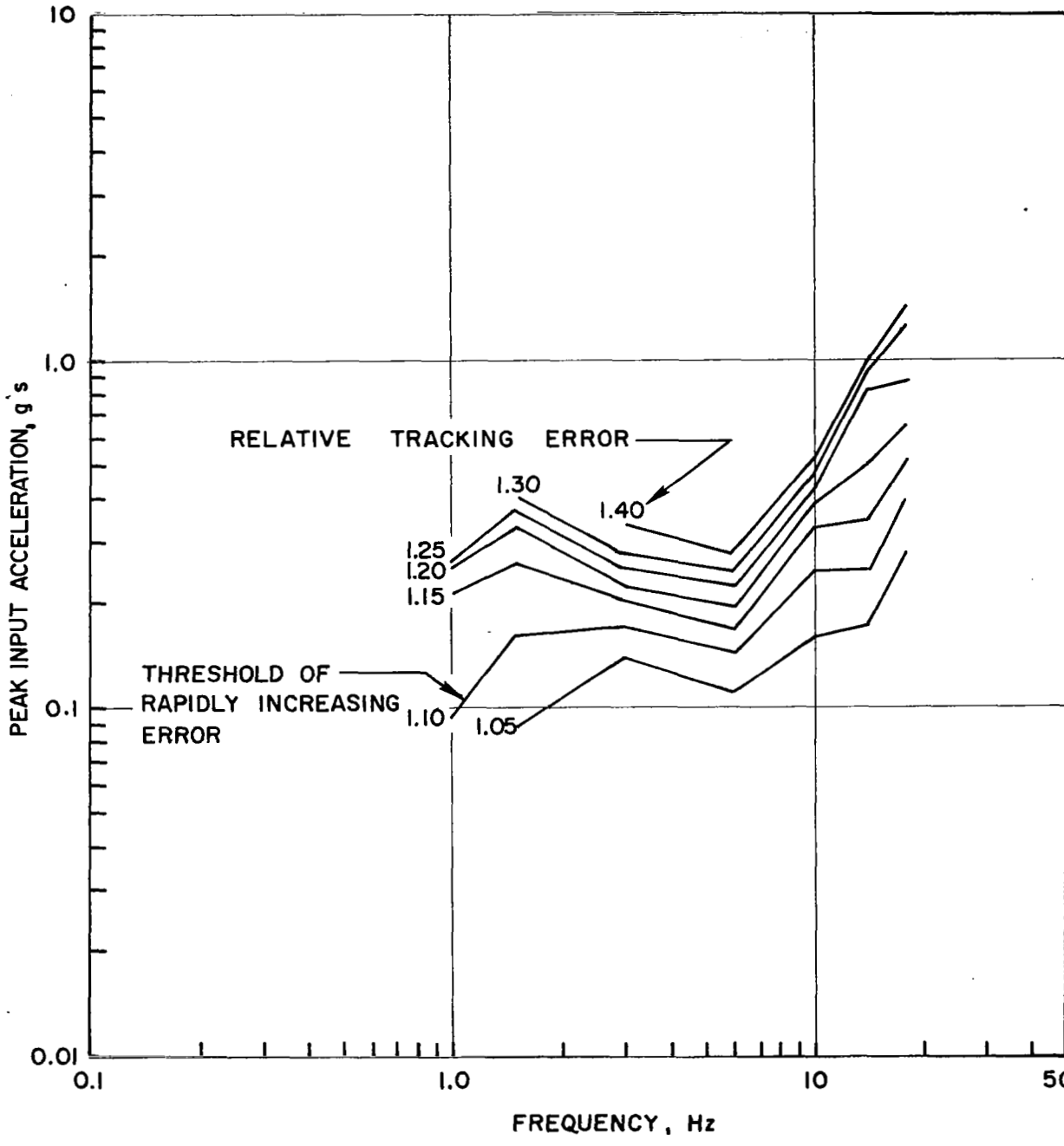

Figure 2: Relative Wheel Tracking Error as a Function of the Amplitude and Frequency of Vertical Sinusoidal Vibration (After Ref. 11)

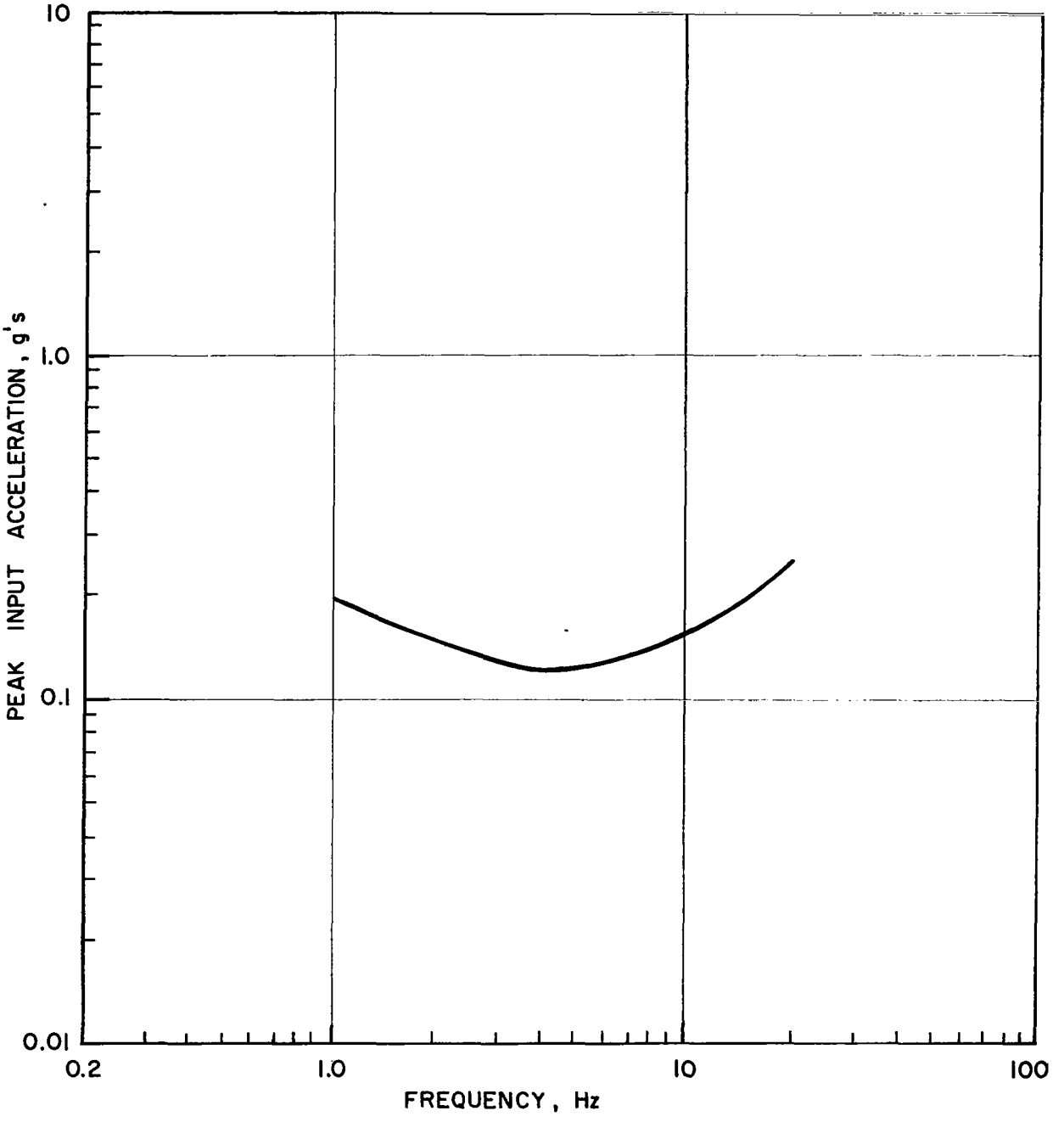

Figure 3: One-Hour Endurance Threshold Curve With Minimal Reduction in Tracking Performance For Seated Human Subjects Being Subjected to Vertical Sinusoidal Vibration (After Ref. 15)

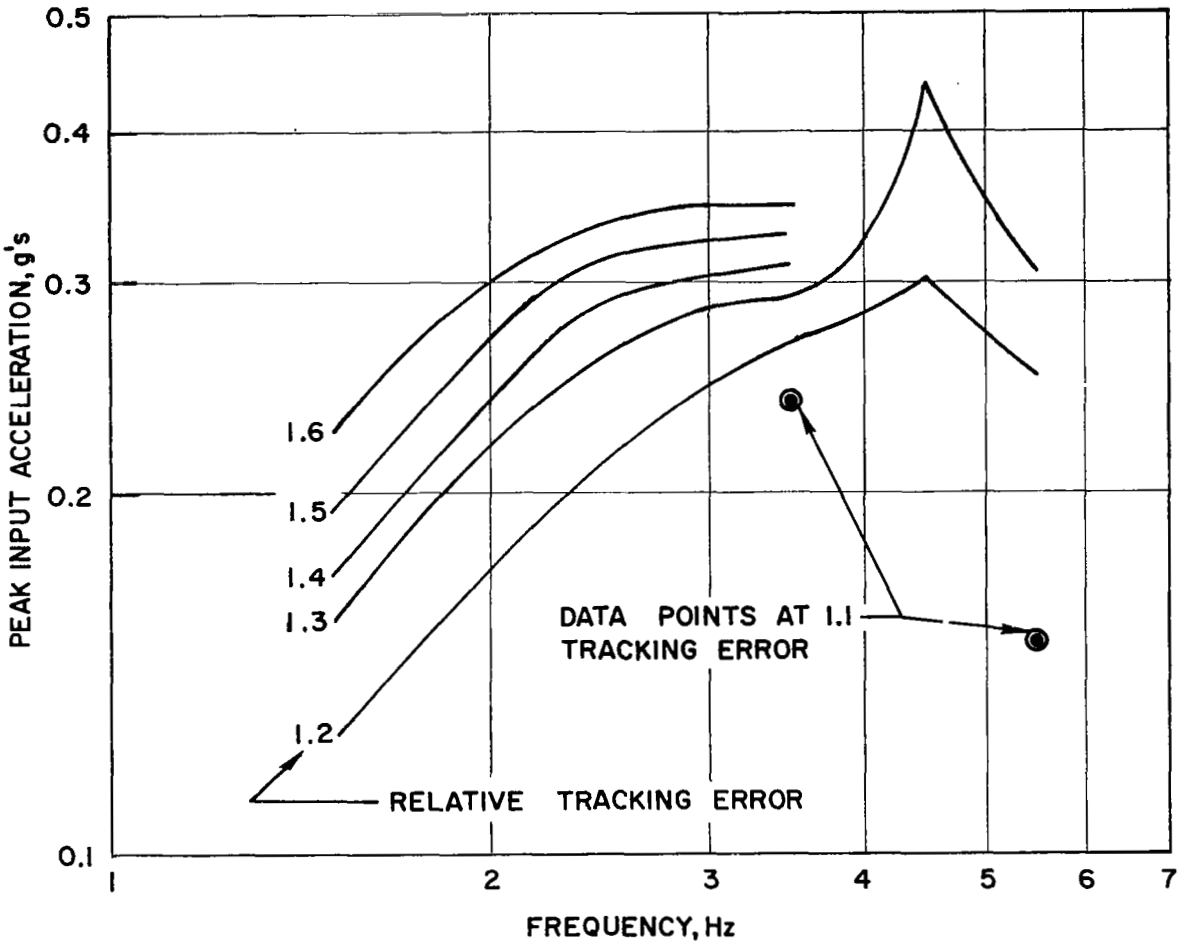

Figure 4: Relative Wheel Tracking Error as a Function of the Amplitude and Frequency of Transverse Sinusoidal Excitation (After Ref. 16)

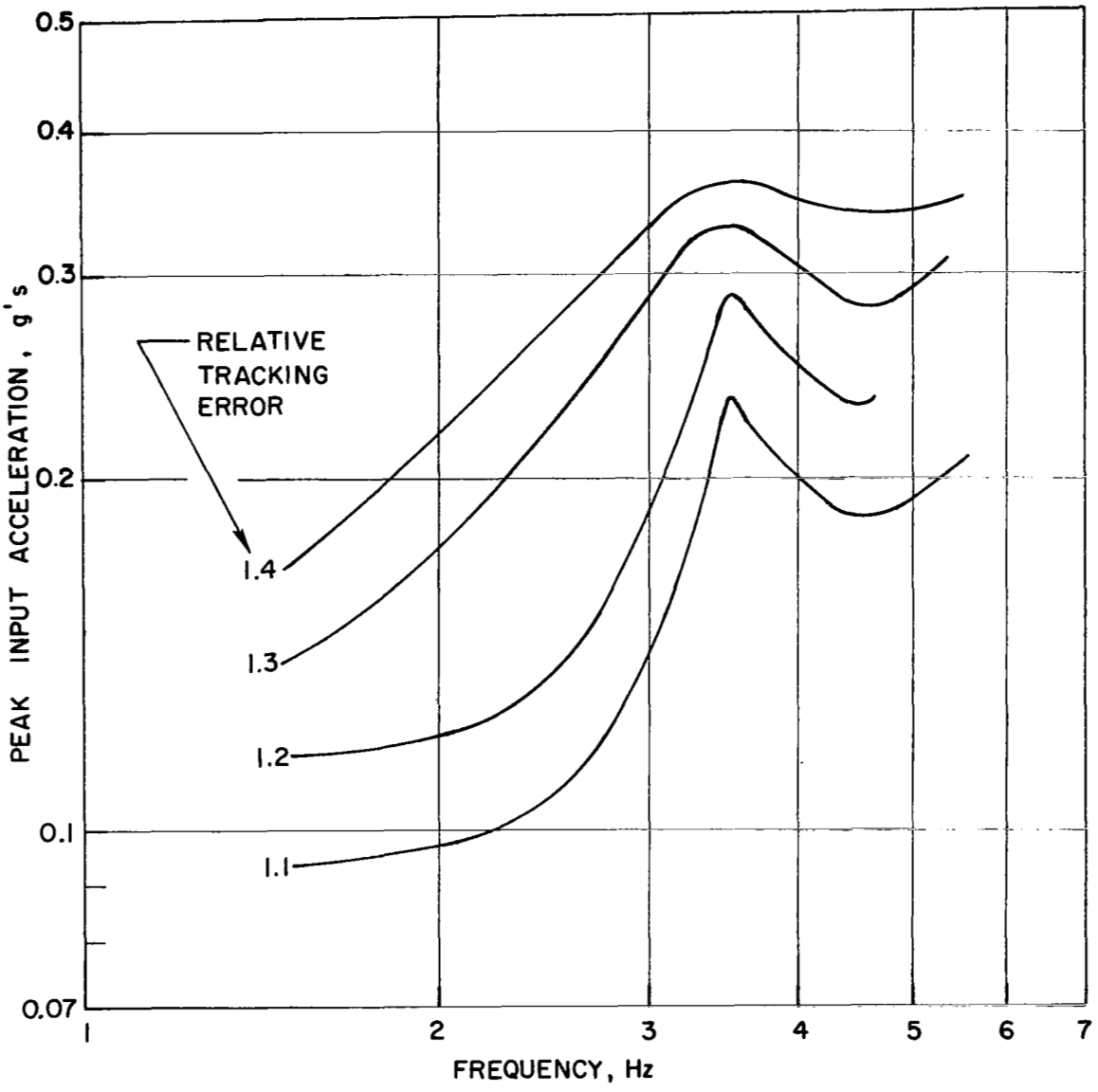

Figure 5: Relative Foot Tracking Error as a Function of the Amplitude and Frequency of Transverse Sinusoidal Vibration (After Ref. 16)

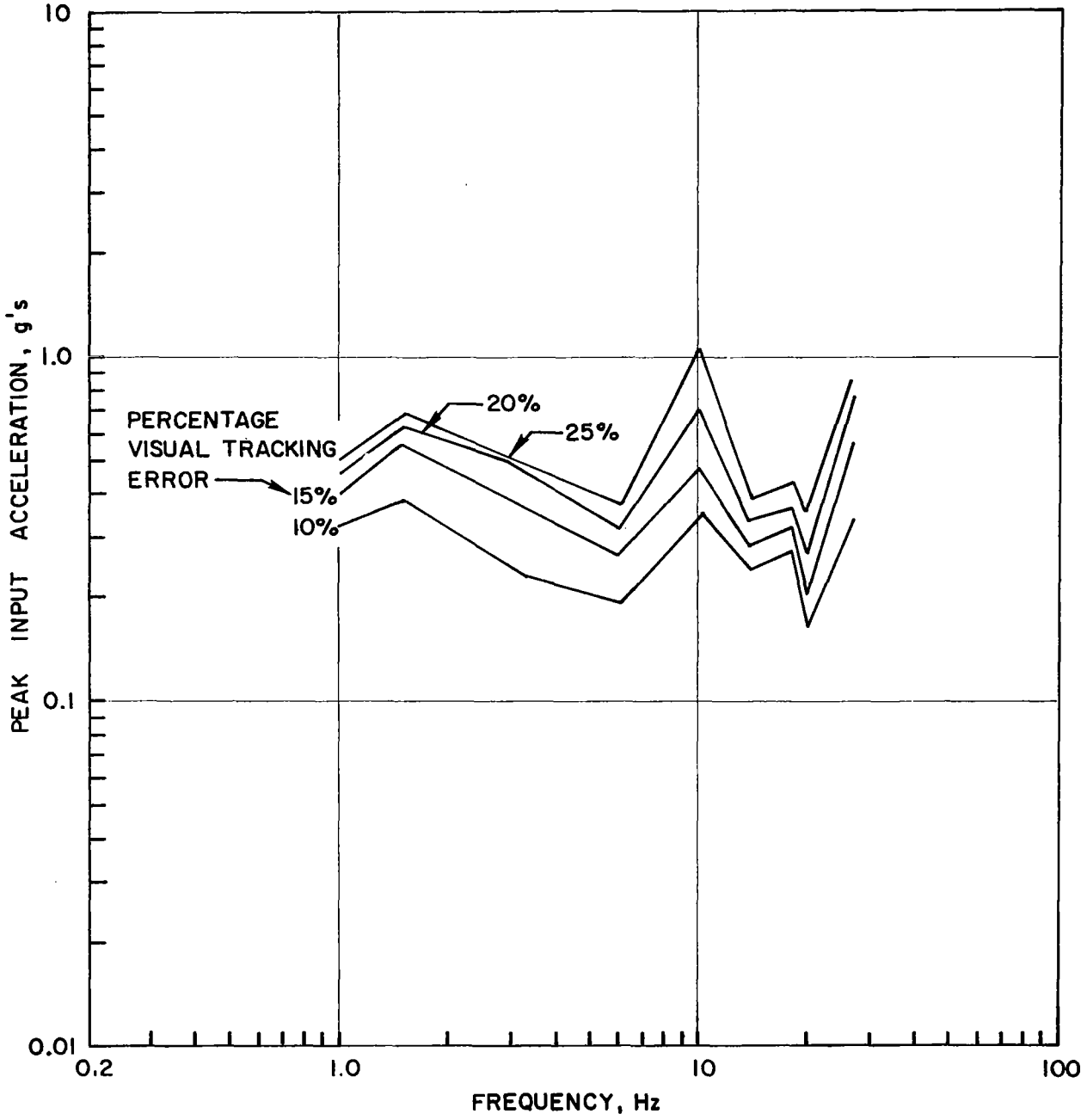

Figure 6: Constant Percentage Visual Tracking Error as a Function of the Amplitude and Frequency of Vertical Sinusoidal Vibration (After Ref. 17)

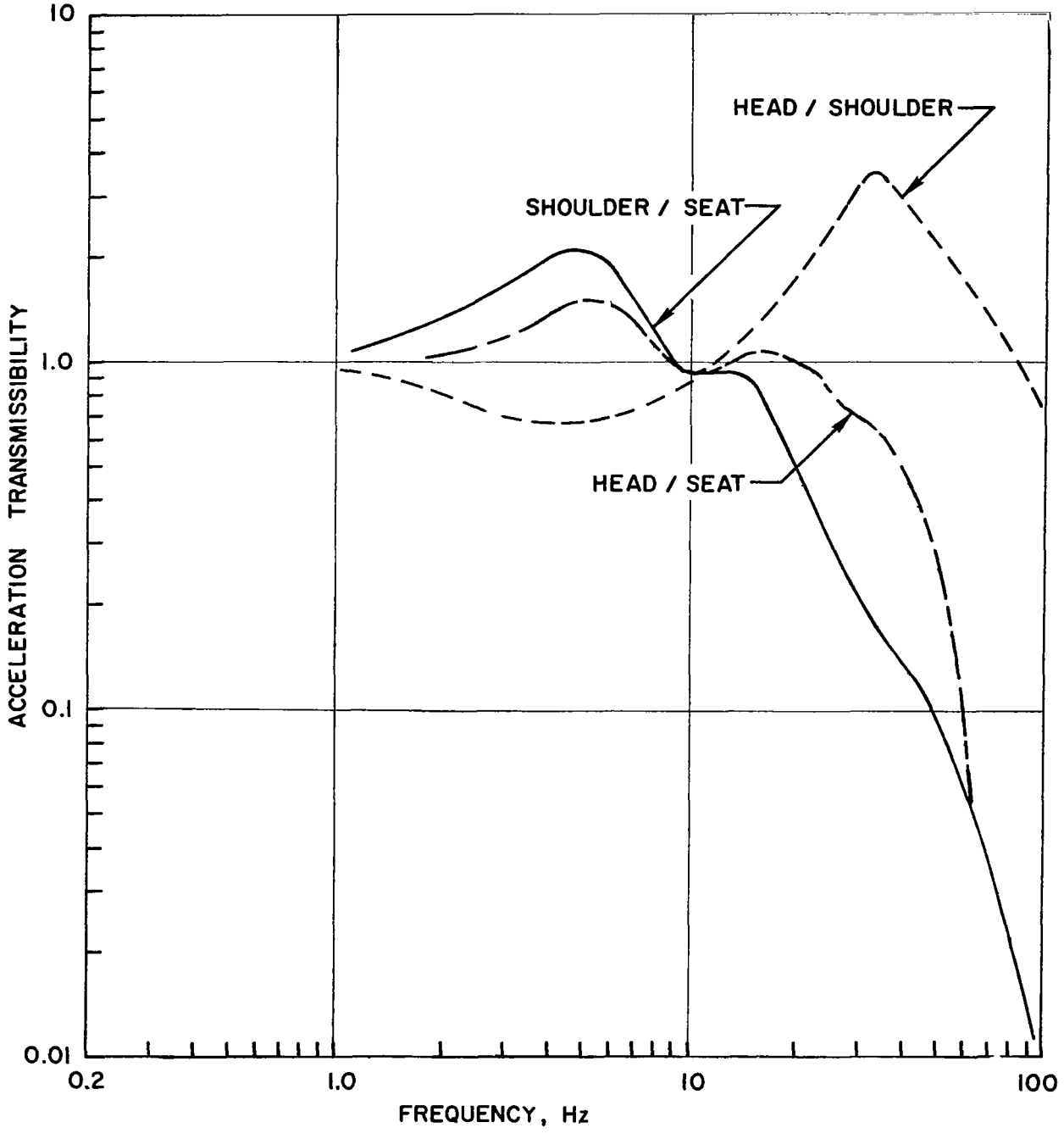

Figure 7: Average Vertical Acceleration Transmissibilities From Rigid Seat to Various Parts of the Body and Between Parts of Body For Seated Human Subject (After Ref. 23 and 24)

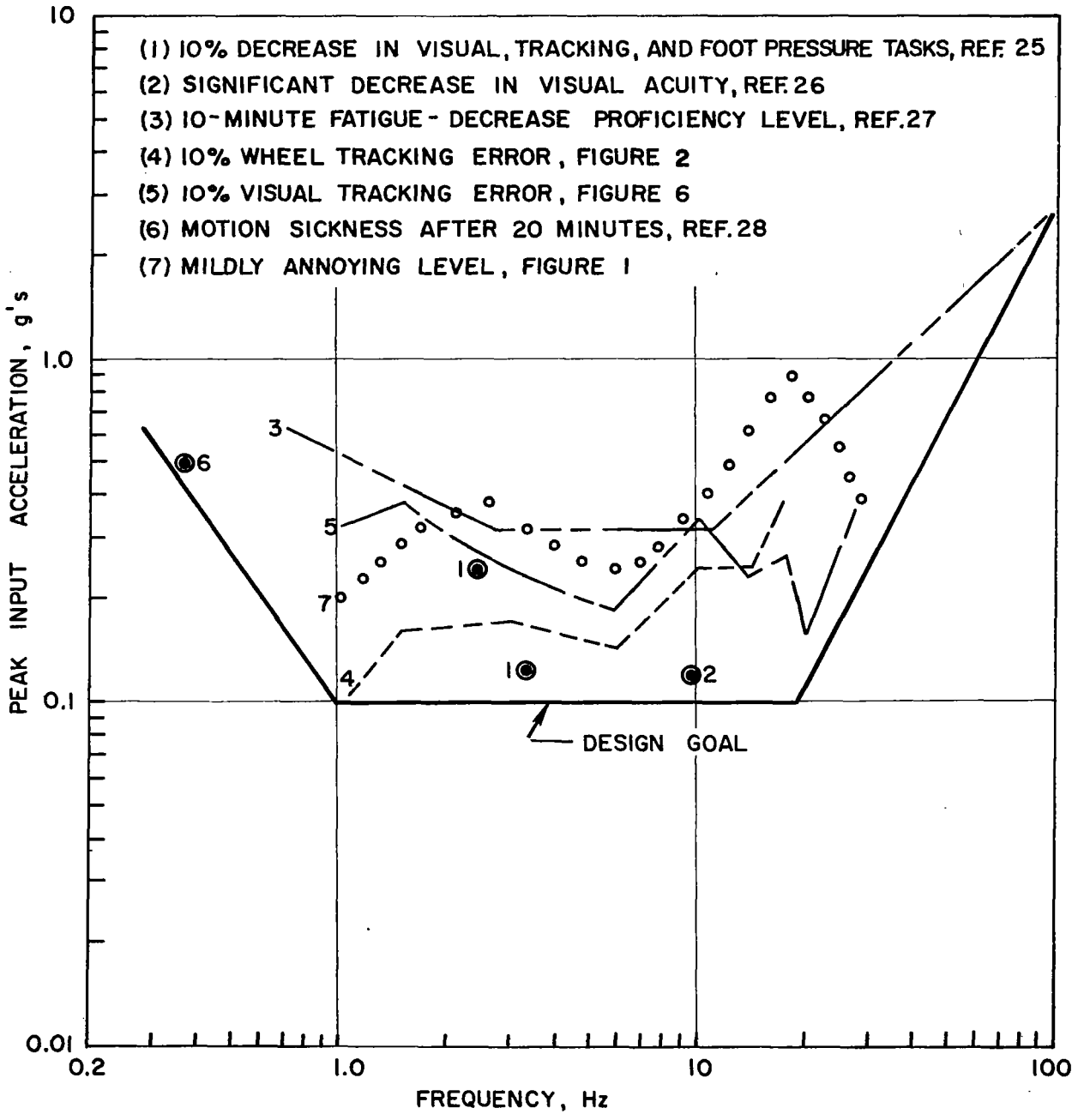

Figure 8: Design Goal For Maximum Vertical Sinusoidal Vibration Levels Which Should be Transmitted to Commercial Jet Transport Pilots

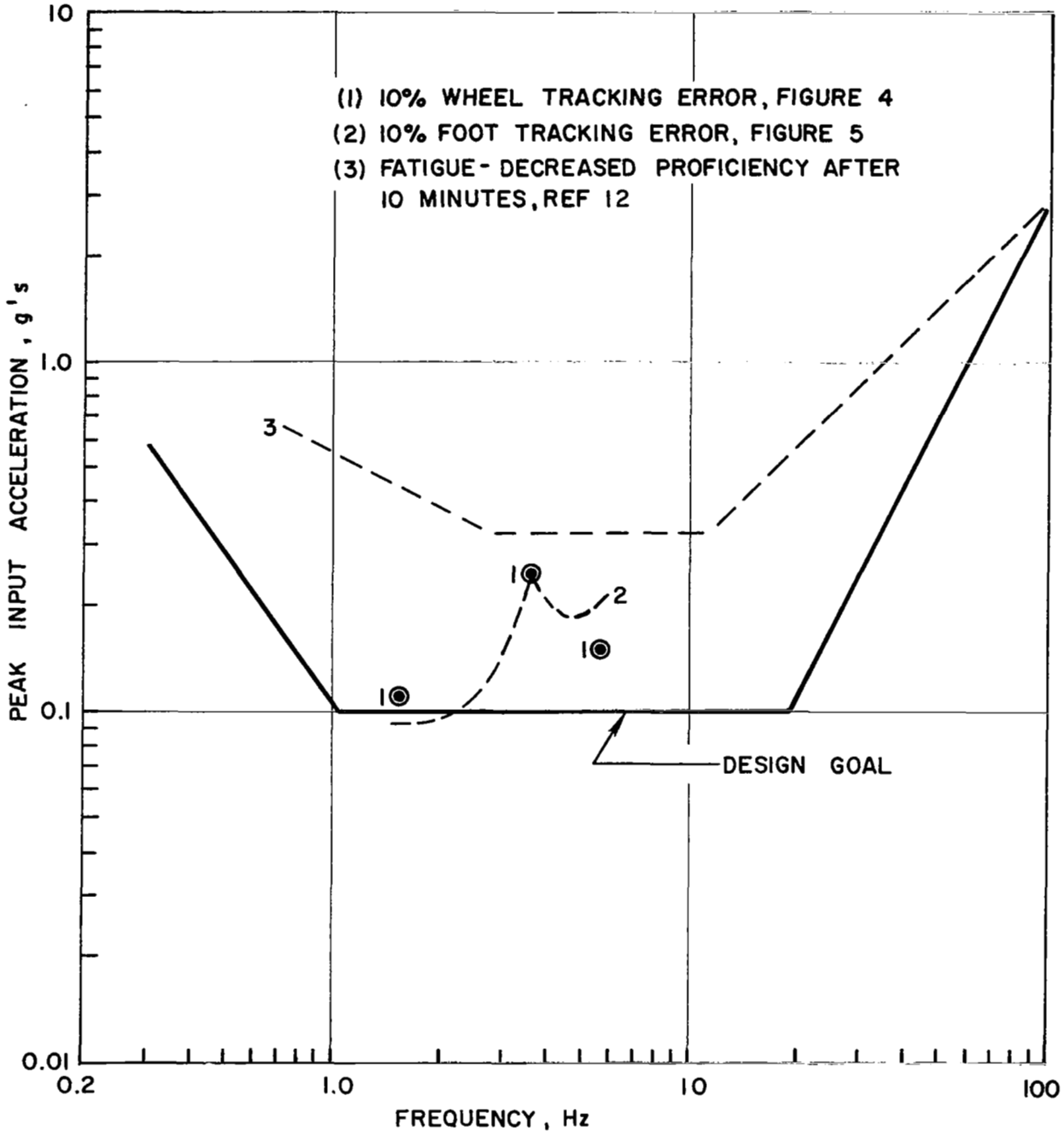

Figure 9: Design Goal For Maximum Transverse Sinusoidal Vibration Level Which Should be Transmitted to Commercial Jet Transport Pilots

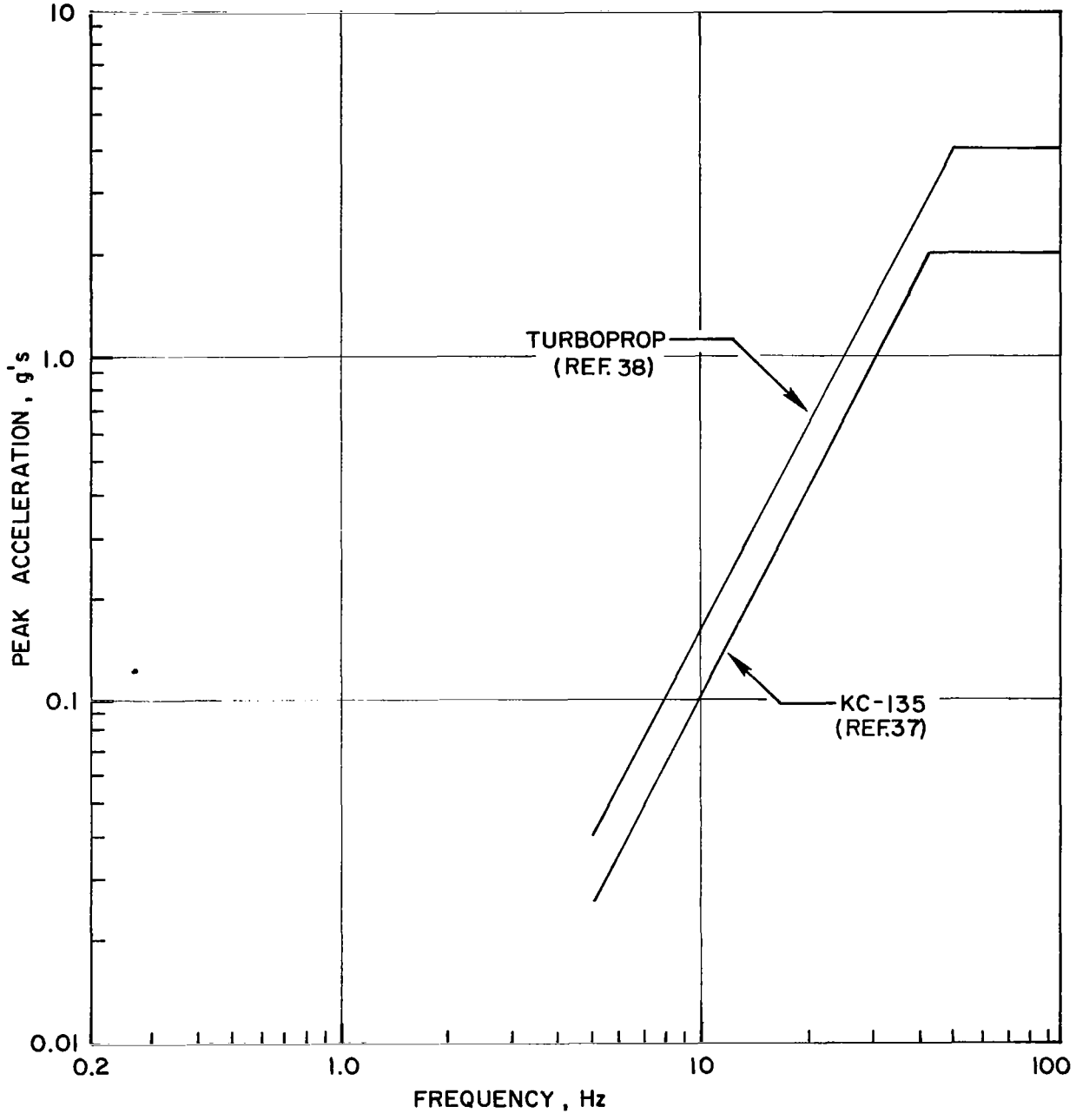

Figure 10: Envelope of Transverse and Normal Equivalent Sinusoidal Vibrations Monitored on Fuselage of Jet Transport Aircraft During Normal Cruise Conditions

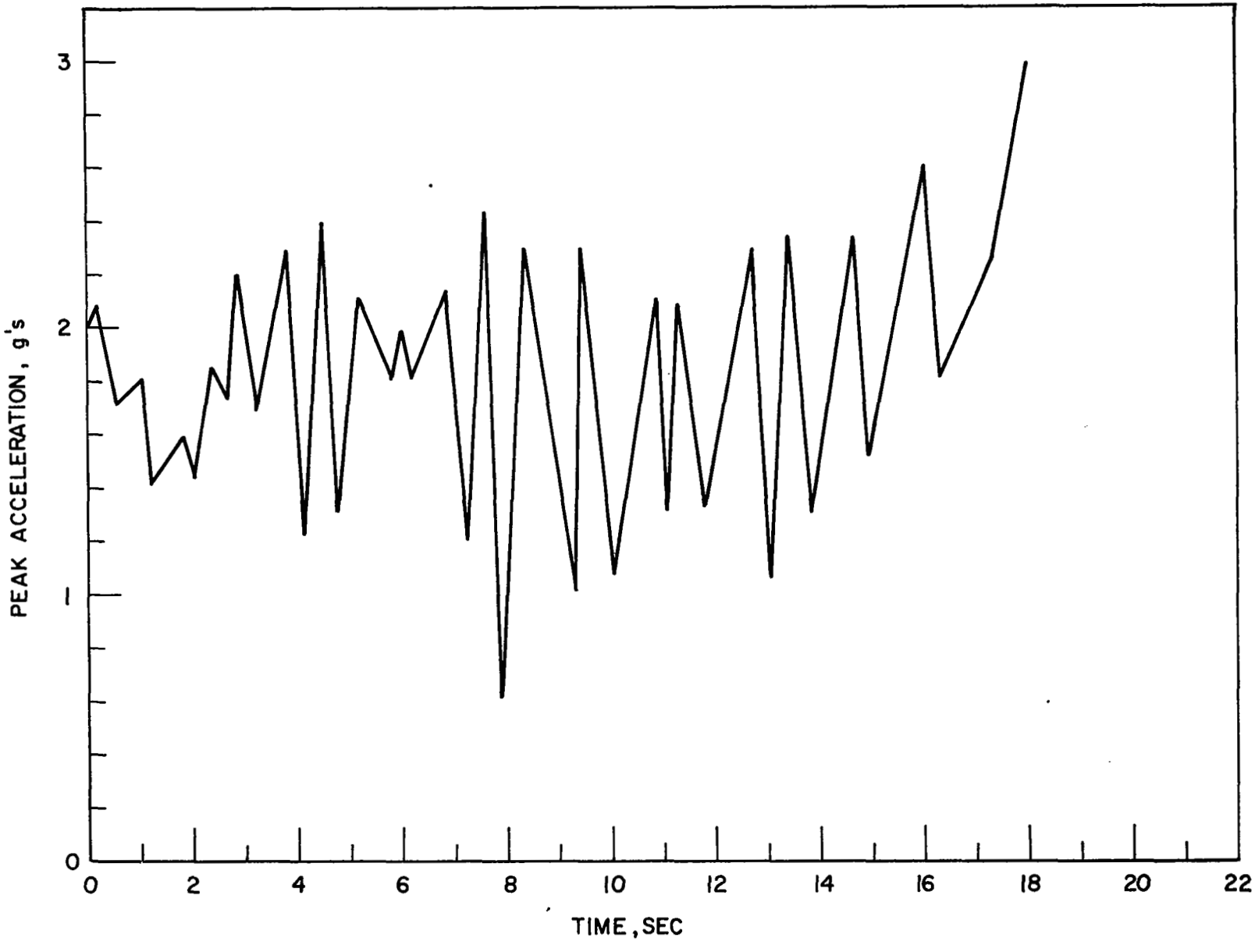

Figure 11: Normal Acceleration Time Response at CG of Jet Airliner During Heavy Buffet

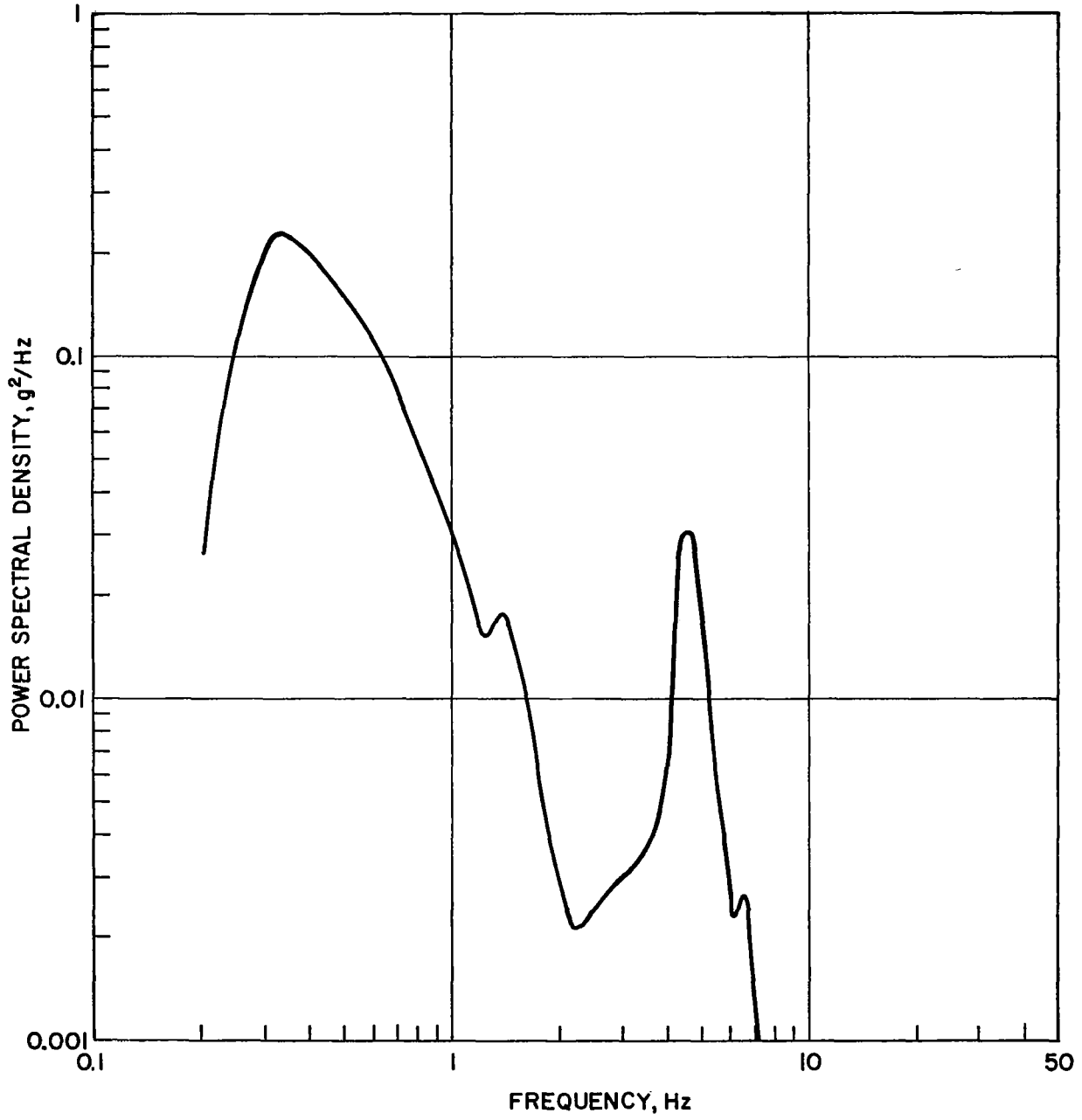

Figure 12: Spectral Density of Maximum Normal Vibrations Expected at Pilot's Cabin of Subsonic Commercial Jet Transport During Turbulent Flight (rms gust velocity = 20 ft/sec)

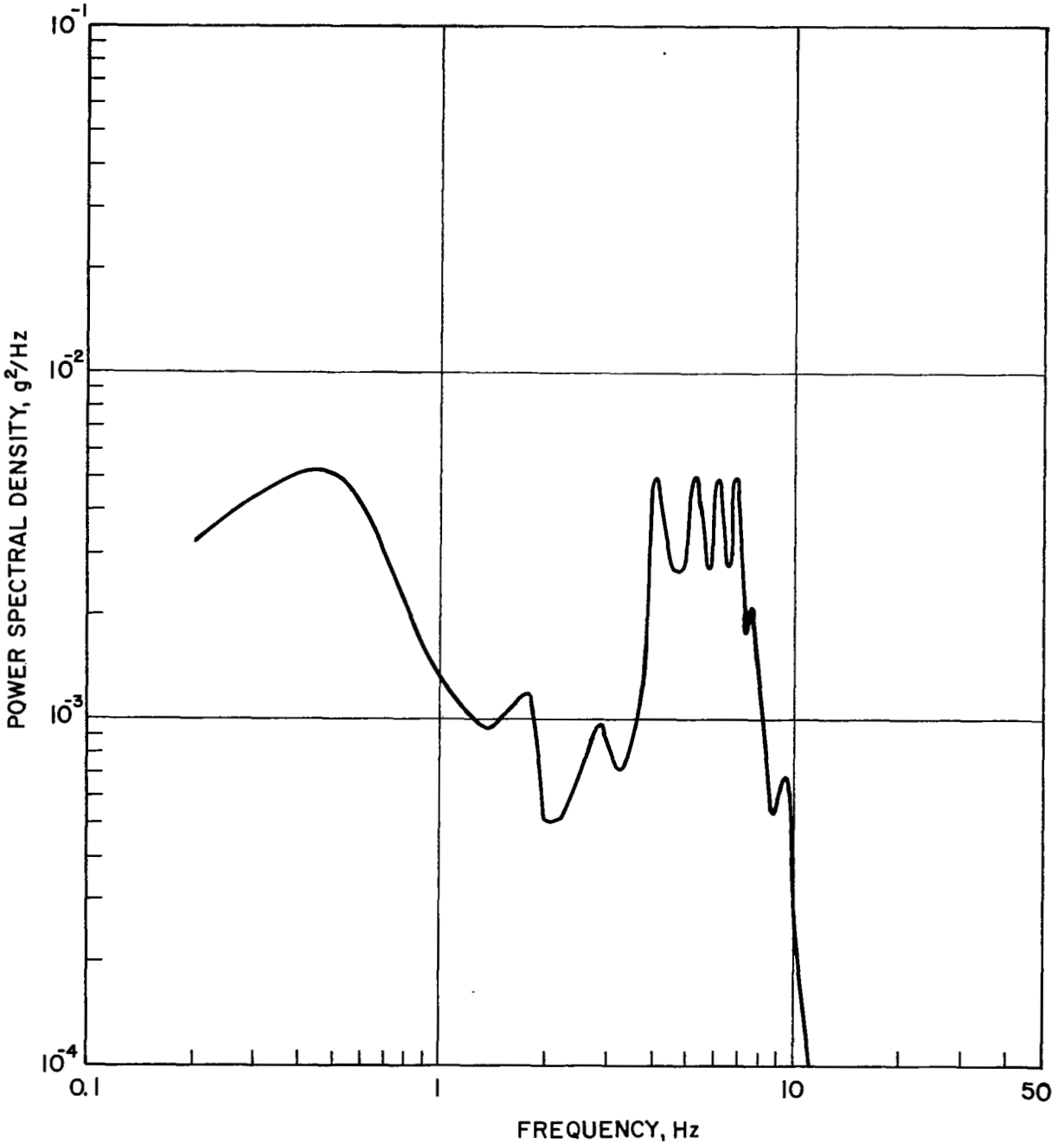

Figure 13: Spectral Density of Maximum Transverse Vibrations Expected at Pilot's Cabin of Subsonic Commercial Jet Transport During Turbulent Flight (rms gust velocity = 20 ft/sec)

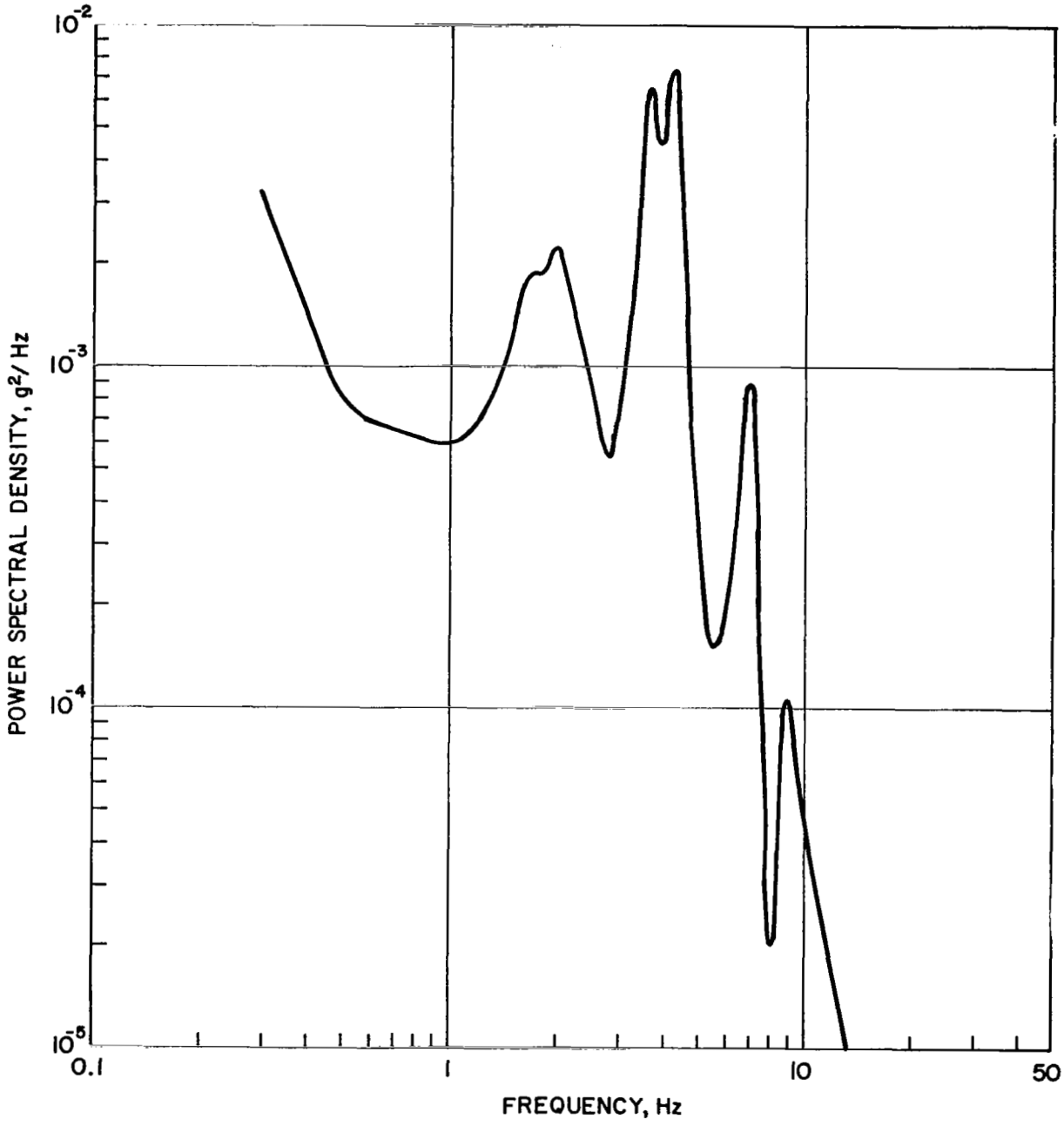

Figure 14: Spectral Density of Normal Vibrations Measured at Pilot's Cabin of the XB-70 in Clear Air Turbulence at 55,000 feet and Mach 2.4

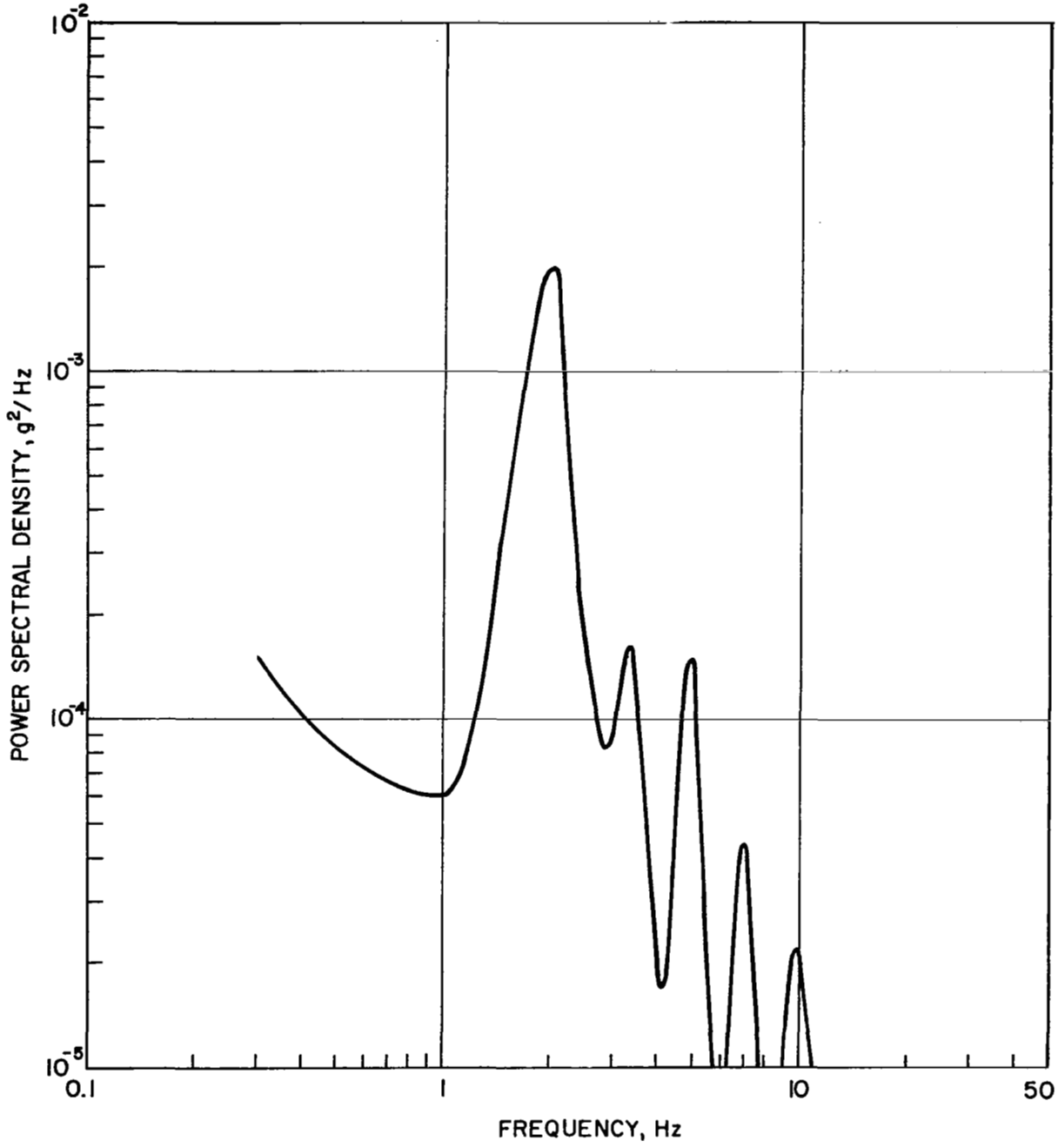

Figure 15: Spectral Density of Transverse Vibrations Measured at Pilot's Cabin of the XB-70 in Clear Air Turbulence at 55,000 feet and Mach 2.4

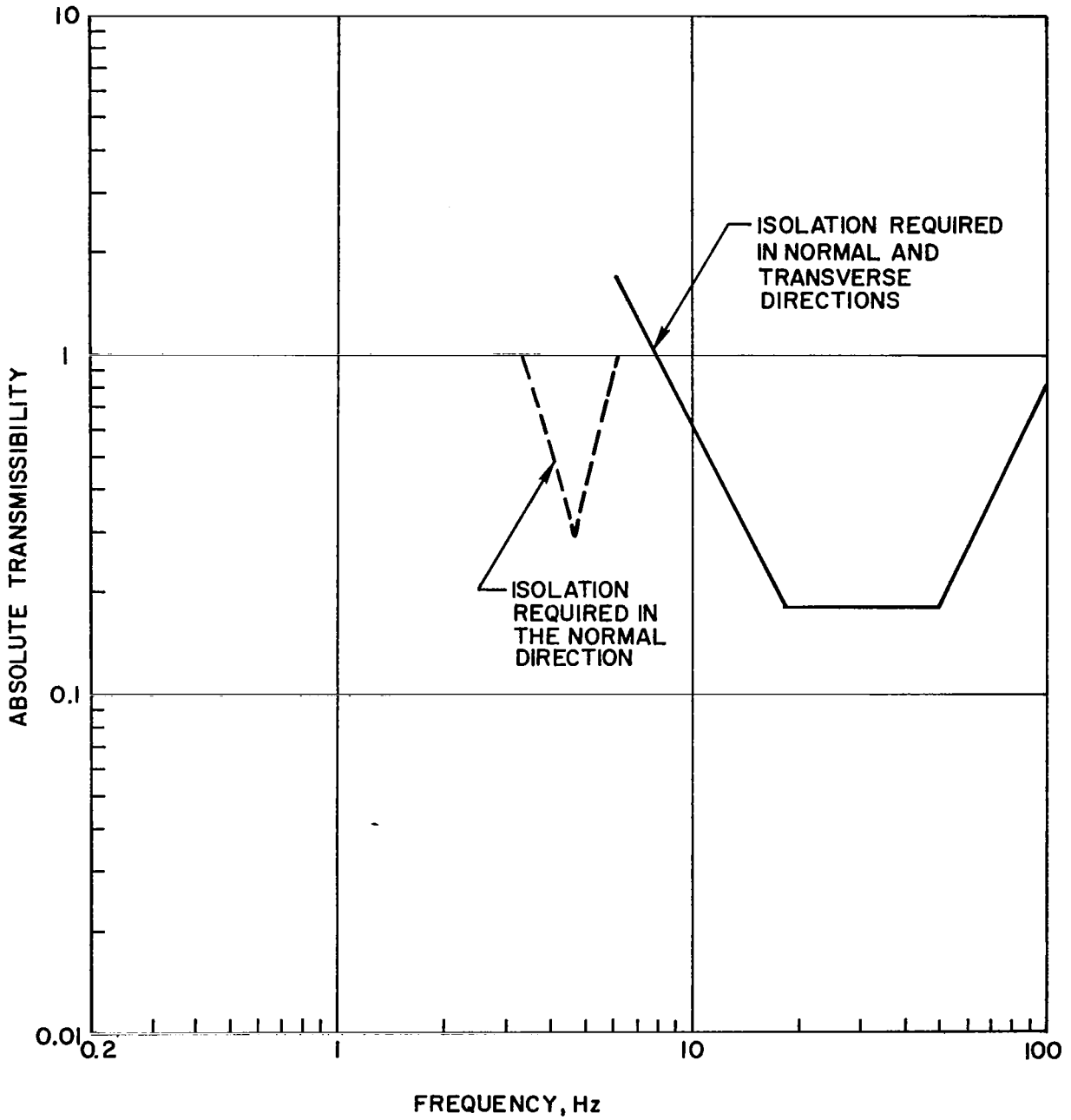

Figure 16: Maximum Allowable Transmissibility Required in Normal and Transverse Directions for Pilot Seat Isolation System

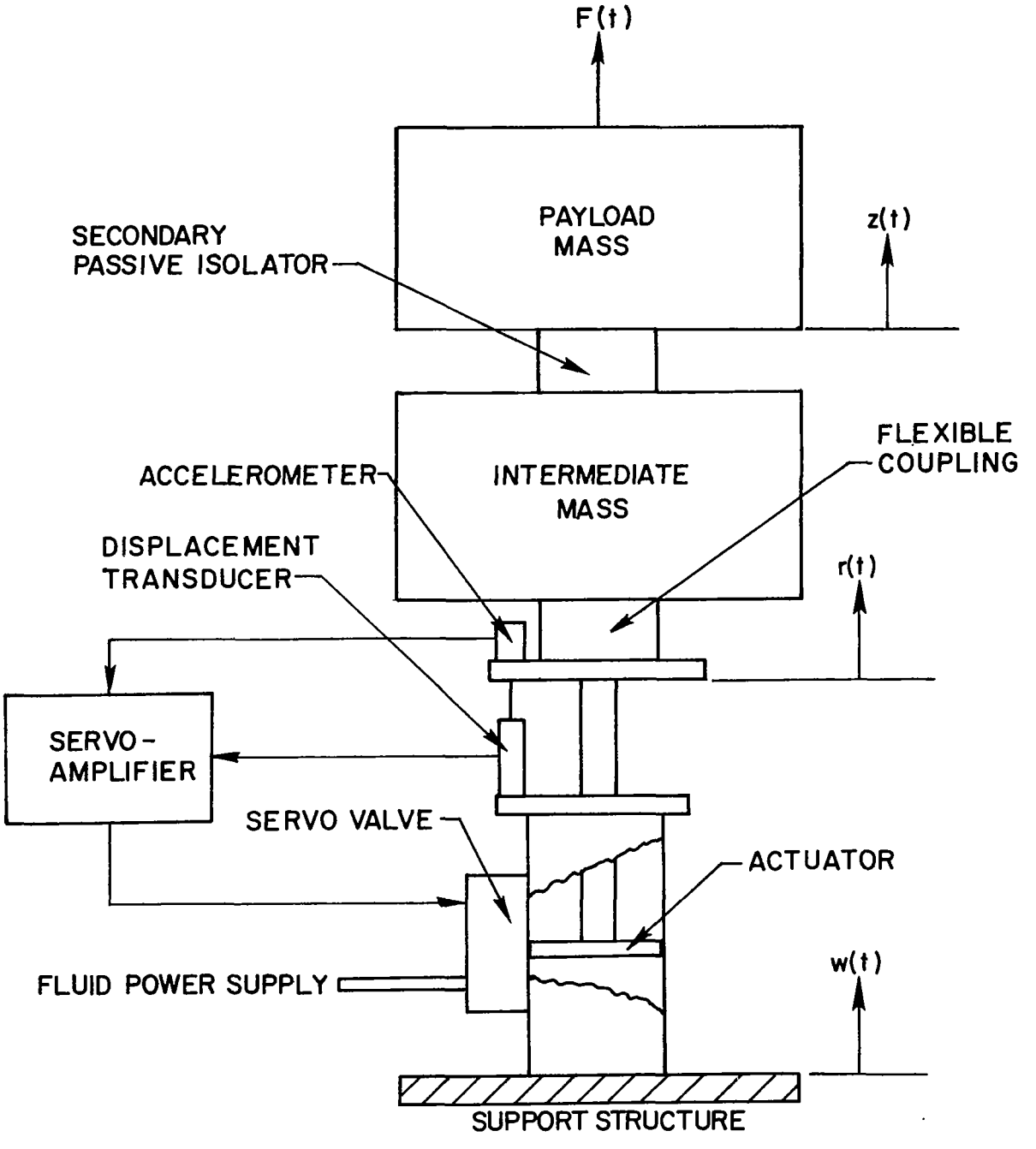

Figure 17: Schematic Diagram of Electrohydraulic Vibration Isolation System with Acceleration Feedback and Flexible Coupling Outside of Control Loop

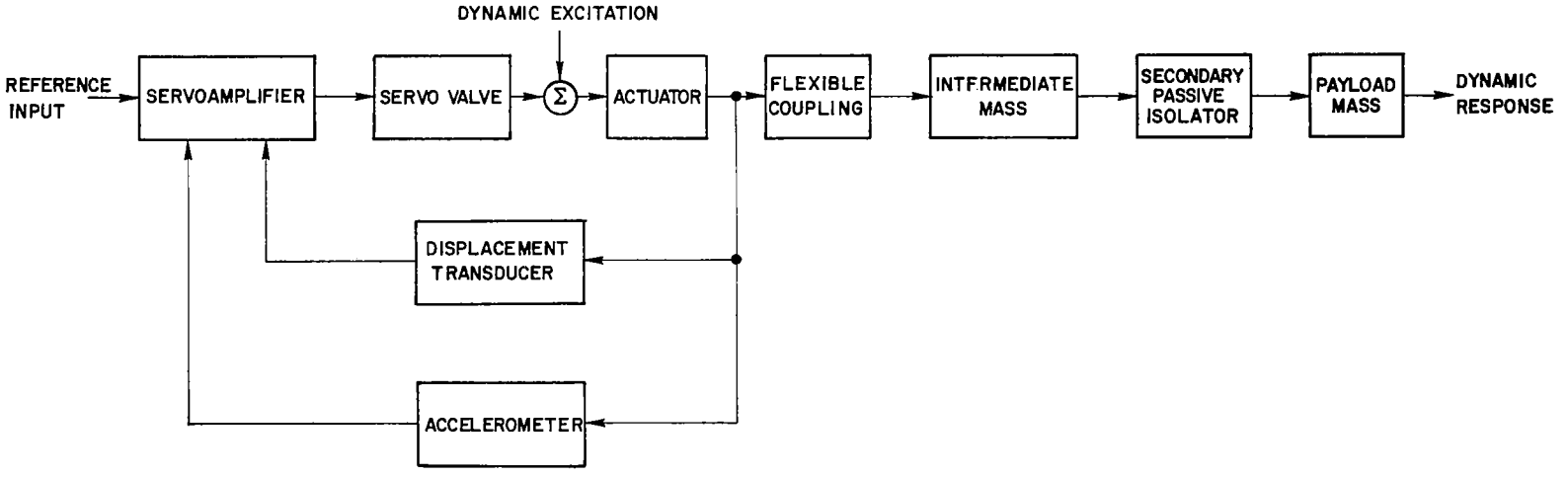

Figure 18 : Schematic Block Diagram of Electrohydraulic Vibration Isolation System with Flexible Coupling Outside of Control Loop

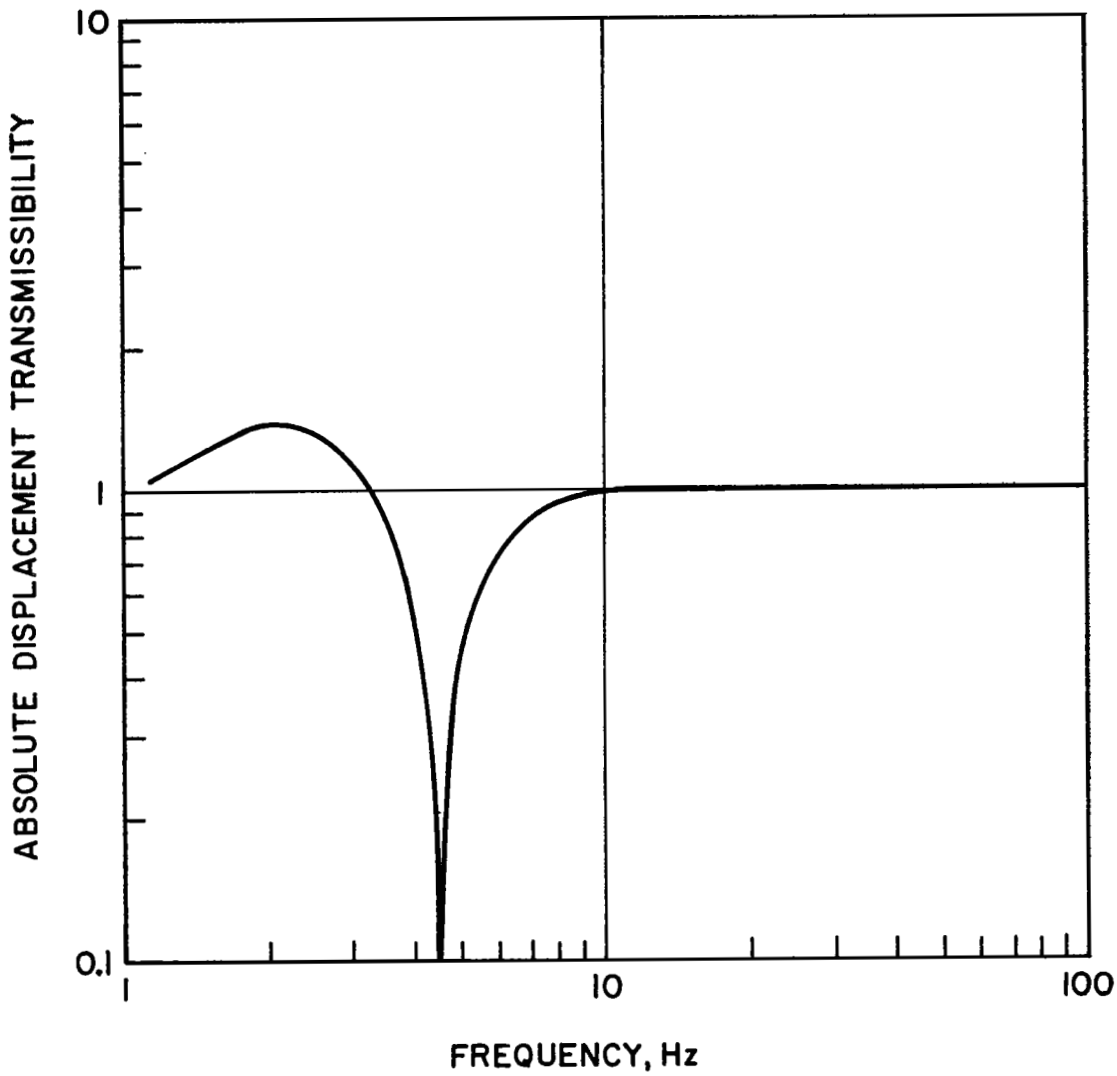

Figure 19: Absolute Displacement Transmissibility Associated with a Typical Notch Type Electrohydraulic Vibration Isolation System

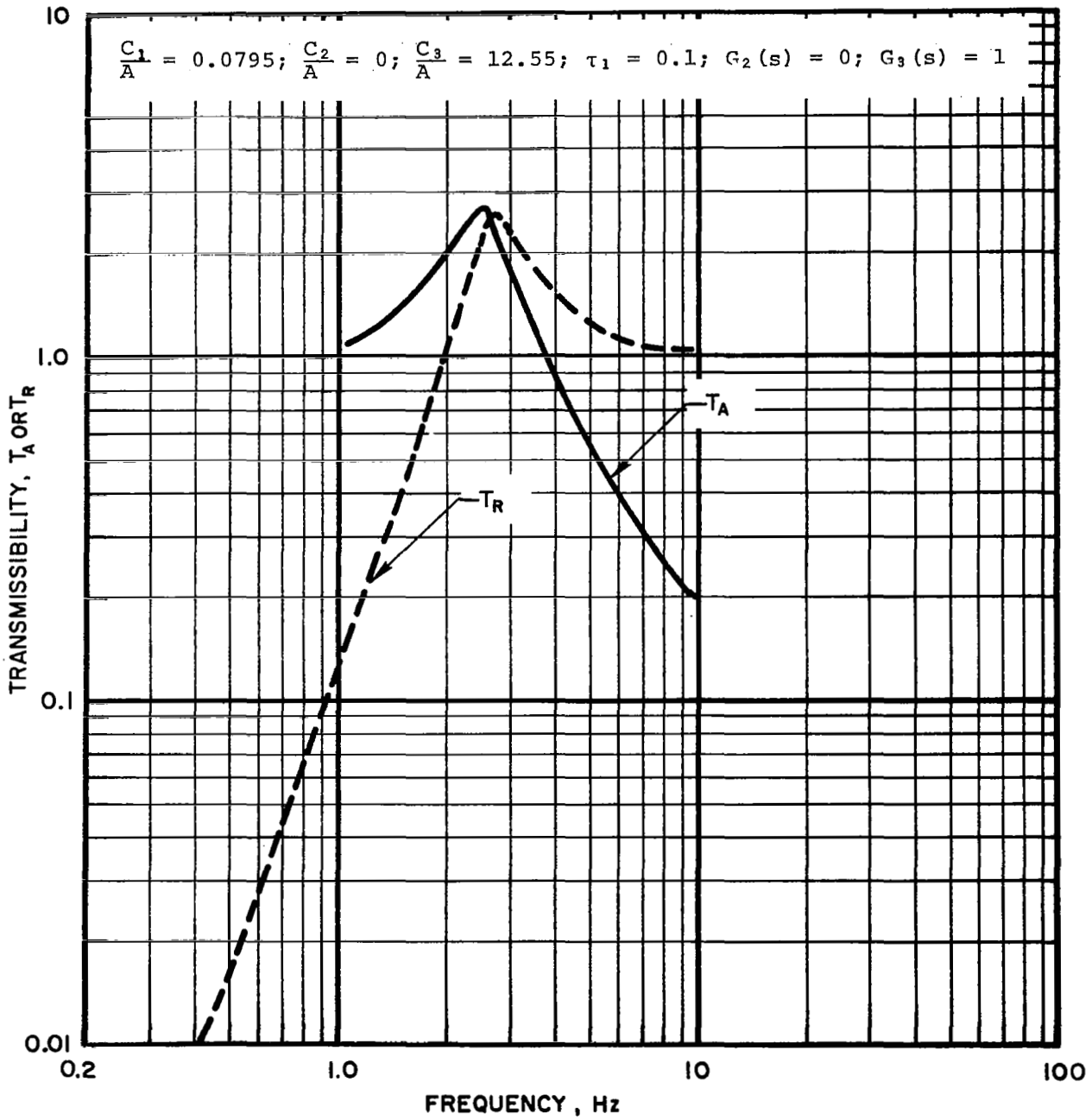

Figure 20: Theoretical Vertical Absolute and Relative Displacement Transmissibilities for a 2.5 Hz Resonant Frequency Electrohydraulic Broad-Band Isolation System With Rigid Payload

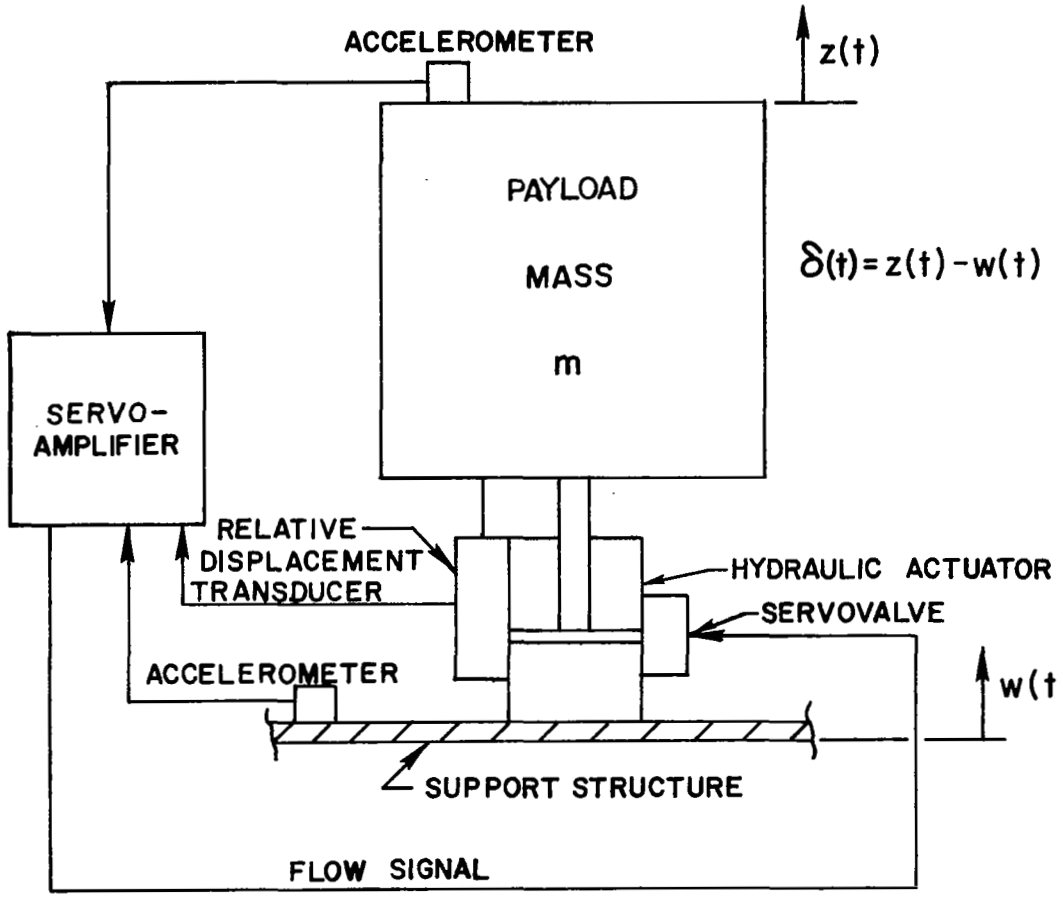

Figure 21: Schematic Diagram of Electrohydraulic Vibration Isolation System With Rigid Payload and Feedforward and Feedback Acceleration

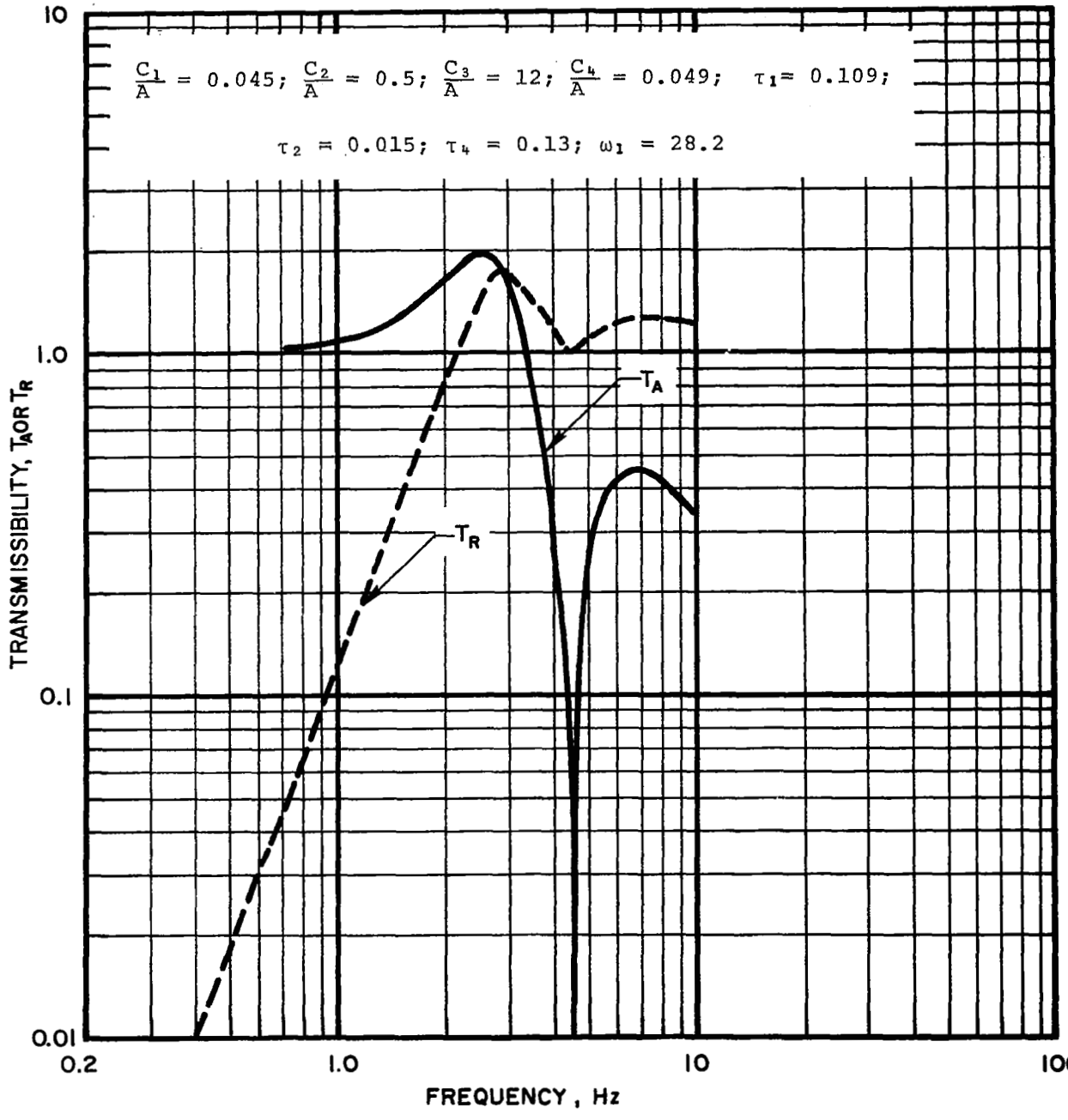

Figure 22: Theoretical Vertical Absolute and Relative Displacement Transmissibilities for a 2.5 Hz Resonant Frequency Electrohydraulic Broad-Band Plus Notch Isolation System With Rigid Payload

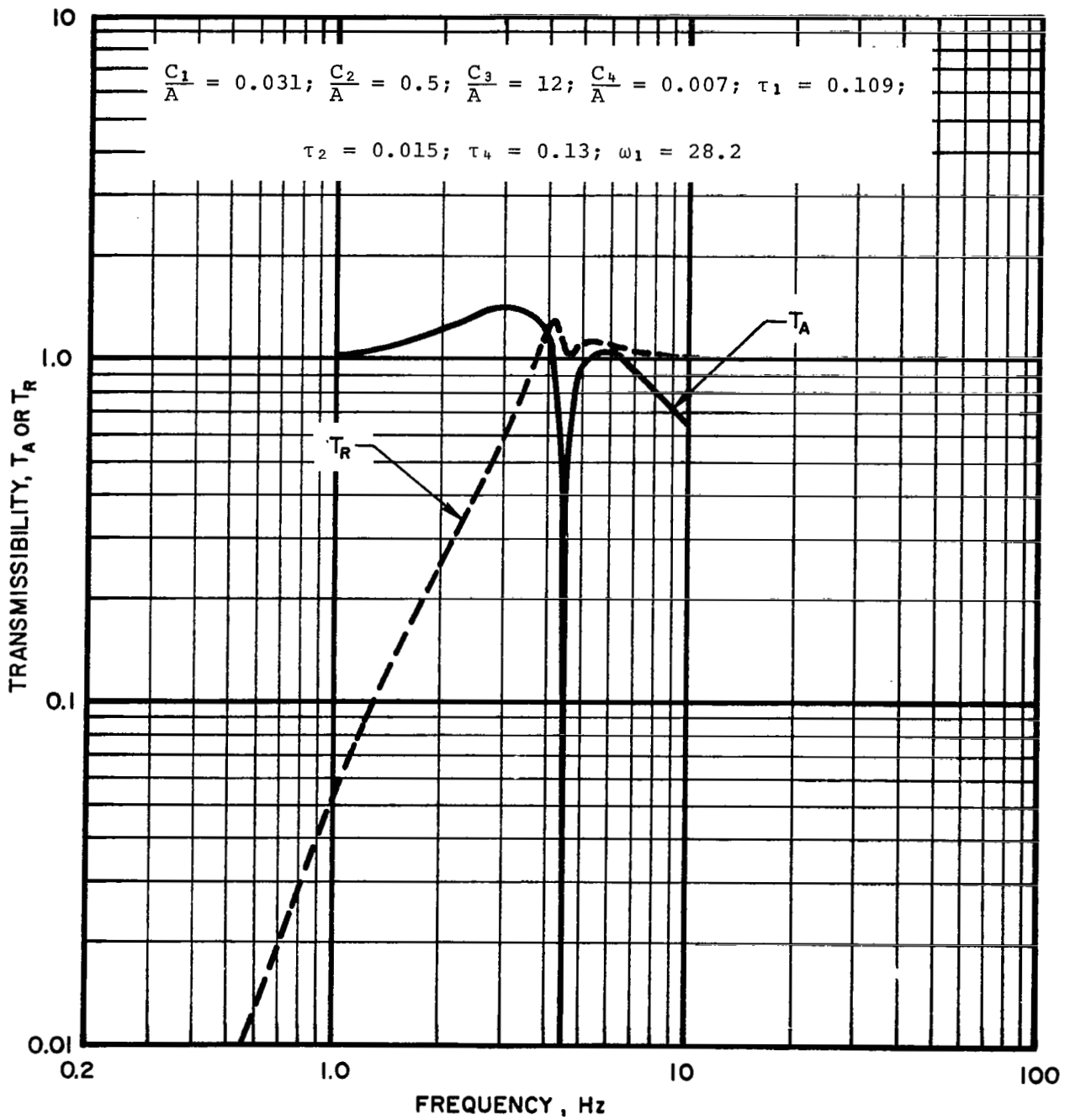

Figure 23: Theoretical Vertical Absolute and Relative Displacement Transmissibilities for Broad-Band Plus Notch Isolation System With Rigid Payload in Nonlinear Range (Small Relative Deflections About Mean Position in Nonlinear Range)

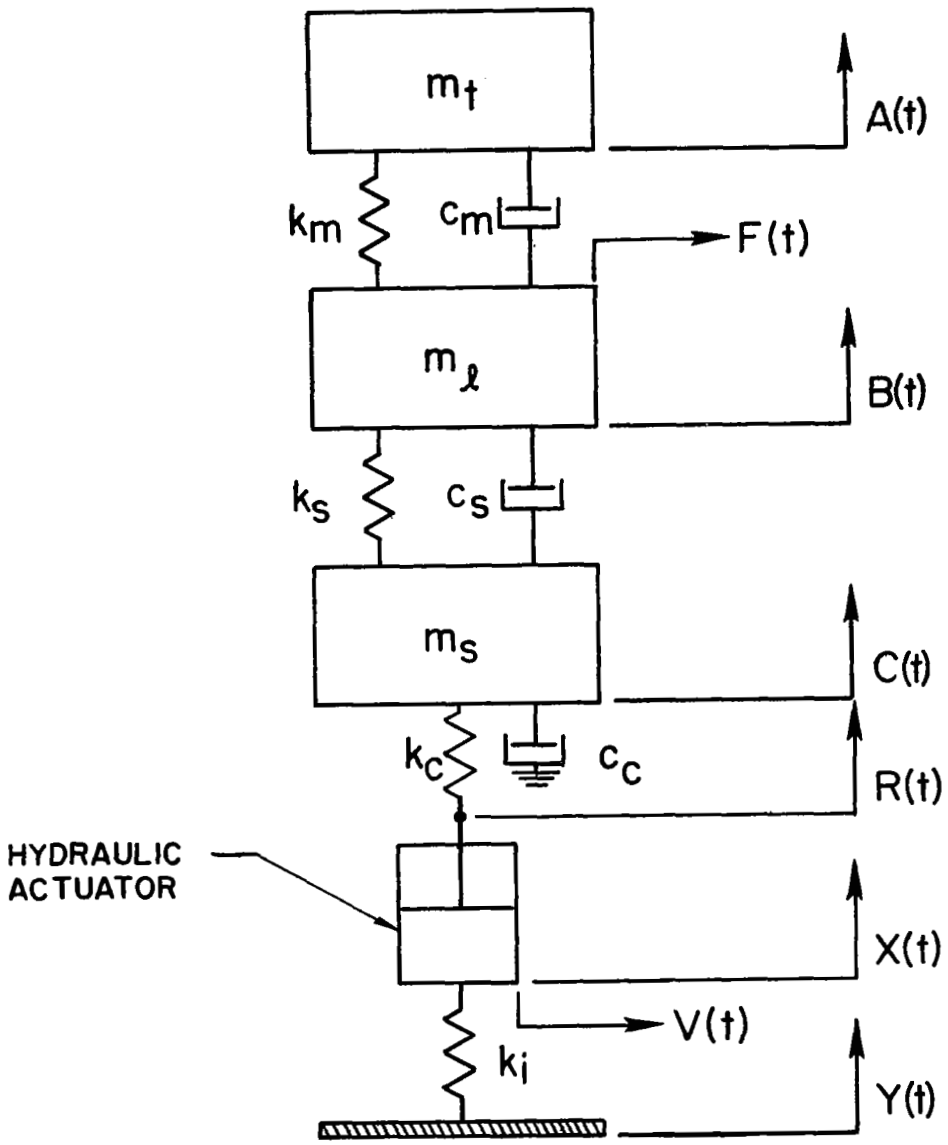

Figure 24: Model of Electrohydraulic Pilot Seat Isolation System With Flexible Payload and Support Structure

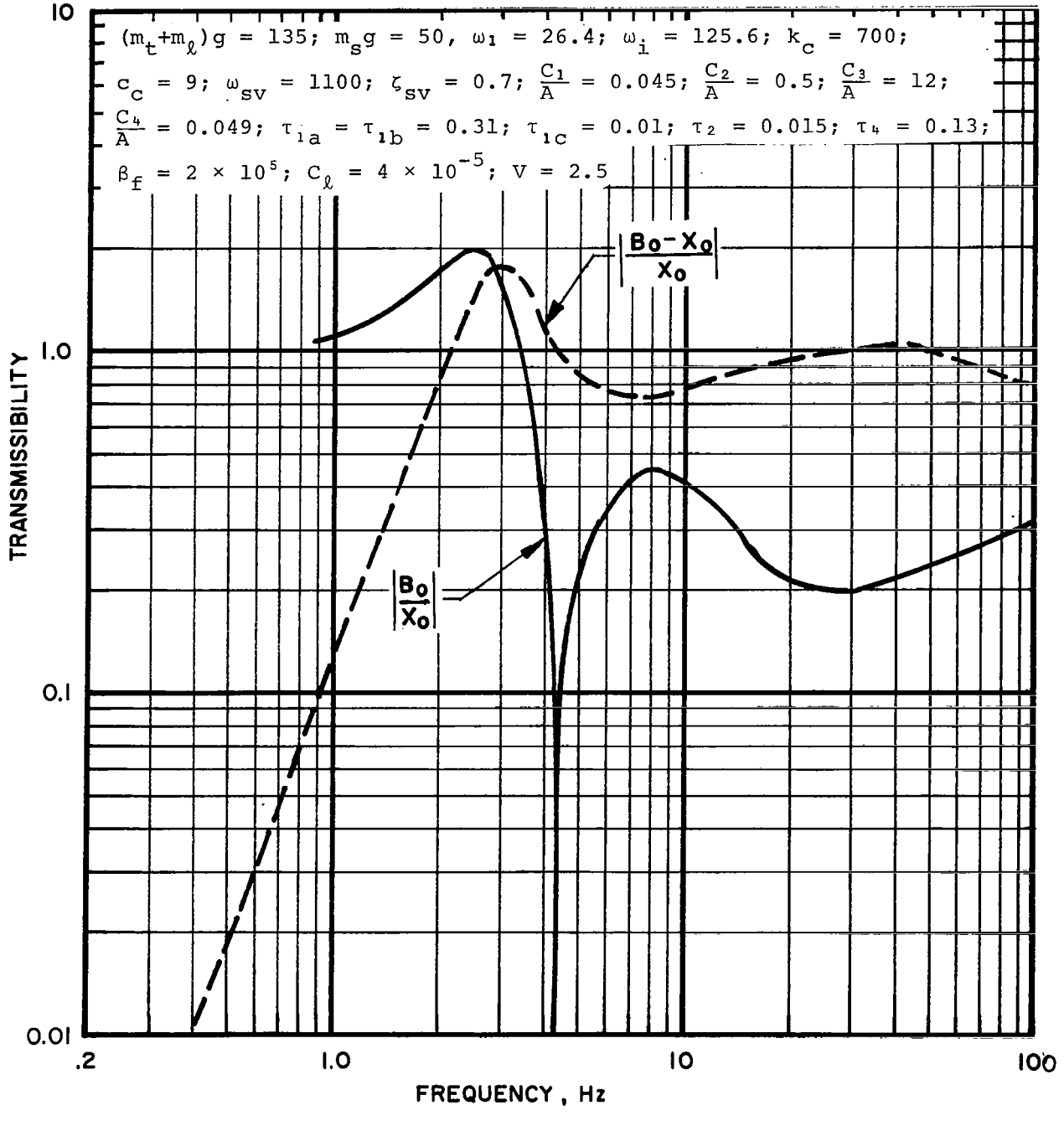

Figure 25: Theoretical Vertical Absolute and Relative Displacement Transmissibilities for Pilot Seat Isolation System With Rigid Payload

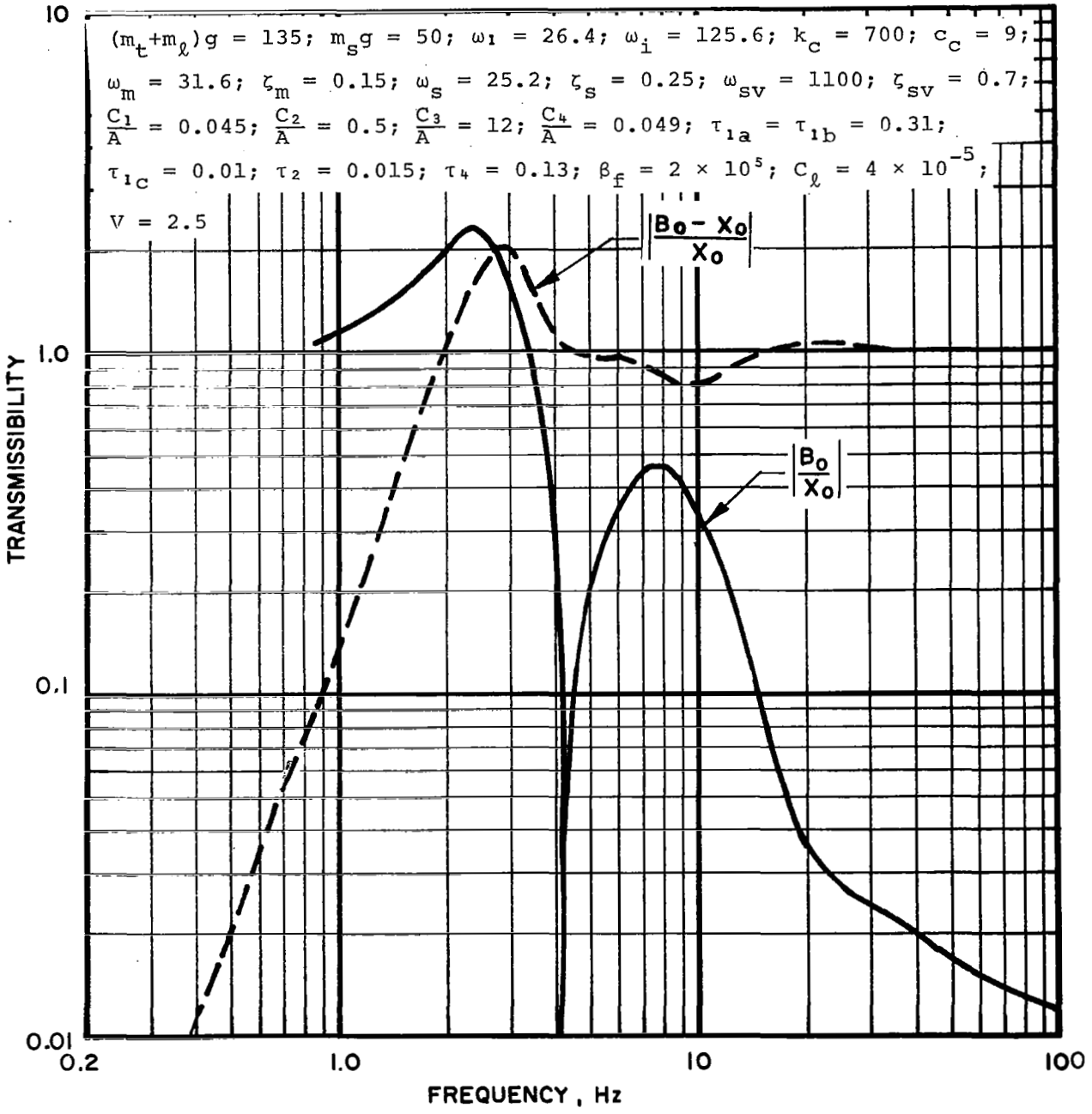

Figure 26: Theoretical Vertical Absolute and Relative Displacement Transmissibilities for Pilot Seat Isolation System With a DC-8 Seat Cushion and 175 Pound Subject

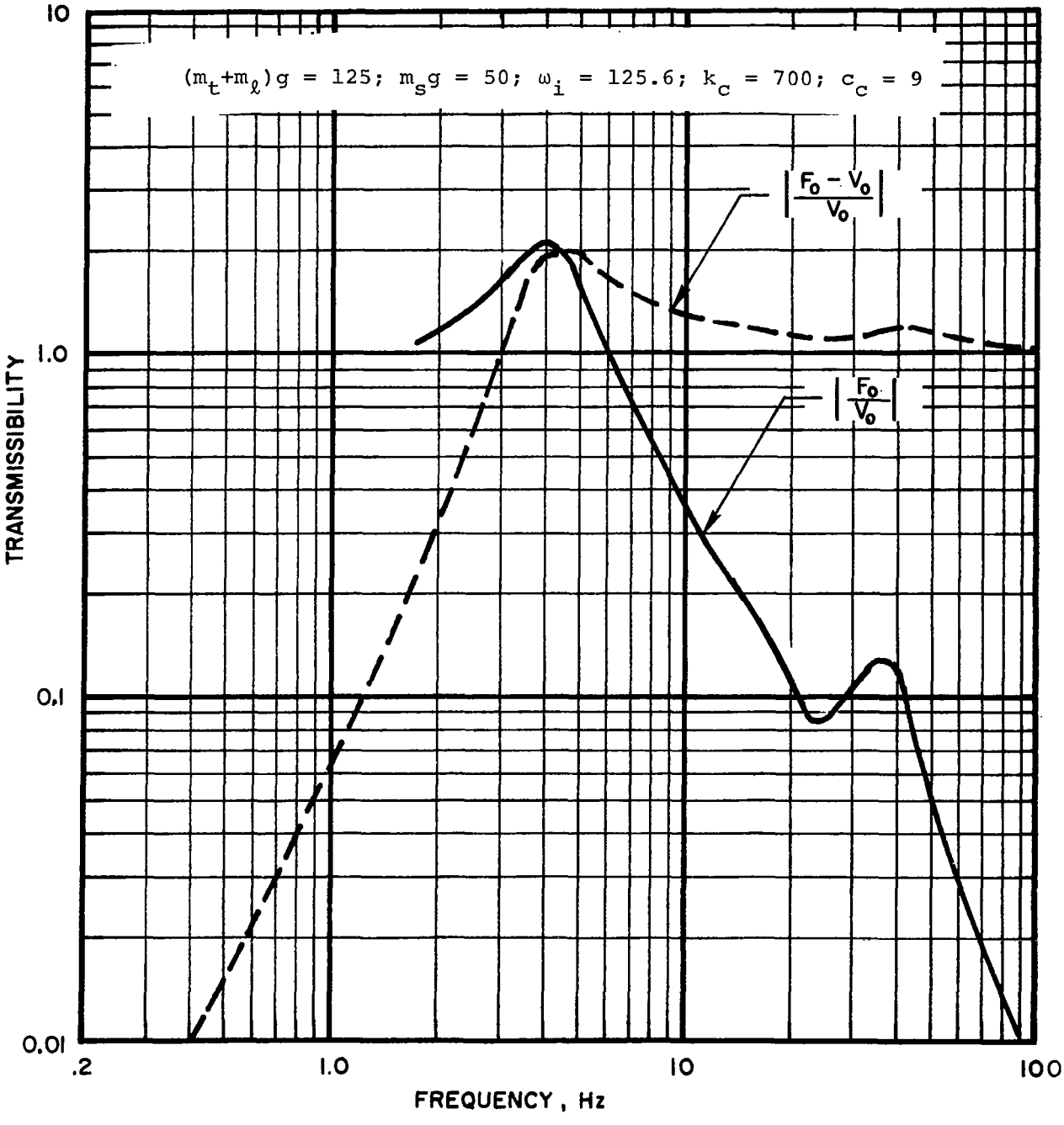

Figure 27: Theoretical Horizontal Absolute and Relative Displacement Transmissibilities for Pilot Seat Isolation System With a DC-8 Seat Cushion and 175 Pound Rigid Payload

CR-1560

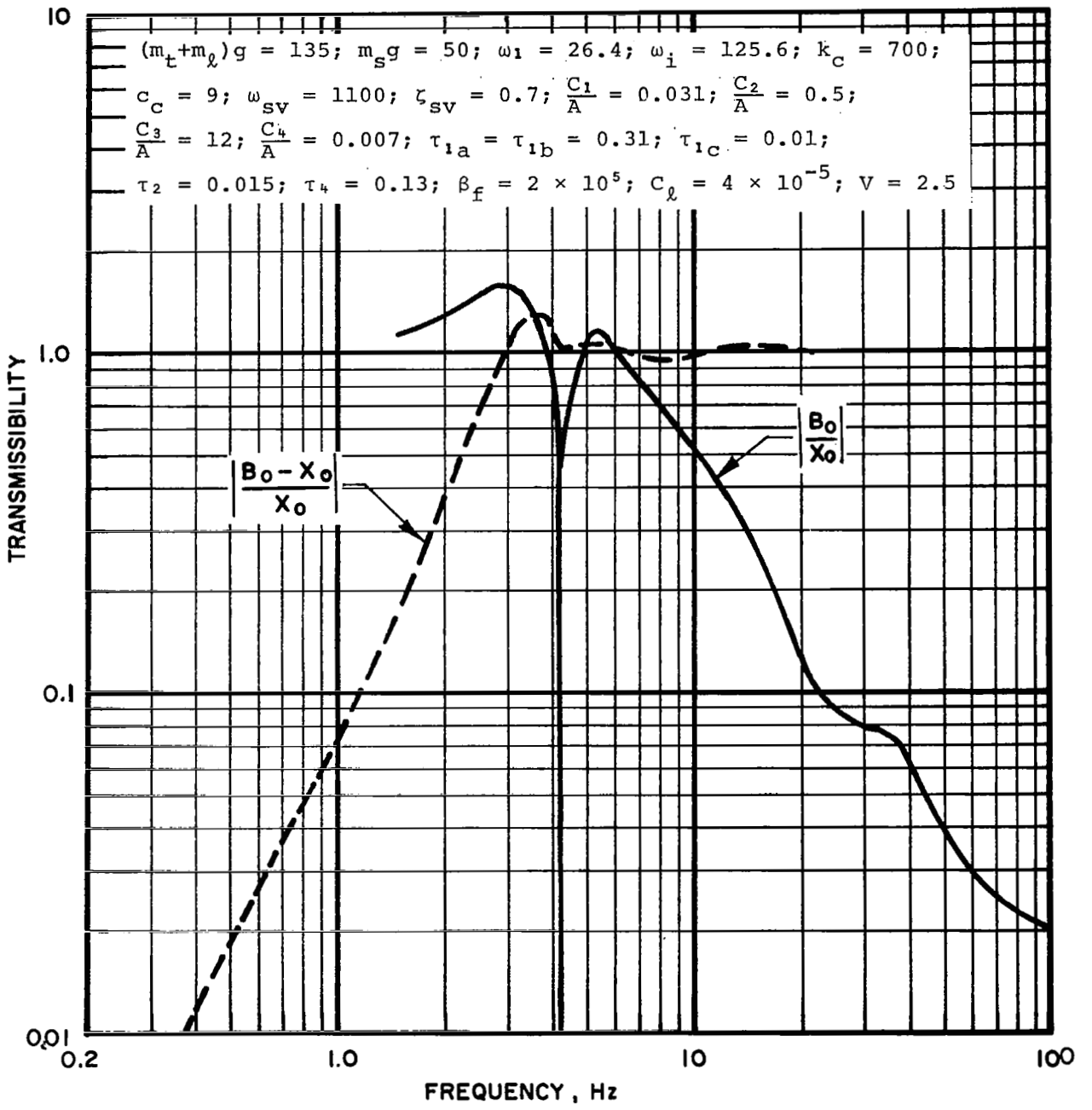

Figure 28: Theoretical Vertical Absolute and Relative Displacement Transmissibilities for Pilot Seat Isolation System at Extreme of Nonlinear Range (Small Relative Deflections About Mean Position in Nonlinear Range) With a DC-8 Seat Cushion and 175 Pound Subject

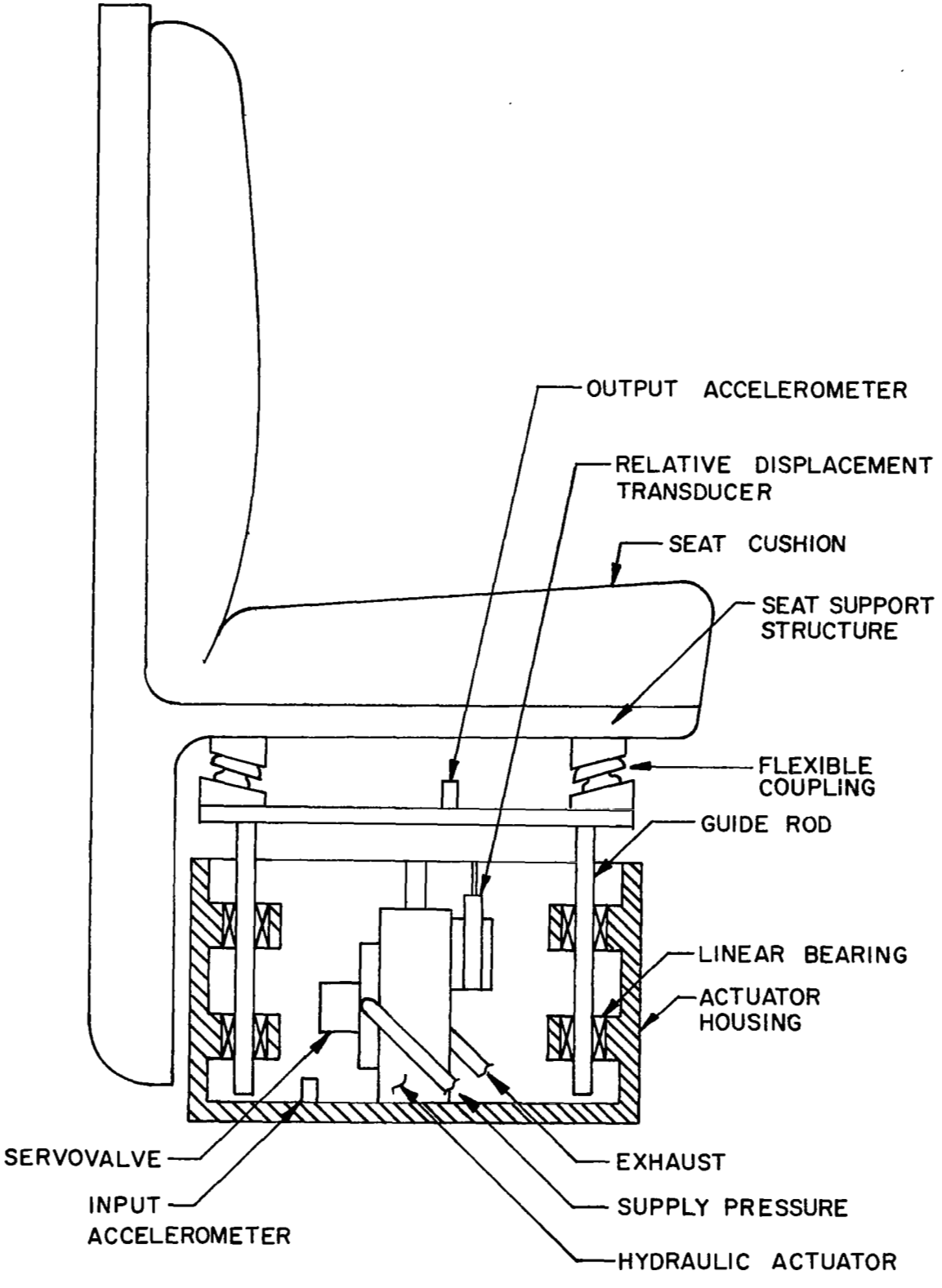

Figure 29 : Diagrammatic Representation of Major Functional Components of Electrohydraulic Pilot Seat

Figure 30 : Photograph of Laboratory Model of the Electrohydraulic Pilot Seat Mounted on the Cockpit Simulator

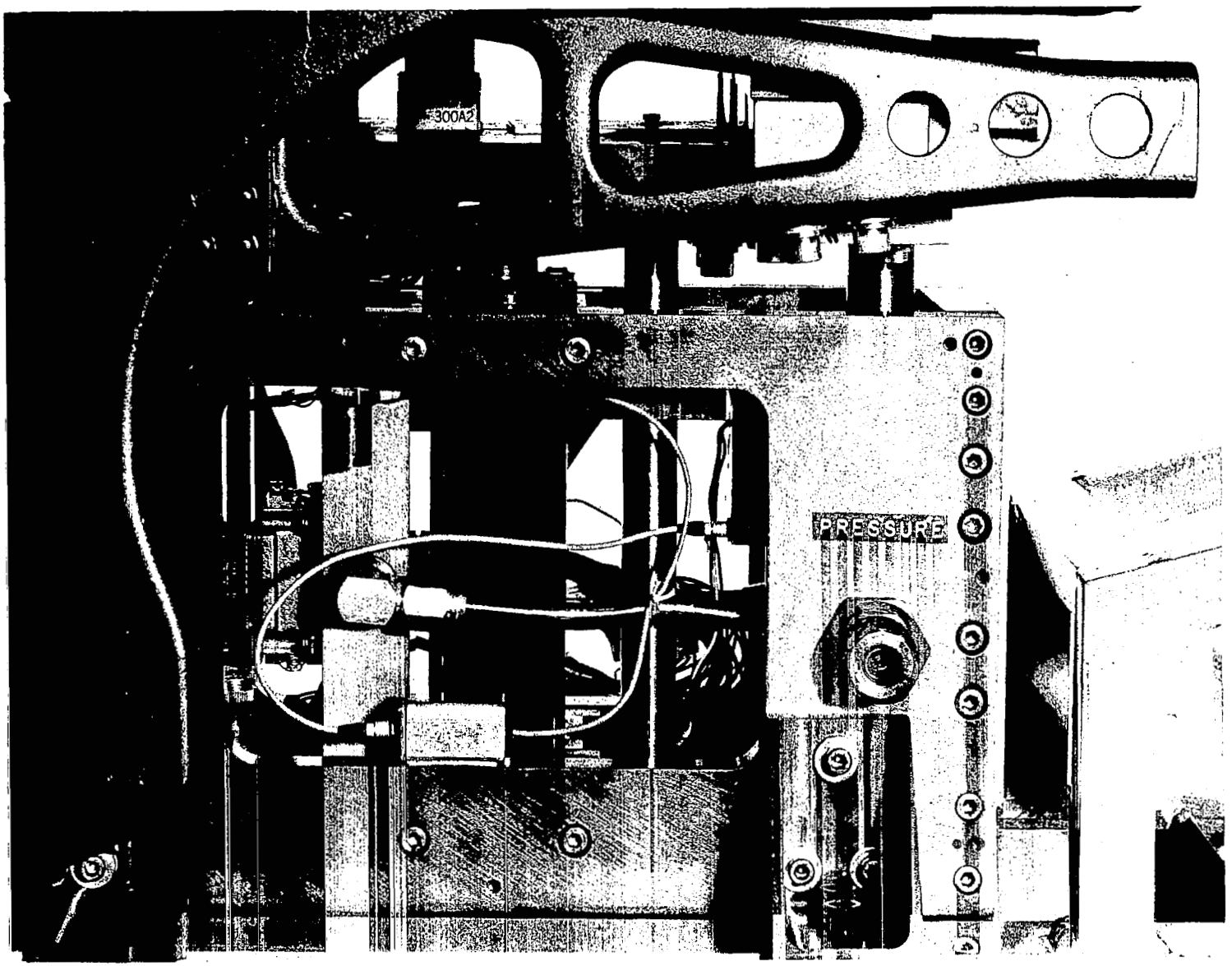

Figure 31: Photograph of Active Portion of the Electrohydraulic Pilot Seat

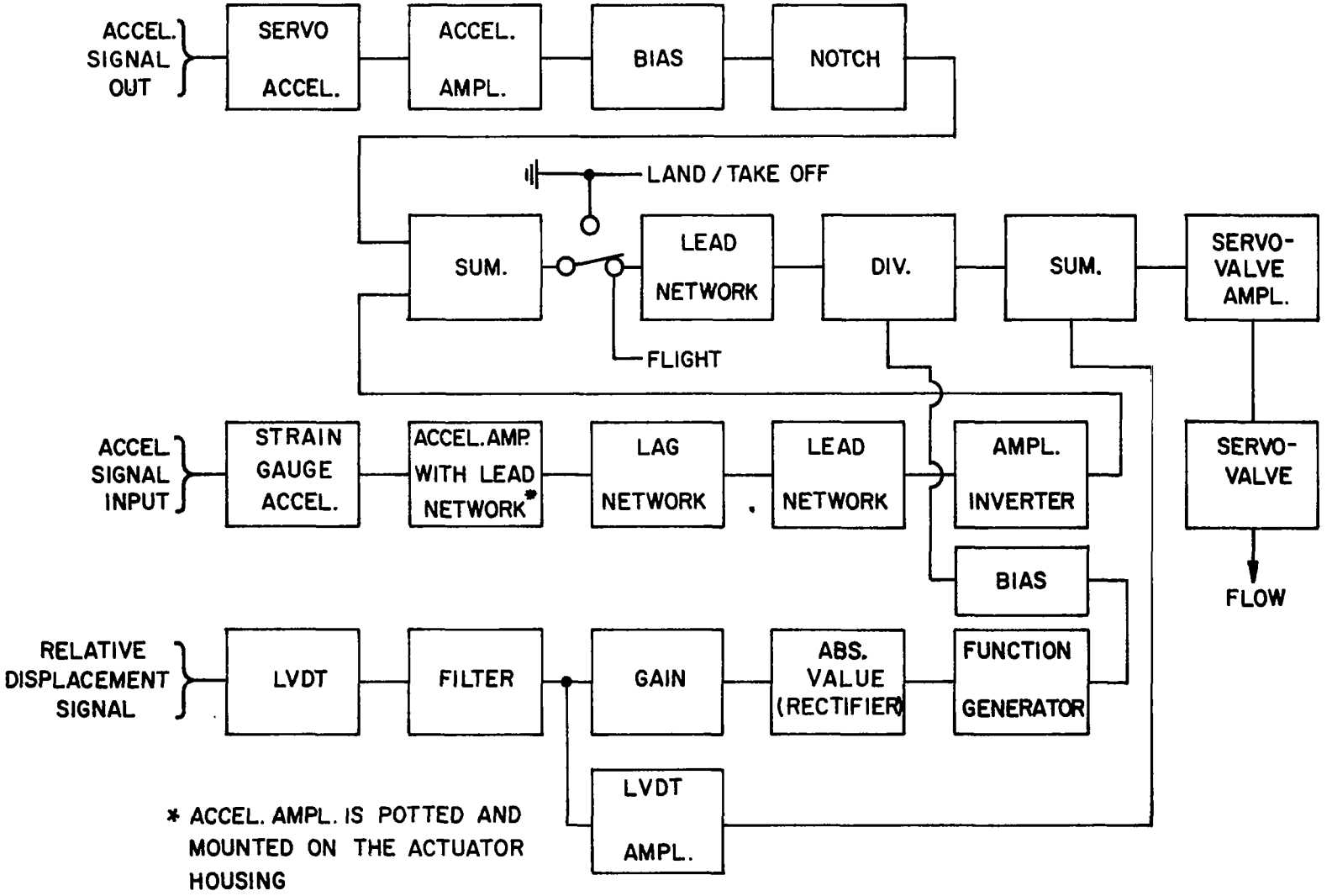

Figure 32: Signal Flow Diagram For Electrohydraulic Pilot Seat Isolation System

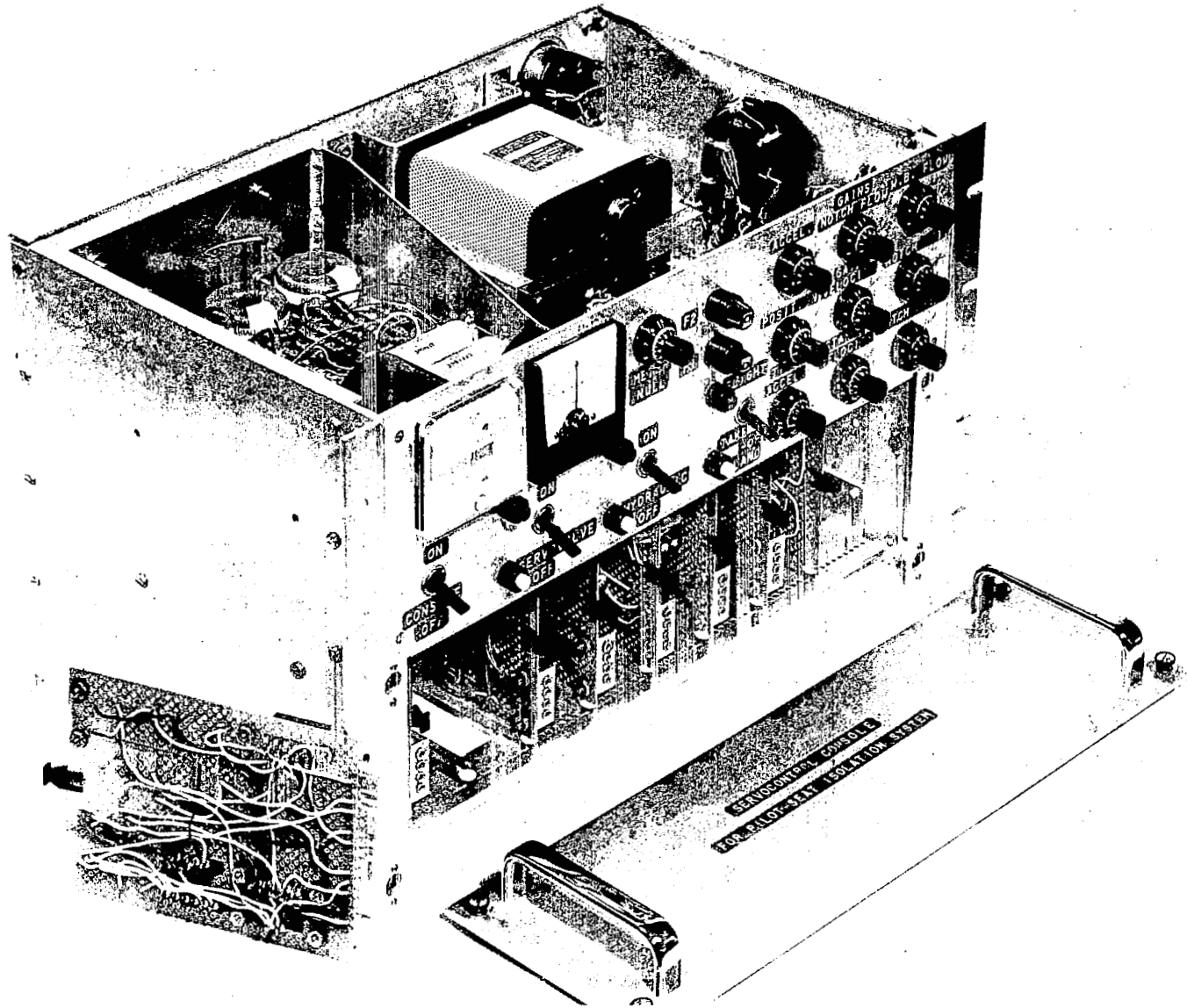

Figure 33: Photograph of Servocontrol Console Breadboard for the Electrohydraulic Pilot Seat

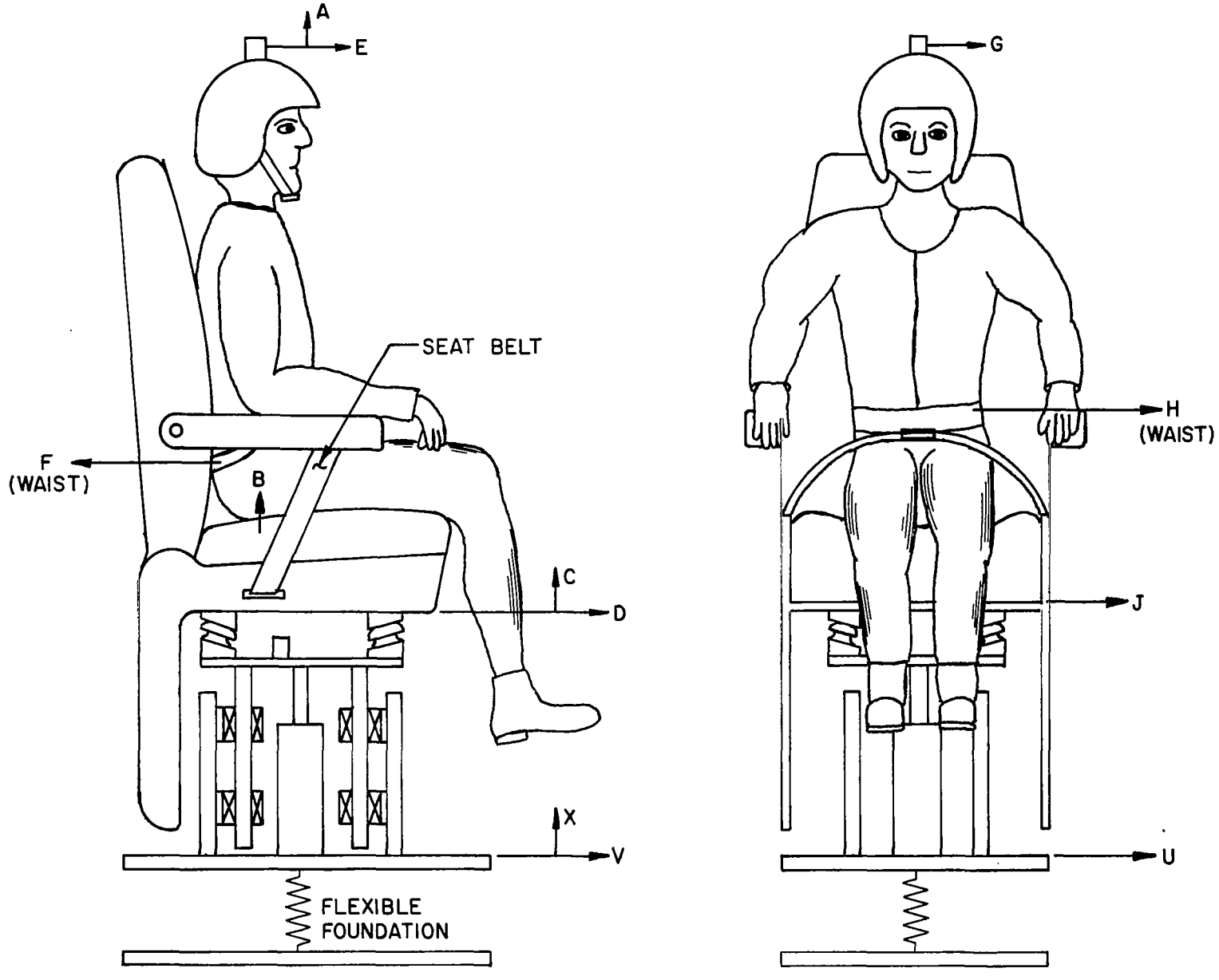

Figure 34: Accelerometer Orientations Employed During Testing Program on Electrohydraulic Pilot Seat Isolation System

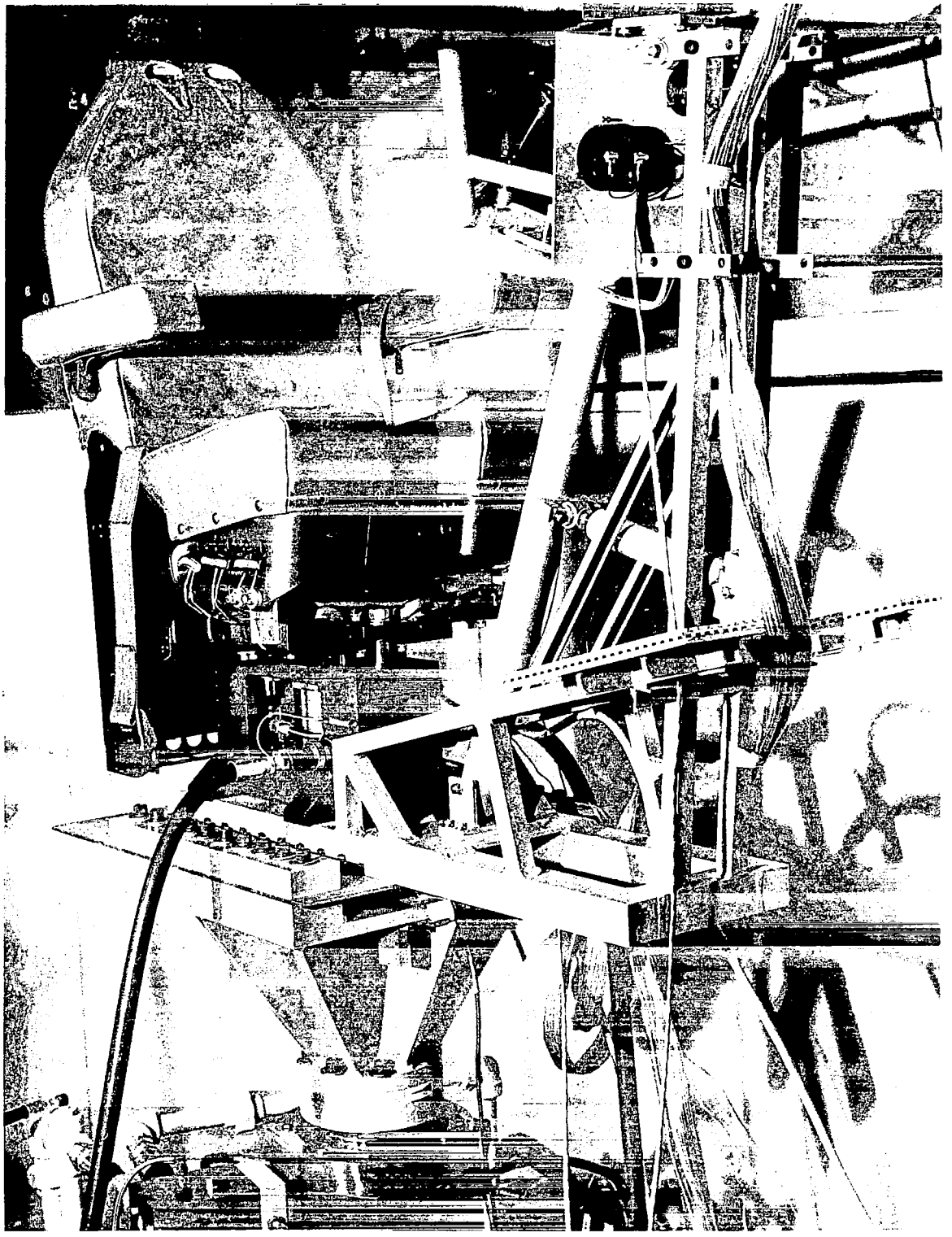

Figure 35: Photograph of Laboratory Model of Electrohydraulic Pilot Seat and Cockpit Simulator Mounted on Hydraulic Shaker

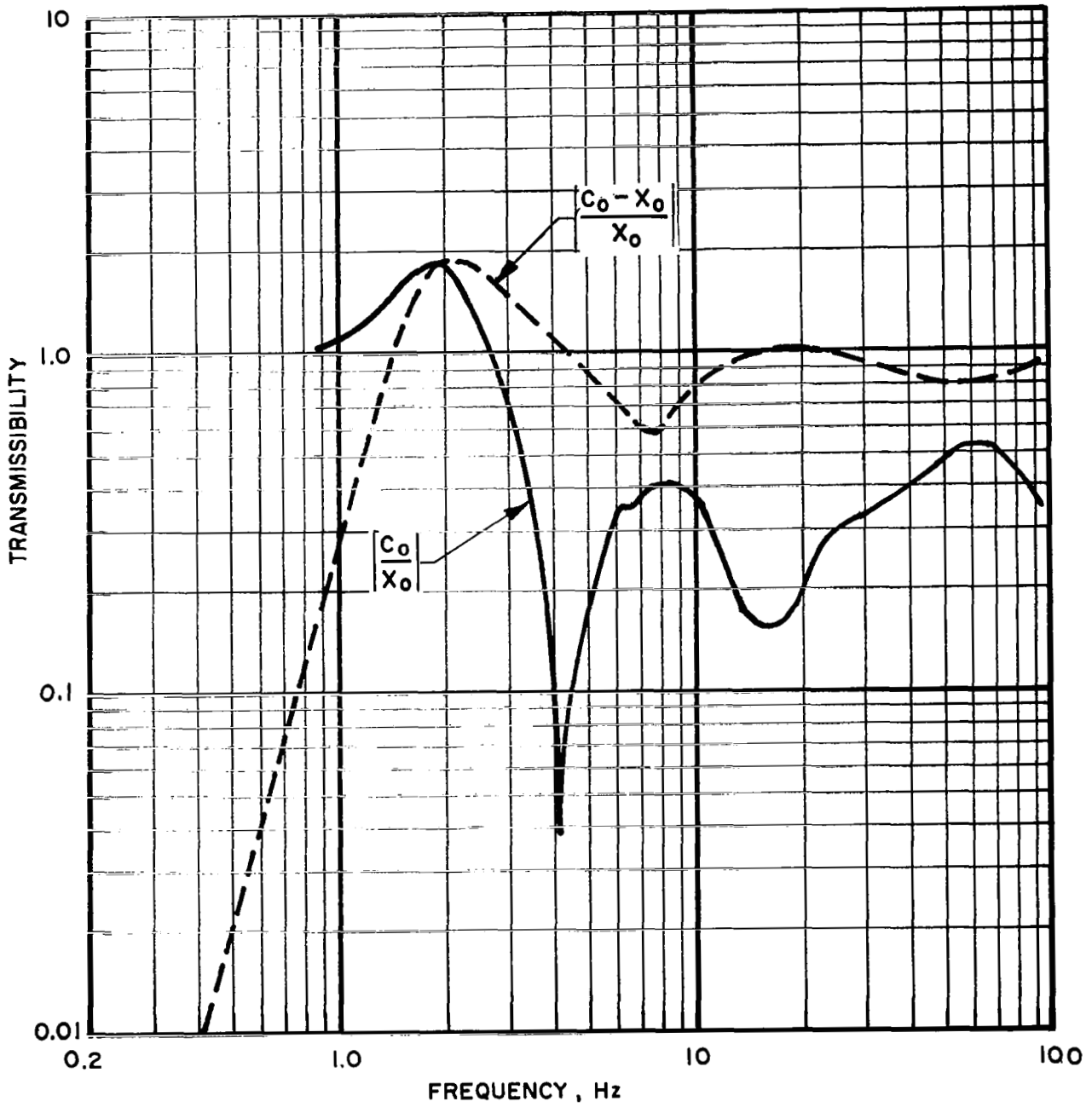

Figure 36: Test Data on Absolute and Relative Vertical Transmissibilities Between the Input and Output of the Flexible Coupling With: a 160 Pound Subject; DC-8 Seat Cushion; Seat Belt Tight; and Isolation System in Flight Mode

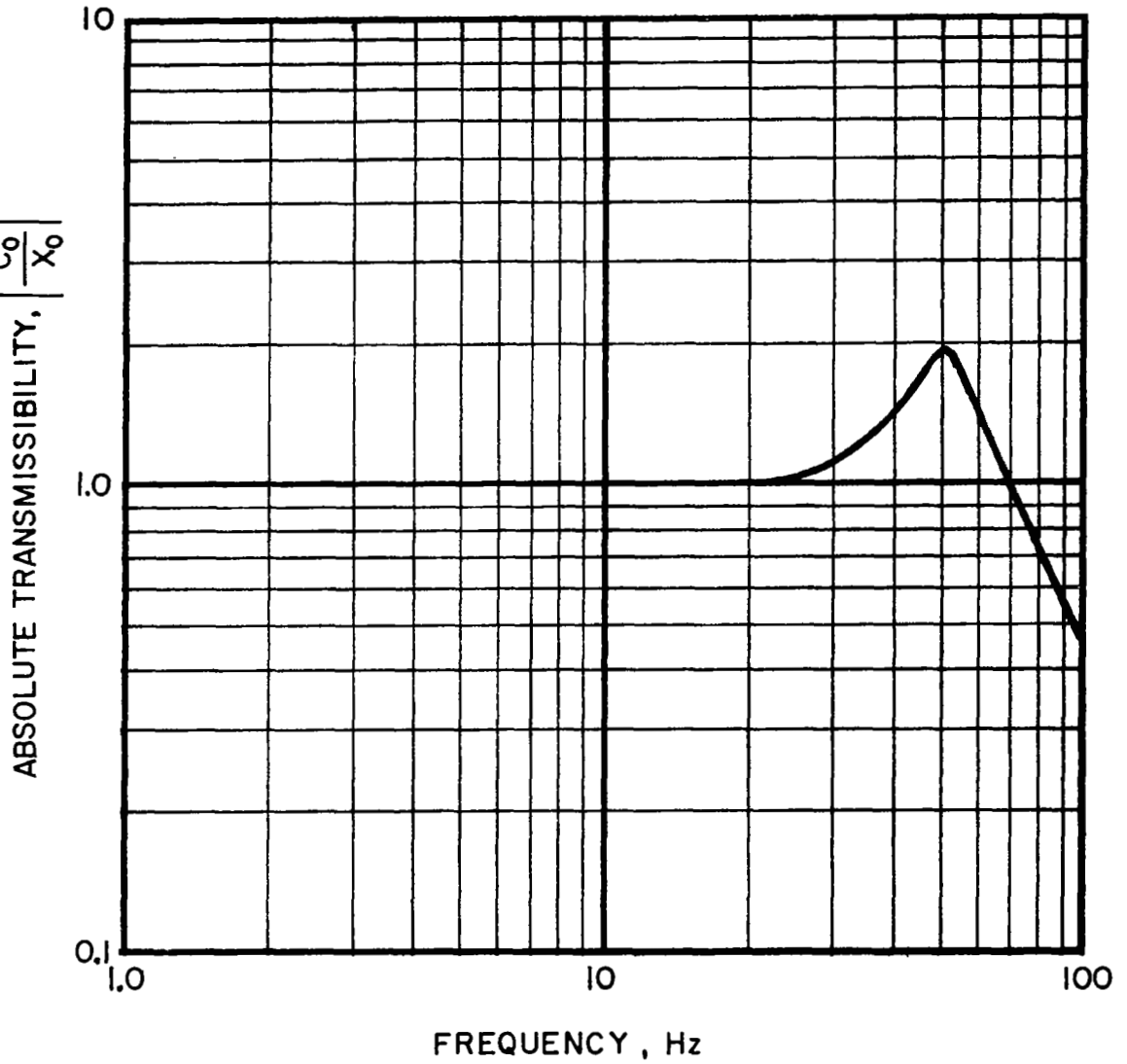

Figure 37: Test Data on Absolute Vertical Transmissibility Between Input and Output of Flexible Coupling With: a 160 Pound Subject; DC-8 Seat Cushion; Seat Belt Tight; and Isolation System in Landing/Takeoff Mode

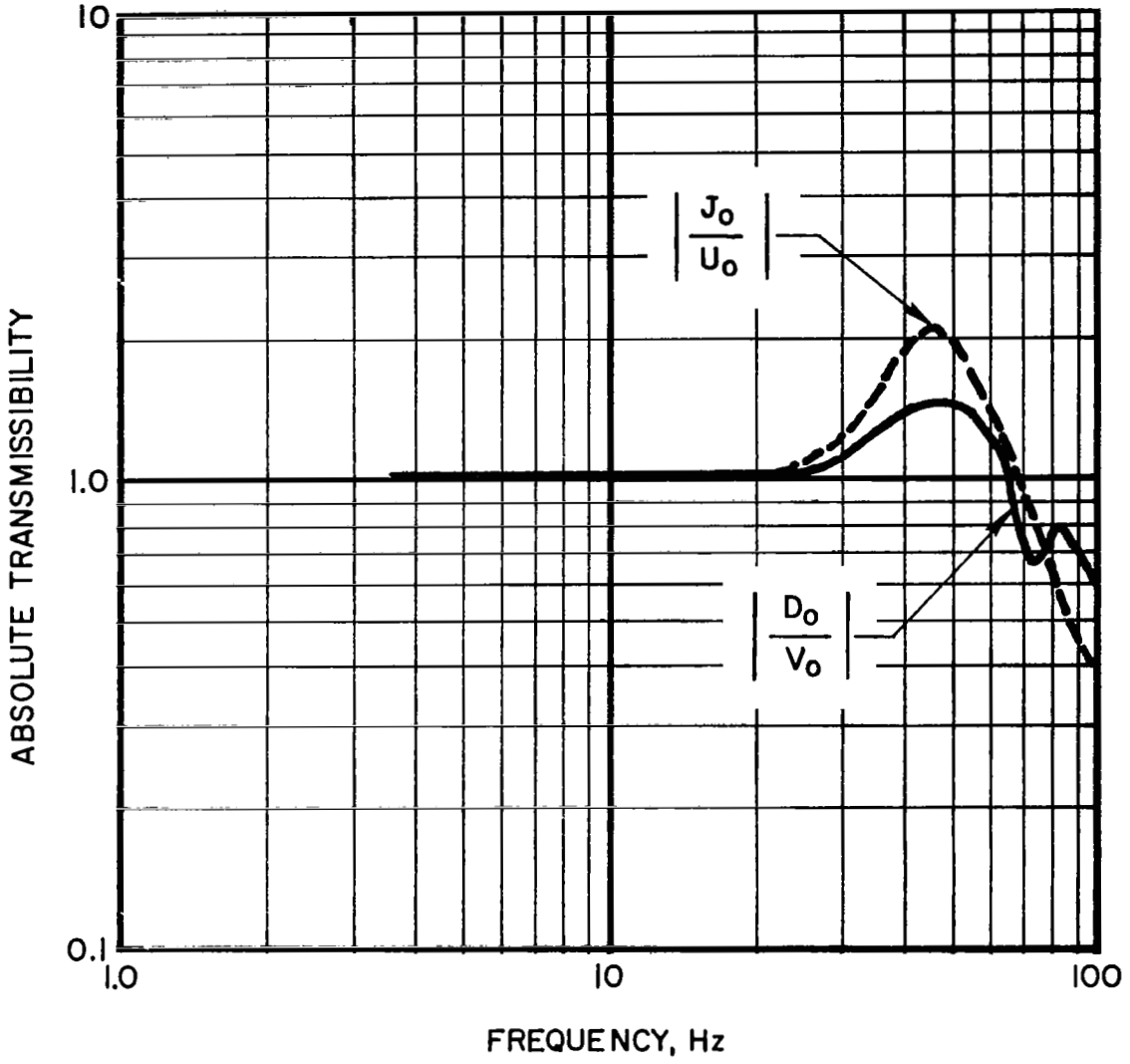

Figure 38: Test Data on the Absolute Horizontal Transmissibilities Between the Input and Output of the Flexible Coupling with: a 160 Pound Subject; DC-8 Seat Cushion; and Seat Belt Tight

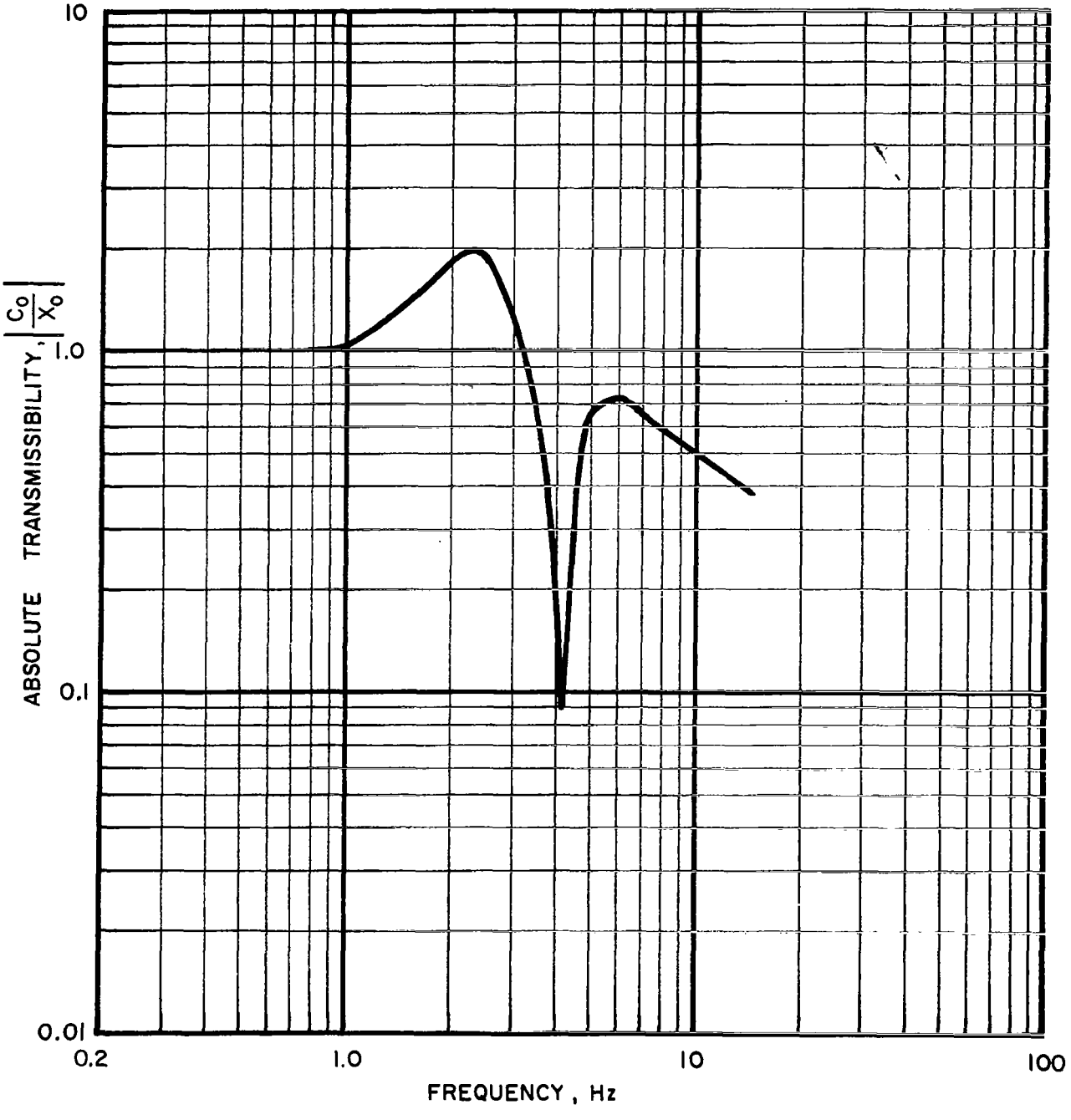

Figure 39: Test Data on Absolute Vertical Transmissibility Between Input and Output of Flexible Coupling With: a 160 pound Subject; DC-8 Seat Cushion; Seat Belt Tight; Mean Actuator Position 1-1/4 in. Above Null; and Isolation System in Flight Mode

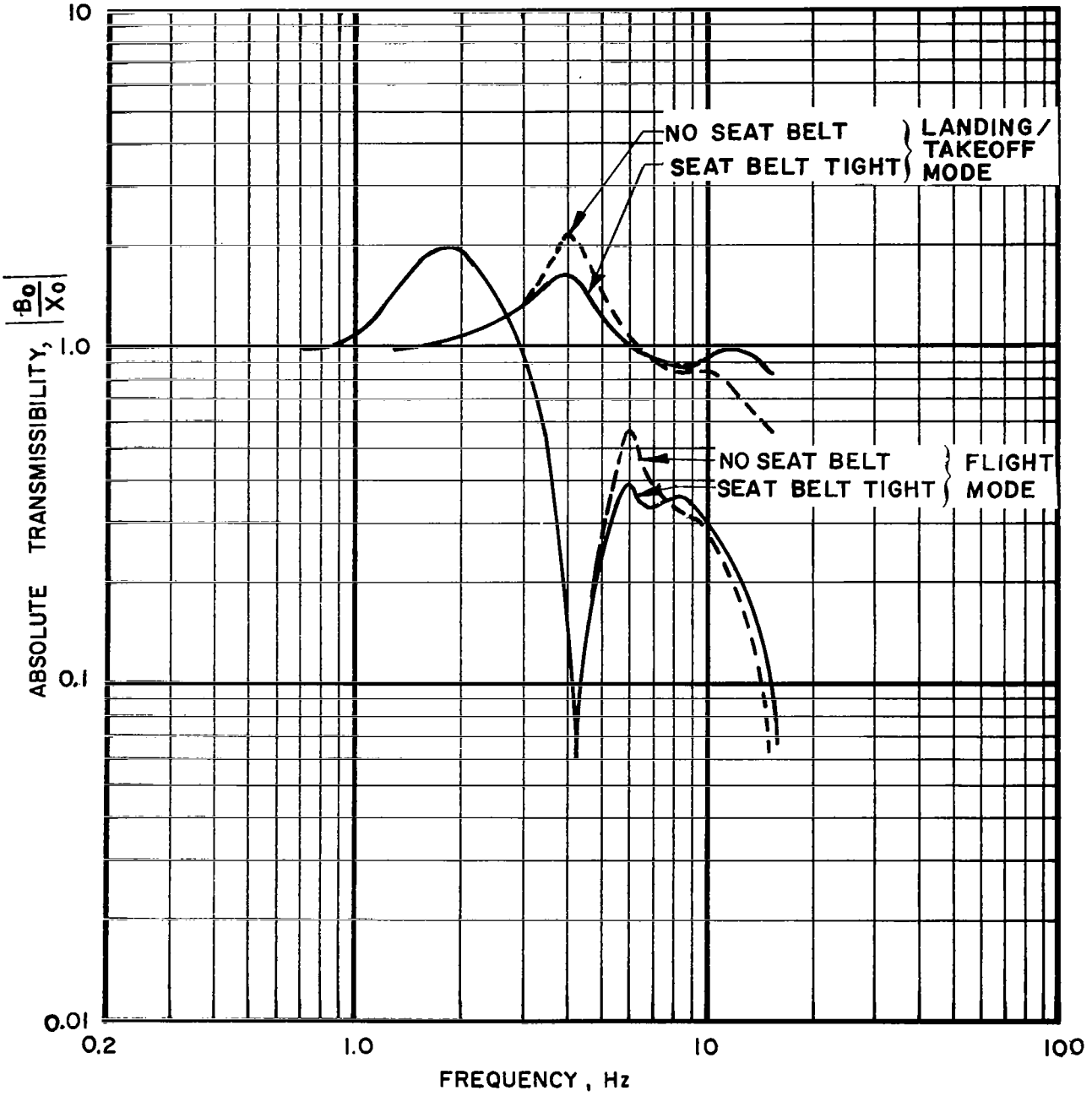

Figure 40: Test Data on Absolute Vertical Transmissibilities Between Input and Buttocks With: a 160 Pound Subject; DC-8 Seat Cushion; and Isolation System in Flight and Landing/Takeoff Modes

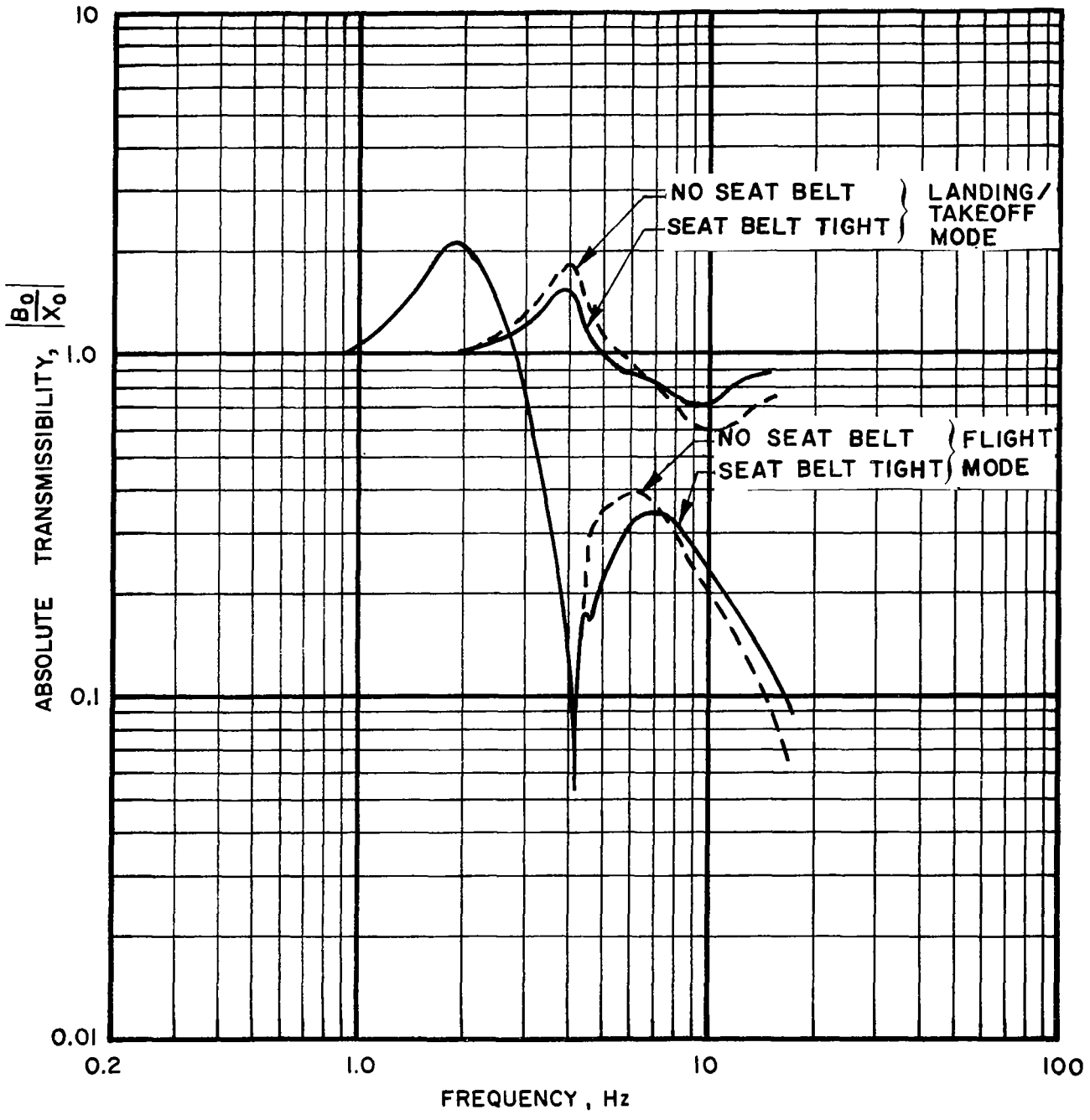

Figure 41: Test Data on Absolute Vertical Transmissibilities Between Input and Buttocks With: a 200 Pound Subject; DC-8 Seat Cushion; and Isolation System in Flight and Landing/Takeoff Modes

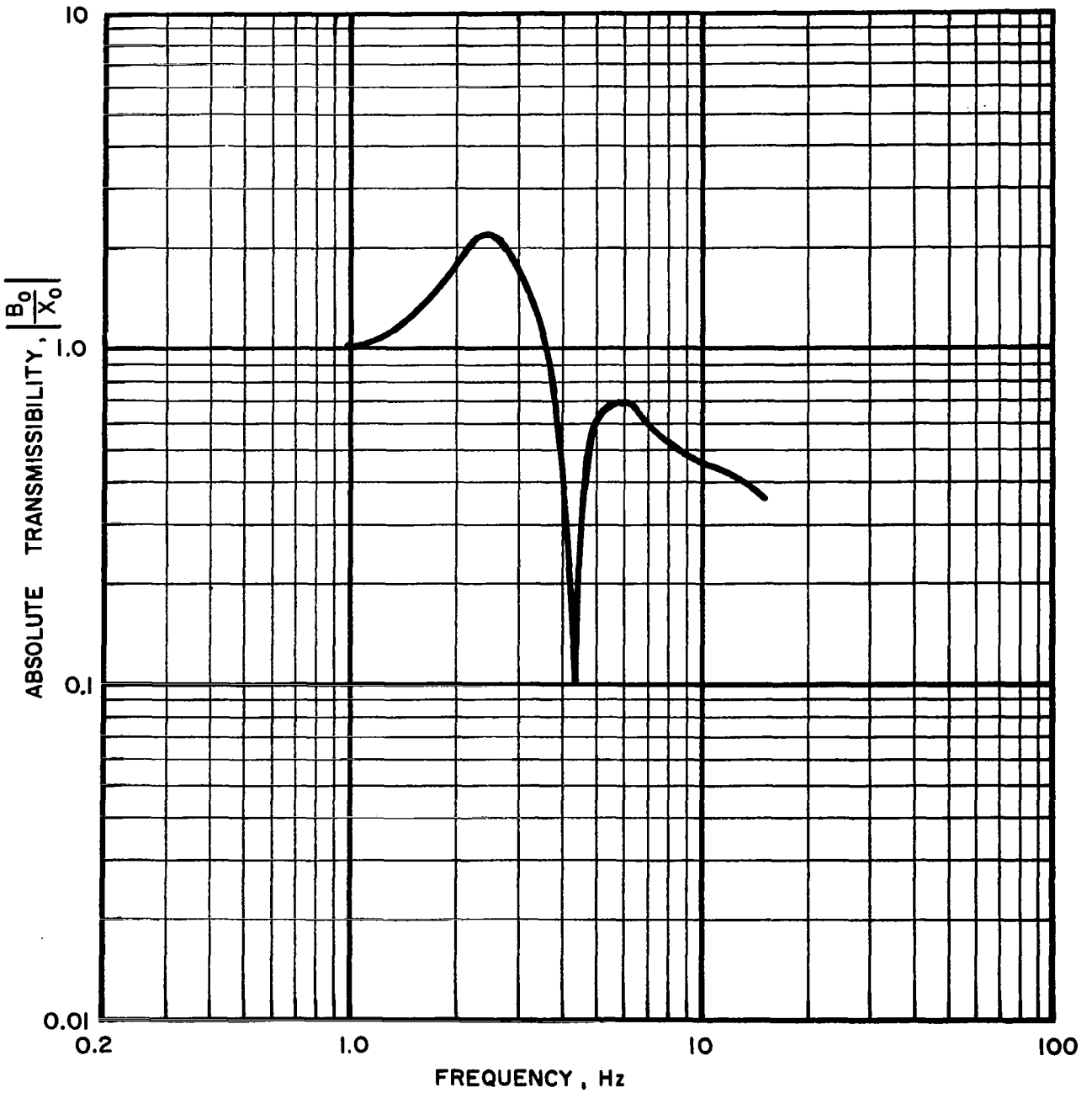

Figure 42: Test Data on Absolute Vertical Transmissibility Between Input and Buttocks With: a 160 Pound Subject; DC-8 Seat Cushion; Seat Belt Tight; Mean Actuator Position 1-1/4 in. Above Null; and Isolation System in Flight Mode

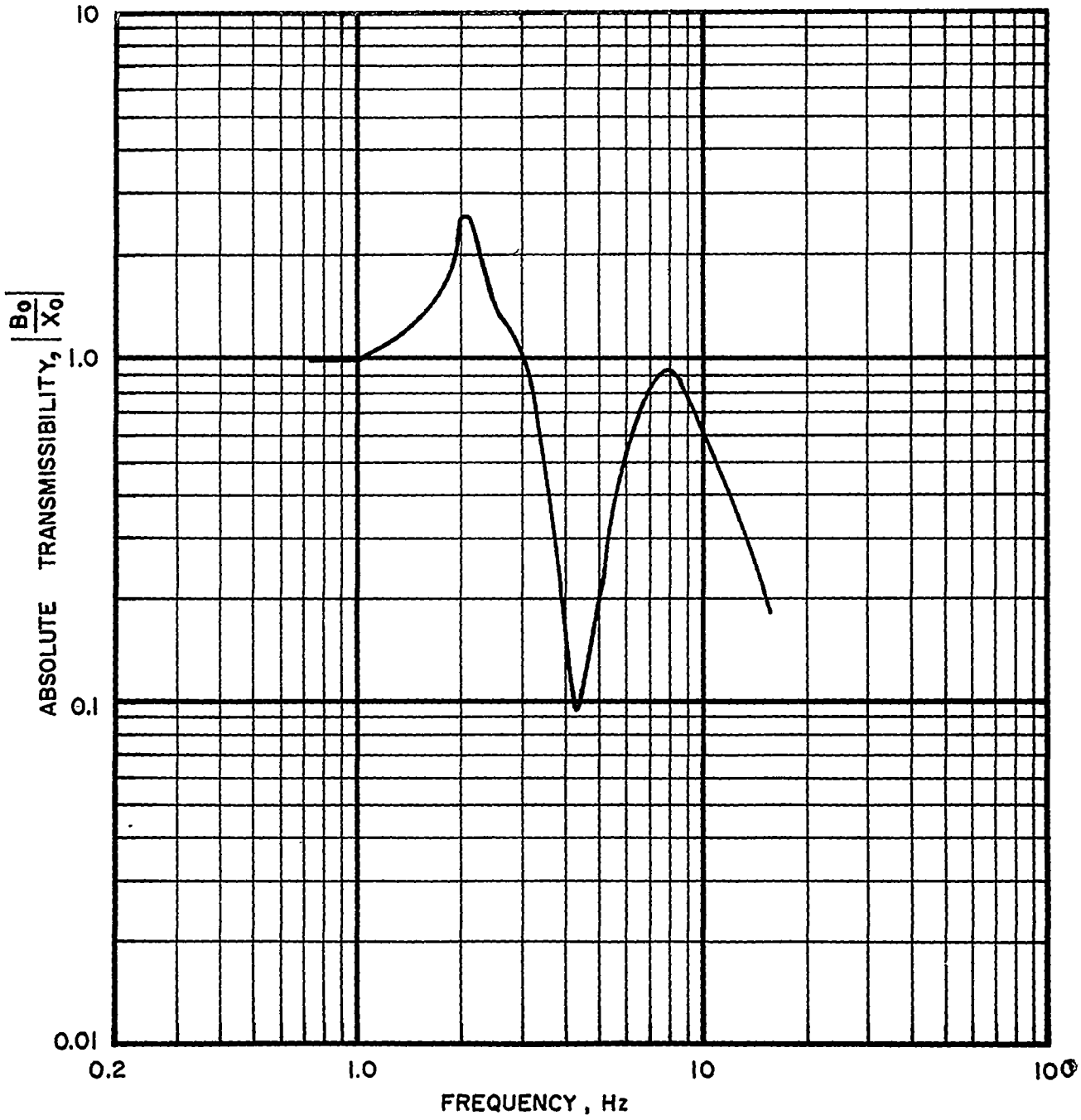

Figure 43: Test Data on Absolute Vertical Transmissibility Between Input and Buttocks With: a 175 Pound Rigid Payload; a DC-8 Seat Cushion; Seat Belt Tight; and Isolation System in Flight Mode

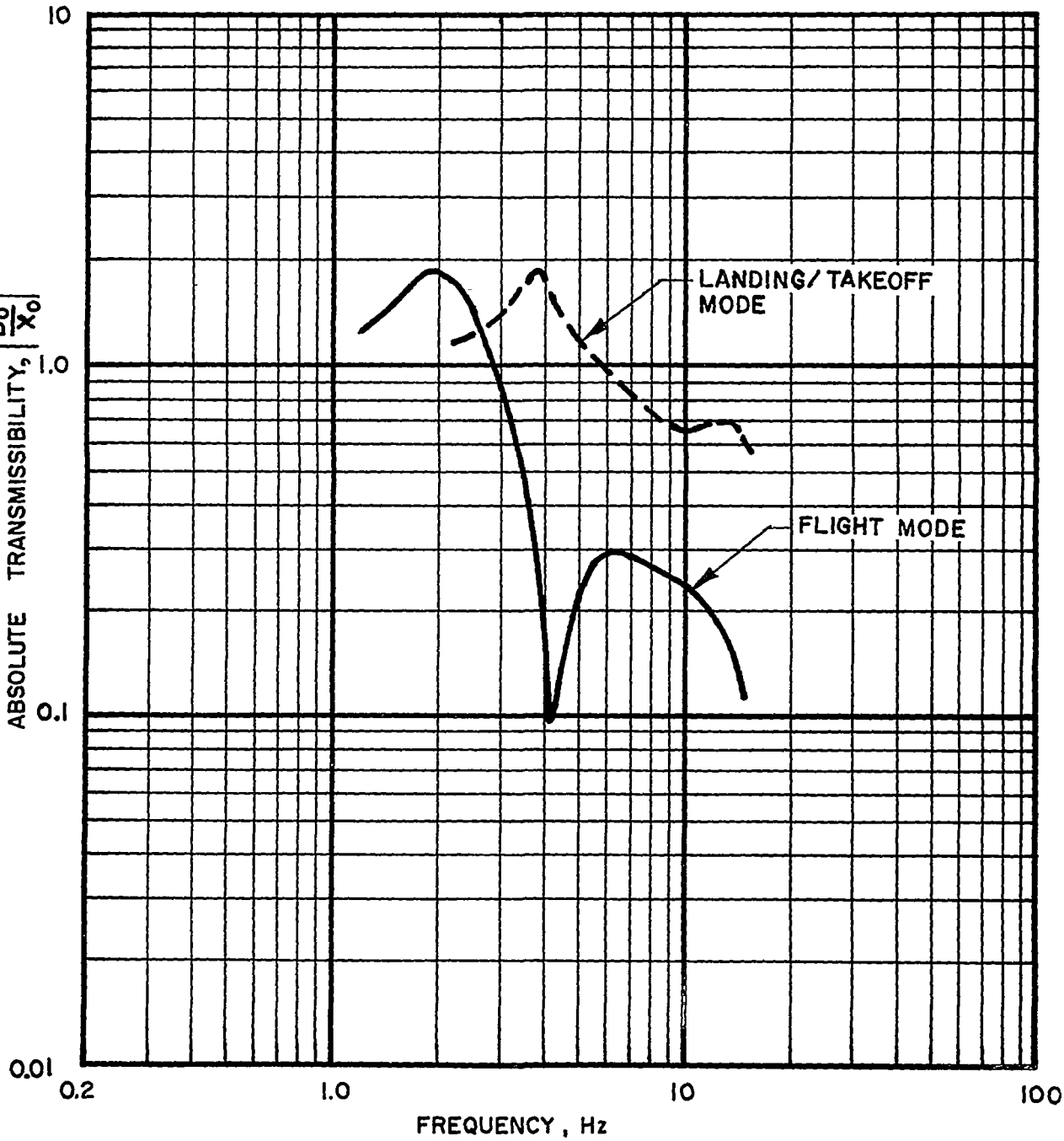

Figure 44: Test Data on Absolute Vertical Transmissibilities Between Input and Buttocks With: a 160 Pound Subject; DC-8 Seat Cushion; Seat Belt Tight; Isolation System in Flight and Landing/Takeoff Modes; and Random Vibration Input

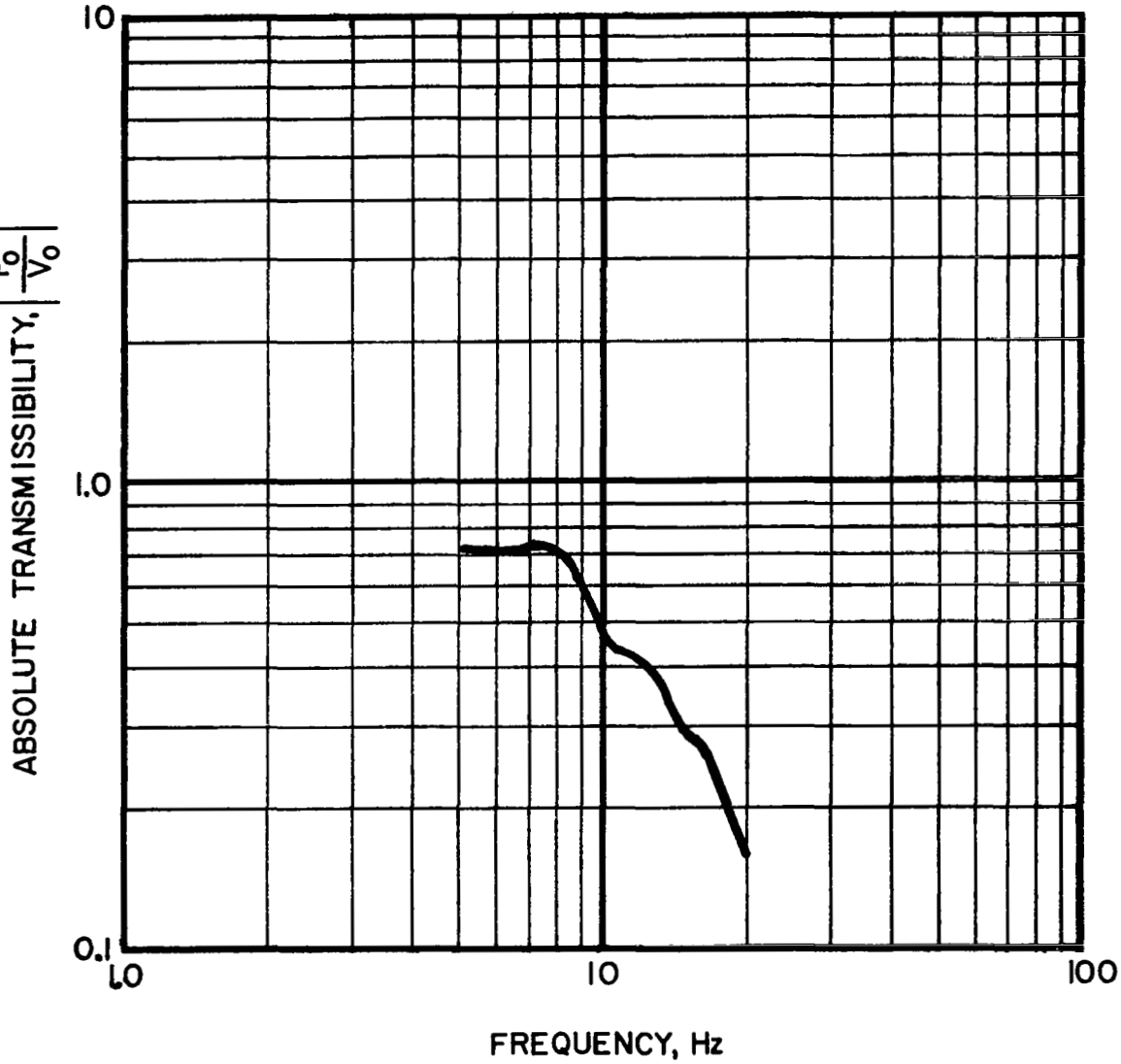

Figure 45: Test Data on Absolute Fore/Aft Transmissibility Between Input and Waist With: a 160 Pound Subject; DC-8 Seat Cushion; and Seat Belt Tight

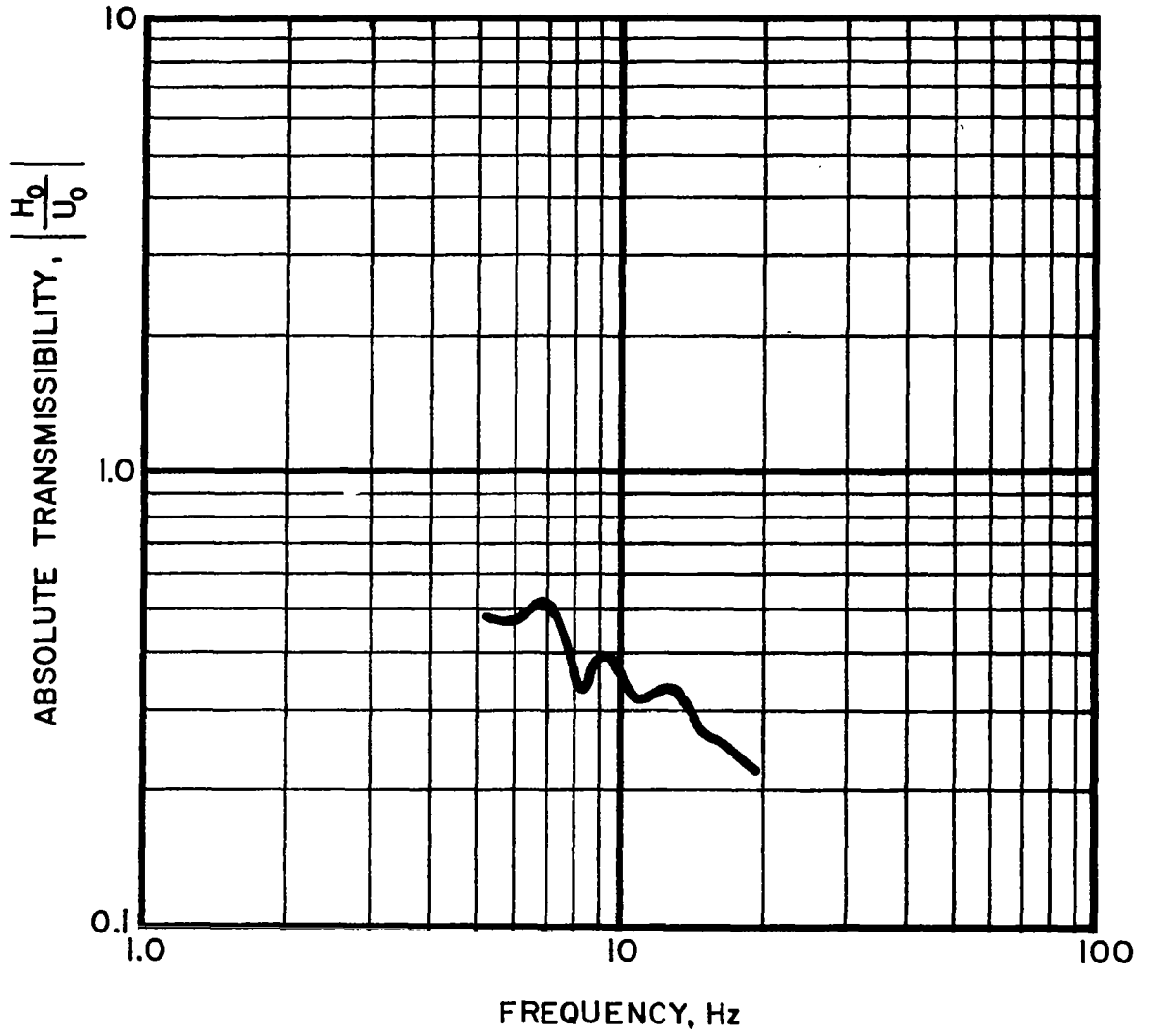

Figure 46: Test Data on Absolute Lateral Transmissibility Between Input and Waist With: a 160 Pound Subject; DC-8 Seat Cushion; and Seat Belt Tight

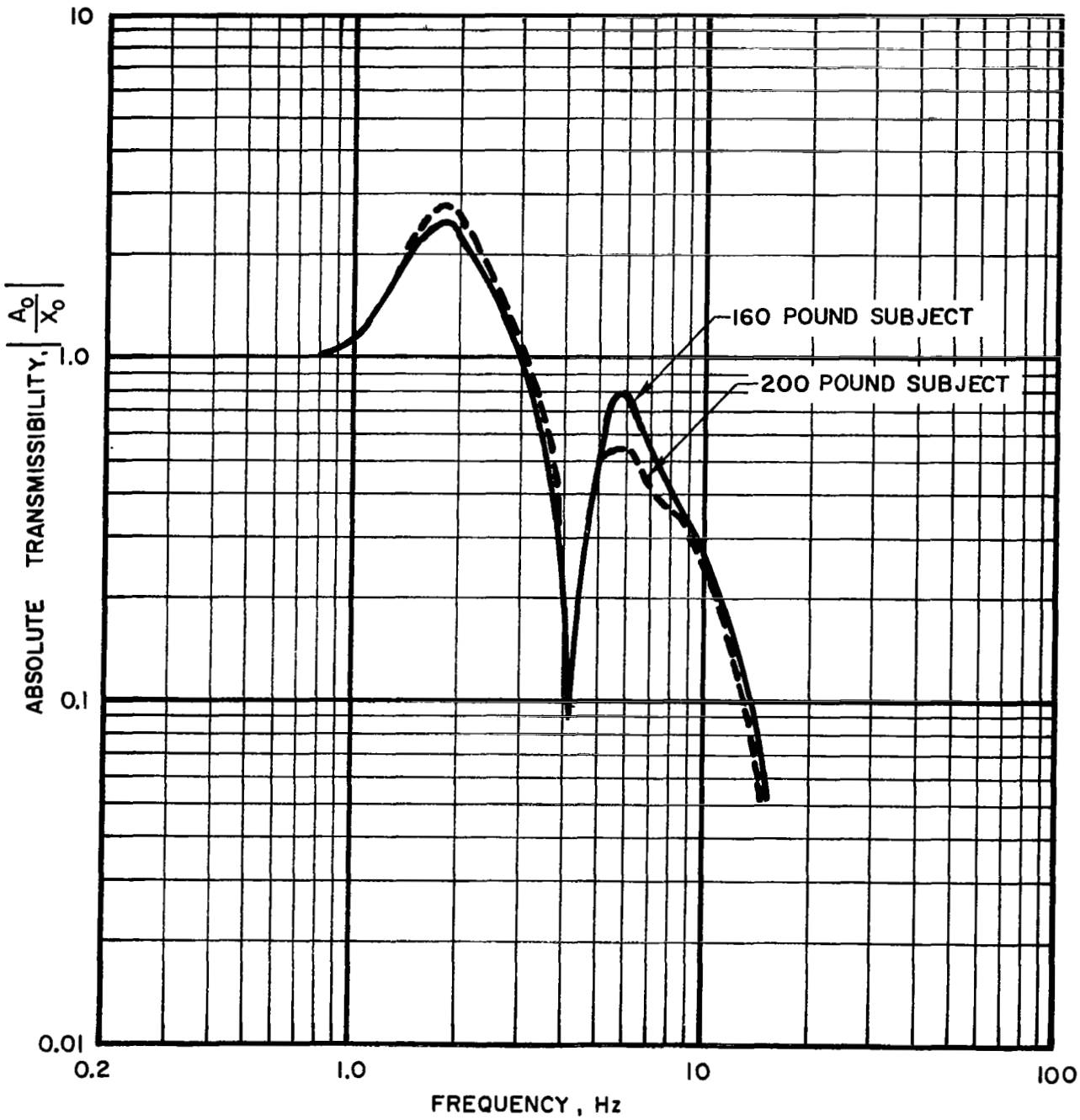

Figure 47: Test Data on Absolute Vertical Transmissibilities Between the Input and Head With: DC-8 Seat Cushion; Seat Belt Tight; and Isolation System in Flight Mode

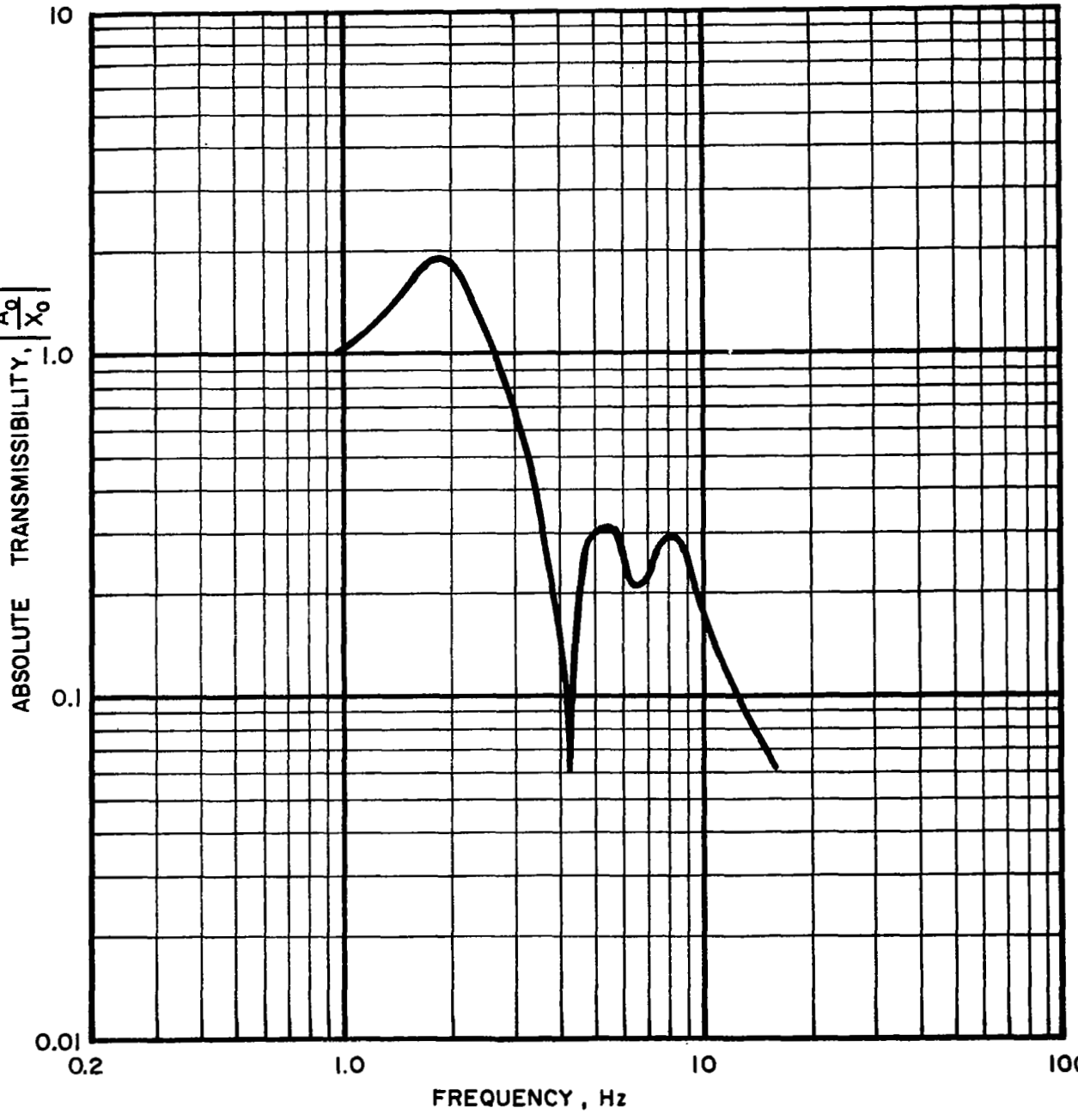

Figure 48: Test Data on Absolute Vertical Transmissibilities Between the Input and Head With: a 200 Pound Subject; Balsa Wood Seat; Seat Belt Tight; and Isolation System in Flight Mode

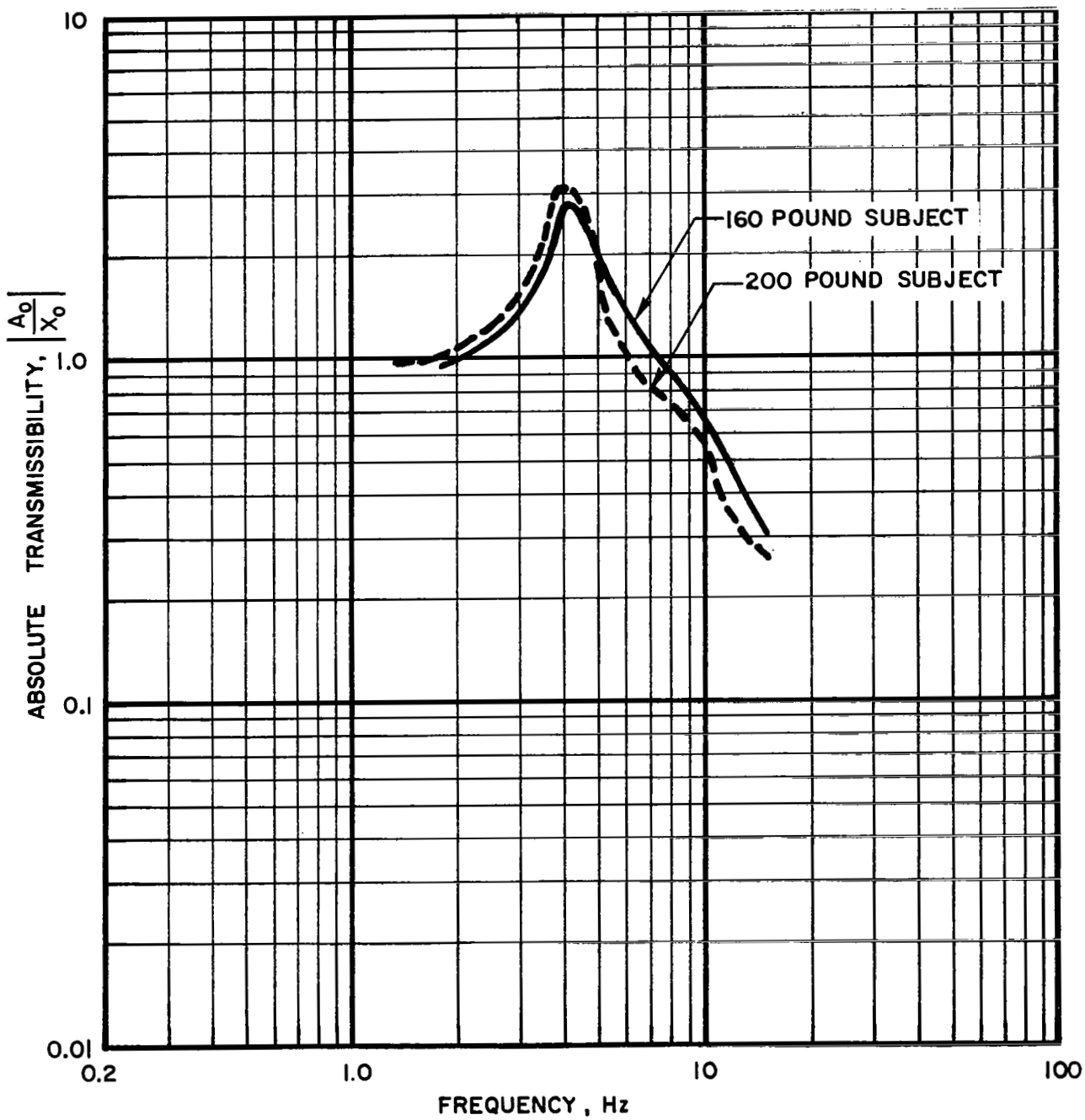

Figure 49: Test Data on Absolute Transmissibilities Between the Input and Head With: DC-8 Seat Cushion; Seat Belt Tight; and Isolation System in Landing/Takeoff Mode

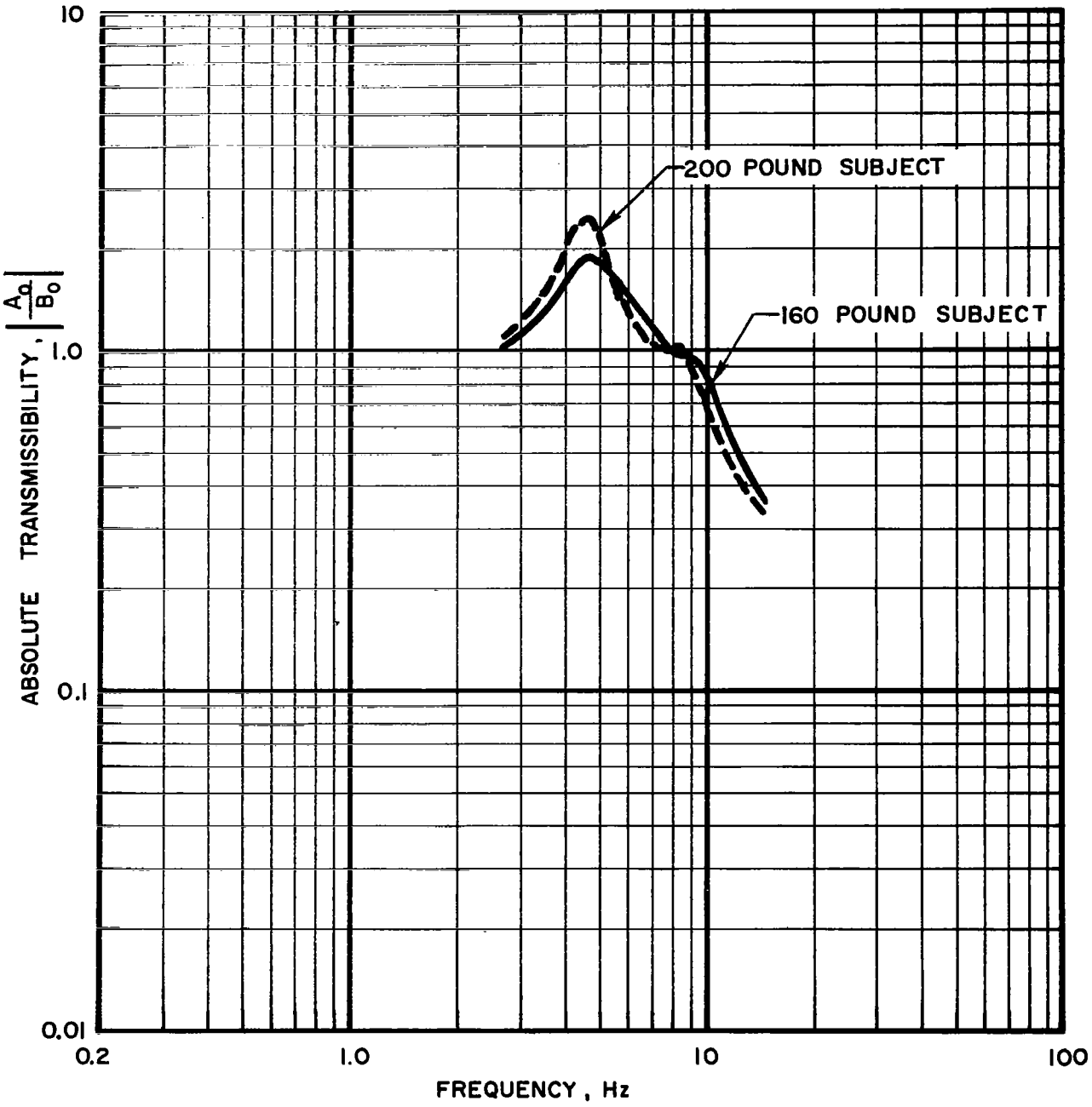

Figure 50: Test Data on Absolute Transmissibilities Between the Buttocks and Head for 160 Pound and 200 Pound Subjects as Determined From Landing/Takeoff Mode Tests

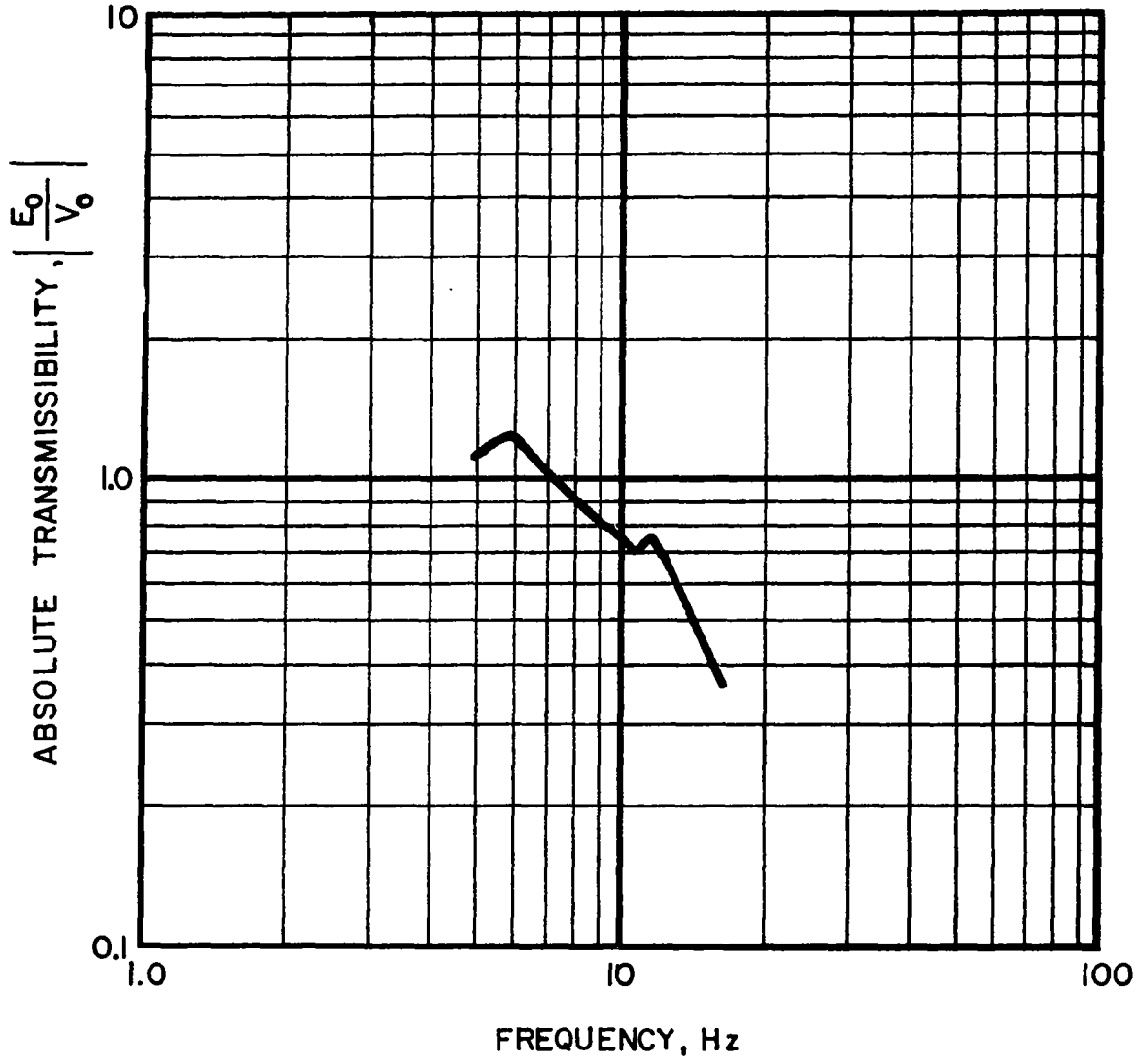

Figure 51: Test Data on Absolute Fore/Aft Transmissibility Between Input and Head With: a 160 Pound Subject; DC-8 Seat Cushion; and Seat Belt Tight

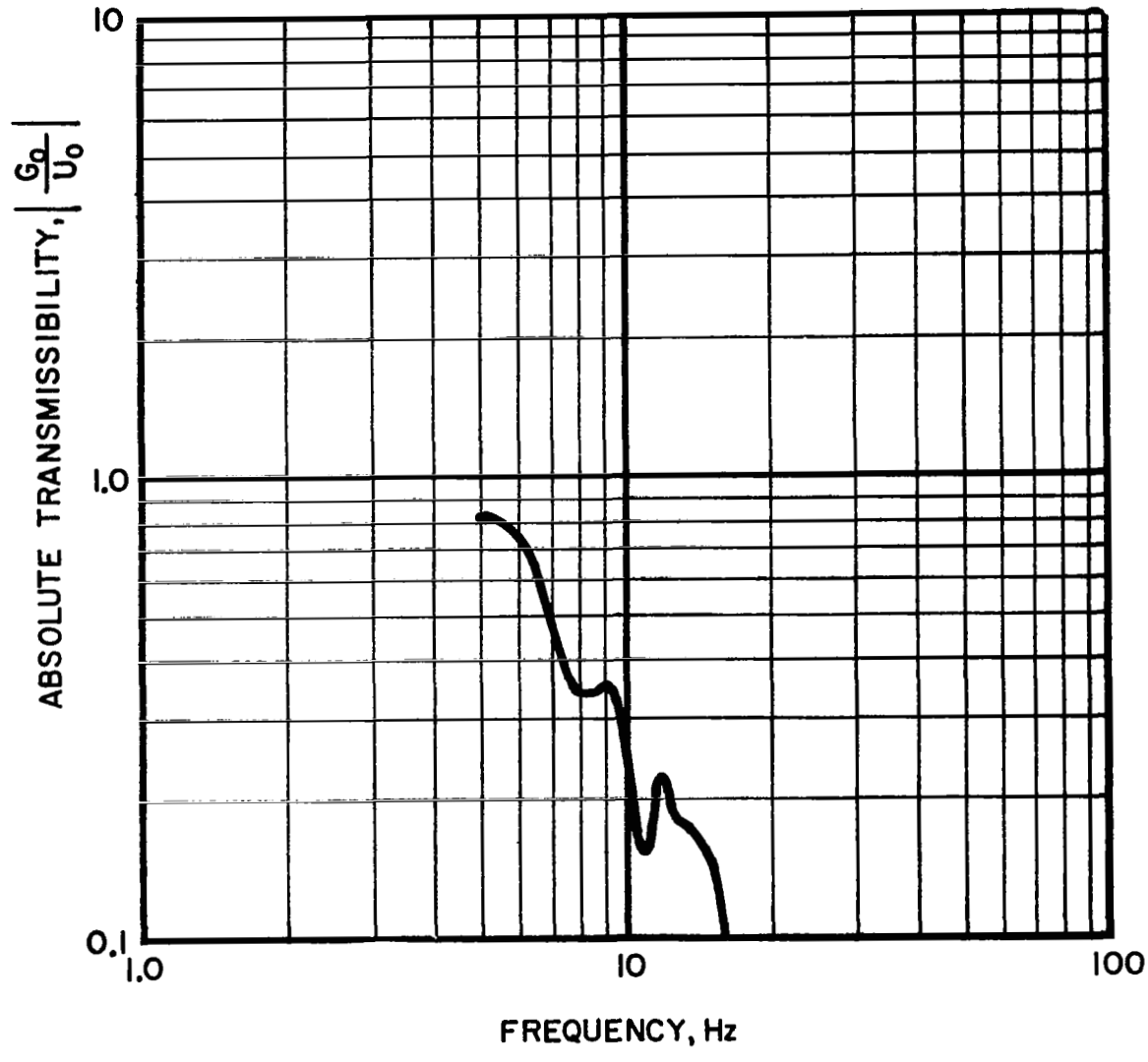

Figure 52: Test Data on Absolute Lateral Transmissibility Between Input and Head With: a 160 Pound Subject; DC-8 Seat Cushion; and Seat Belt Tight